

NATIONAL CENTER FOR EARTHQUAKE
ENGINEERING RESEARCH

State University of New York at Buffalo

A THREE-DIMENSIONAL ANALYTICAL STUDY OF SPATIAL VARIABILITY OF SEISMIC GROUND MOTIONS

by

L-L. Hong and A.H-S. Ang

Department of Civil Engineering
University of California-Irvine
Irvine, California 92717

Technical Report NCEER-90-0025

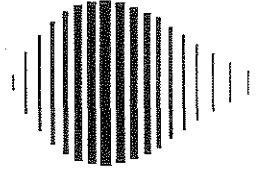
October 30, 1990

This research was conducted at the University of California-Irvine and was partially supported by the National Science Foundation under Grant No. ECE 86-07591.

NOTICE

This report was prepared by the University of California-Irvine as a result of research sponsored by the National Center for Earthquake Engineering Research (NCEER). Neither NCEER, associates of NCEER, its sponsors, the University of California-Irvine, nor any person acting on their behalf:

- a. makes any warranty, express or implied, with respect to the use of any information, apparatus, method, or process disclosed in this report or that such use may not infringe upon privately owned rights; or
- b. assumes any liabilities of whatsoever kind with respect to the use of, or the damage resulting from the use of, any information, apparatus, method or process disclosed in this report.



**A THREE-DIMENSIONAL ANALYTICAL STUDY OF
SPATIAL VARIABILITY OF SEISMIC GROUND MOTIONS**

by

L-L. Hong¹ and A.H-S. Ang²

October 30, 1990

Technical Report NCEER-90-0025

NCEER Contract Number 88-3015

NSF Master Contract Number ECE 86-07591

- 1 Assistant Professor, Department of Civil Engineering, National Cheng-Kung University, Tainan, Taiwan
- 2 Professor, Department of Civil Engineering, University of California - Irvine

NATIONAL CENTER FOR EARTHQUAKE ENGINEERING RESEARCH
State University of New York at Buffalo
Red Jacket Quadrangle, Buffalo, NY 14261

PREFACE

The National Center for Earthquake Engineering Research (NCEER) is devoted to the expansion and dissemination of knowledge about earthquakes, the improvement of earthquake-resistant design, and the implementation of seismic hazard mitigation procedures to minimize loss of lives and property. The emphasis is on structures and lifelines that are found in zones of moderate to high seismicity throughout the United States.

NCEER's research is being carried out in an integrated and coordinated manner following a structured program. The current research program comprises four main areas:

- Existing and New Structures
- Secondary and Protective Systems
- Lifeline Systems
- Disaster Research and Planning

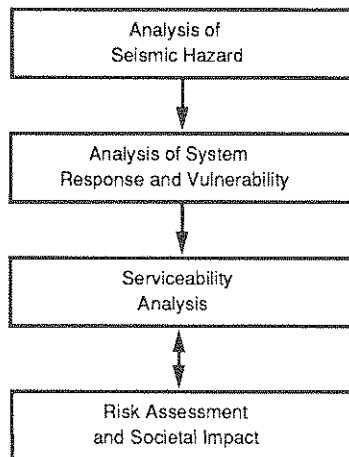
This technical report pertains to Program 3, Lifeline Systems, and more specifically to water delivery systems.

The safe and serviceable operation of lifeline systems such as gas, electricity, oil, water, communication and transportation networks, immediately after a severe earthquake, is of crucial importance to the welfare of the general public, and to the mitigation of seismic hazards upon society at large. The long-term goals of the lifeline study are to evaluate the seismic performance of lifeline systems in general, and to recommend measures for mitigating the societal risk arising from their failures.

From this point of view, Center researchers are concentrating on the study of specific existing lifeline systems, such as water delivery and crude oil transmission systems. The water delivery system study consists of two parts. The first studies the seismic performance of water delivery systems on the west coast, while the second addresses itself to the seismic performance of the water delivery system in Memphis, Tennessee. For both systems, post-earthquake fire fighting capabilities will be considered as a measure of seismic performance.

The components of the water delivery system study are shown in the accompanying figure.

Program Elements:



Tasks:

Wave Propagation, Fault Crossing
Liquefaction and Large Deformation
Above- and Under-ground Structure Interaction
Spatial Variability of Ground Motion

Soil-Structure Interaction, Pipe Response Analysis
Statistics of Repair/Damage
Post-Earthquake Data Gathering Procedure
Leakage Tests, Centrifuge Tests for Pipes

Post-Earthquake Firefighting Capability
System Reliability
Computer Code Development and Upgrading
Verification of Analytical Results

Mathematical Modeling
Socio-Economic Impact

In this study, an approach for the analytical solution of wave propagation in three-dimensional solids has been extended to a half-space subjected to finite dislocation representing fault rupture from an earthquake. With specified rupture area and dislocation speed, analytical solutions of the ground motions at the surface, or near the surface, at specified distances from the rupture are calculated. Using the results at specific ground surface stations obtained analytically for a given set of source parameters, appropriate transfer functions can be obtained through time-domain system identification techniques to represent seismic wave transmission between the fault rupture and ground station. This should then permit a definition of spatially varying ground motions useful for lifeline studies.

ABSTRACT

A hybrid deterministic and stochastic method is developed to estimate the spatial variation of seismic ground motions which is necessary for the analysis and design of lifeline systems. An analytical model for wave propagating through a three-dimensional half-space is first proposed to evaluate the ground responses. The incoherent slip over a fault plane is then represented by an autocorrelation function of the dislocation velocity, from which the source motion is modeled as a random process specified by a power spectral density function. To separate the path effect from the source effect, a multi-degree-of-freedom system is chosen as the "substitute system" which is characterized by the equivalent transmission effect to the deterministic wave propagation model. The frequency transfer function of the substitute system is obtained through system identification. With the resulting transfer function of the system and the given power spectral density at the source, the power spectral density of absolute and differential ground motions can be estimated.

The results obtained through the model are compared with the field data from an actual earthquake recorded at a dense strong motion array. The analytical results should be applicable for the seismic response analysis and design of pipeline systems.

ACKNOWLEDGMENTS

This report is based on the studies conducted by Dr. L-L. Hong as part of his dissertation for the Ph.D. at the University of Illinois at Urbana-Champaign. The work was supported by the National Center for Earthquake Engineering Research under contract NCEER 88-3015, and constitutes part of the US-Taiwan cooperative research on lifeline reliability and design.

The authors are indebted to Professors C. S. Yeh, C. H. Loh, P. L. Chen, and M. K. Kuo, and Mr. T. K. Wang of Taiwan for their contributions to the cooperative study.

TABLE OF CONTENTS

SECTION	TITLE	PAGE
1	INTRODUCTION	1-1
1.1	Introductory Remarks	1-1
1.2	Objectives and Scope	1-2
1.3	Organization	1-3
1.4	Summary of Notations	1-4
2	ANALYTICAL GROUND MOTIONS IN TRANSFORM DOMAIN	2-1
2.1	Review of Earthquake Source Models	2-1
2.2	The Haskell Model.....	2-6
2.2.1	Horizontal Fault	2-6
2.2.2	Oblique Fault	2-14
3	ANALYTICAL GROUND MOTIONS IN TIME DOMAIN	3-1
3.1	Introduction	3-1
3.2	Inverse Laplace Transform	3-2
3.2.1	Cagniard Path Contribution	3-2
3.2.2	Branch Cut Contribution	3-4
3.2.3	Pole Contribution	3-4
3.3	Analytical Formulation	3-7
3.4	Case Studies	3-12
4	ANALYSIS OF SEISMIC GROUND MOTIONS	4-1
4.1	Deterministic Analysis	4-1
4.1.1	The Event 5	4-1
4.1.2	Model Parameters	4-2
4.2	Stochastic Analysis	4-13
4.2.1	Randomness of Earthquake Source	4-14
4.2.2	The Substitute System	4-18
4.2.3	Stochastic Characteristics of Ground Motion	4-30
5	APPLICATIONS TO PIPELINES	5-1
5.1	Introduction	5-1
5.2	Differential Axial Motion Across Joint	5-2
5.2.1	Deterministic Analysis	5-2
5.2.2	Stochastic Analysis	5-5
5.3	Differential Transverse Motion Across Joint	5-6
5.3.1	Deterministic Analysis	5-6
5.3.2	Stochastic Analysis	5-11
5.4	Comparison of Results	5-12
6	SUMMARY AND CONCLUSIONS	6-1
6.1	Summary	6-1
6.2	Conclusions	6-2
6.3	Suggestions for Further Study.....	6-4

TABLE OF CONTENTS (Cont'd)

SECTION	TITLE	PAGE
7	REFERENCES	7-1
APPENDIX A	LAPLACE TRANSFORM ELEMENTS FOR OBLIQUE FAULT	A-1
APPENDIX B	ANALYTICAL SOLUTION OF HASKELL MODEL	B-1
APPENDIX C	POWER SPECTRAL DENSITY OF BASE VELOCITY	C-1
APPENDIX D	LISTING OF COMPUTER PROGRAM	D-1

LIST OF ILLUSTRATIONS

FIGURE	TITLE	PAGE
2.1	Shear Dislocation in a Rectangular Fault	2-7
2.2	Schematic Diagrams of Superposition of Four Quadrantal Dislocations	2-10
2.3	Coordinate Systems of Half-Space and Fault.....	2-15
2.4	Incident and Reflected Waves at a Receiver	2-20
3.1	Poles and Cagniard Paths in Complex σ -Plane	3-3
3.2	Poles and Cagniard Paths in Complex a -Plane	3-6
3.3	Poles and Cagniard Paths in Complex β -Plane	3-8
3.4	Vertical Fault and Ground Station	3-13
3.5	Displacements in Case I	3-15
3.6	Displacements in Case II	3-16
3.7	Accelerations for Different Rise Times	3-18
4.1	Seven Stations in the SMART-1 Array	4-3
4.2	Accelerograms Along Epicentral Direction	4-4
4.3	Accelerograms Normal to Epicentral Direction	4-5
4.4	The Rupture Velocity	4-7
4.5	Focal Mechanisms of Event 5	4-10
4.6	Analytic Velocities at Station C00 with $T_r = 0$ sec	4-11
4.7	Accelerations for Different Rise Times at Station C00	4-12
4.8	Schematic Diagrams of Dislocation and Its Autocorrelation Function	4-15
4.9	Velocities from Analytic Model and Substitute System at Station C00 ($0.05 < \xi_j < 1$)	4-25
4.10	Velocities from Analytic Model and Substitute System at Station C00 ($0.1 < \xi_j < 1$)	4-26
4.11	Velocities from Analytic Model and Substitute System at Station C00 ($0.2 < \xi_j < 1$)	4-27
4.12	Velocities from Analytic Model and Substitute System at Station O06 ($0.1 < \xi_j < 1$)	4-28
4.13	Velocities from Analytic Model and Substitute System at Station O12 ($0.1 < \xi_j < 1$)	4-29
4.14	Power Spectral Densities of Acceleration at Station O06	4-33
4.15	Power Spectral Densities of Acceleration at Station M06	4-33
4.16	Power Spectral Densities of Acceleration at Station I06	4-34
4.17	Power Spectral Densities of Acceleration at Station C00	4-34
4.18	Power Spectral Densities of Acceleration at Station I12	4-35
4.19	Power Spectral Densities of Acceleration at Station M12	4-35
4.20	Power Spectral Densities of Acceleration at Station O12	4-36
4.21	Power Spectral Densities of Differential Ground Acceleration	4-40
4.22	Power Spectral Densities of Differential Ground Velocity	4-42
4.23	Power Spectral Densities of Differential Ground Displacement	4-44

LIST OF ILLUSTRATIONS (Cont'd)

FIGURE	TITLE	PAGE
5.1	Discrete Model for Differential Axial Motion Across Joint.....	5-3
5.2	Discrete Model for Differential Transverse Motion Across Joint	5-4
5.3	Differential Axial Displacement Response Spectra ($\xi_0=5\%$)	5-16
5.4	Differential Axial Displacement Response Spectra ($\xi_0=10\%$)	5-18
5.5	Differential Transverse Displacement Response Spectra ($\xi_{1,2,3}=5\%$)	5-20
5.6	Differential Transverse Displacement Response Spectra ($\xi_{1,2,3}=10\%$)	5-22

SECTION I

INTRODUCTION

1.1 Introductory Remarks

The spatial variation of seismic ground motions is necessary for the proper design and analysis of lifeline systems. Lifeline systems, such as oil and gas pipelines, water distribution systems, as well as communication and transportation networks, offer varying needs for a modern city. Once their performance are interrupted during an earthquake, the influence to the safety and health of the public could be very significant.

One obvious difference of a lifeline from buildings is that its length is much greater than its other dimensions. Therefore, the seismic excitations along the axis of a lifeline should not be considered to be coherent motions. Since the incoherent excitations generate the differential motion between any two points along the pipeline axis, it is of particular concern to investigate the damage at the joints caused by the relative ground motions.

To study the out-of-phase seismic ground motions, the observations from a dense array of strong motion seismographs are needed. The SMART-1 (Strong Motion ARray in Taiwan) provides this opportunity. The array consisted of 37 triaxial accelerometers configured in three concentric circles of radii 0.2 km (Inner), 1 km (Middle), and 2 km (Outer). There are twelve equally spaced stations numbered 1 through 12 on each ring and one central station named C00. This specially installed array presents much information of the spatially varying seismic ground motions.

The spatial variation of the seismic ground motions recorded by the SMART-1 array has been extensively analyzed, for example, by Loh, *et al.* (1983), Harada (1984) and Loh (1985). The evaluation is entirely based on the field data. In particular, the focal mechanism of an earthquake from which the recordings are generated is not considered, and thus the results are applicable only for a specific earthquake.

For the purpose of presenting a model to study the general spatial variation of ground motions from an earthquake an analytical model to simulate the focal mechanism is required. Such a model should account for the rupture process at the source and the wave propagation through the semi-infinite soil medium.

Similar attempts have been made by Zerva, *et al.* (1985) as well as Suzuki and Kiremidjian (1988) when both the stochastic rupture process and the wave propagation were combined together either to investigate the spatial variation of ground motions or to estimate the seismic hazard. Zerva, *et al.* (1985) used an anti-plane shear plus a plane-strain model to simulate the three-dimensional problem. Suzuki and Kiremidjian (1988) adopted the normal mode method to evaluate seismic ground motions; because no radiation condition at infinity was considered when the normal modes were calculated, an empirical attenuation factor was needed in this approach.

1.2 Objectives and Scope

The objective of this study is to develop a three-dimensional analytical model to determine the characteristics of seismic excitations pertinent to lifelines. The

seismic ground motions are expressed in stochastic terms, such as power and cross spectral density functions of the differential motion. To achieve this goal, the faulting at the source is described stochastically and the transmission through the soil is substituted by an N-degree-of-freedom system whose output is equivalent to the wave motions obtained through a theoretical 3-D wave propagation solution in a half space subjected to a specified rupture process at the focus.

The spatially varying ground motions are then used as the seismic input to a pipeline to investigate the maximum differential displacements across the joints represented in terms of the differential response spectra.

The validity of the analytical results are examined using empirical results from field recordings, specifically the SMART-1 array.

1.3 Organization

In Section 2, several models for simulating ground motions induced by earthquakes are reviewed. The Haskell kinematic dislocation model is then described and the analytical ground motions in the transform domain is obtained for a general fault with an arbitrary dip angle.

Section 3 presents the analytical ground motions in the time domain. Inversion of the Laplace transform presented in Section 2 is performed with the Cagniard-de Hoop technique. To validate the resulting solutions, the displacements obtained with the model for a vertical fault are compared with those obtained by other methods.

An explicit form is proposed in Section 4 for introducing the randomness at the source. The wave transmission effect is simulated by a substitute system, with

parameters obtained through system identification. On this basis, numerical solutions are obtained to simulate an earthquake (Event 5) recorded by the SMART-1 array. The results, in terms of the power spectral density of the absolute and differential motions, for this earthquake are evaluated and compared with those obtained from the corresponding field data.

Discrete models of pipelines subjected to axial and lateral ground motions are introduced in Section 5. Pertinent maximum responses of the pipeline predicted with the analytical ground motion model are compared with corresponding results obtained for the ground motions recorded in Event 5.

Finally, Section 6 presents the summary and major conclusions of the current study.

1.4 Summary of Notations

A_{\pm} , B_{\pm}	Cagniard paths in the complex α - and β -planes, respectively
B , \dot{B}	base displacement and velocity of substitute system, respectively
b_p , b_s	P- and S-wave slowness, respectively
C_{\pm}	circular paths in the complex plane
c_p , c_s	dampings of joint and soil, respectively
D , \dot{D}	dislocation and its velocity, respectively
D_0	final dislocation
$D_{..}$	receiver functions
E	error function
F_p , F_s	Laplace transformed elements for an oblique fault
$F_{0,1,2,3}$	ground excitations to discrete pipeline systems

f	source time function
g_p, g_s	phase functions of P- and S-wave, respectively
$g'_{p, s}$	phase functions for local system (fault)
H	Heaviside step function
H, H^*	frequency transfer functions
h, h_*	impulse response functions
J_p, J_s	Jacobian determinants related to P- and S-wave, respectively
k_L^{-1}	correlation length
k_T^{-1}	correlation time
k_p, k_s	stiffnesses of joint and soil, respectively
L	fault length
l	separation distance of pipe segments
M_L	local magnitude
m	lumped mass of pipe segment
R	Rayleigh function
R_0	distance from a station to the corner of a fault
R^{**}	reflection coefficients
r	amplitude of position vector in xy plane
S_p, S_v, S_H	source functions of P-, SV- and SH-wave, respectively
$S'_{p, v, H}$	source functions of P-, SV- and SH-wave, respectively
$S_{..}$	power or cross spectral density functions
s	Laplace transform parameter
sgn	sigma function
T_r	rise time in linear ramp-time source function

T_0	duration of spreading rupture
t_i, t_f	initial and final times of a record, respectively
t_{1h}	arrival time of conical head wave
t_{1p}, t_{1s}	arrival time of spherical P- and S-wave, respectively
t_{2h}, t_{3h}	arrival time of plane head wave
t_{2p}, t_{2s}	arrival time of conical P- and S-wave, respectively
t_{3p}, t_{3s}	arrival time of cylindrical P- and S-wave, respectively
u_x, u_y, u_z	displacement components
$\bar{u}_x, \bar{u}_y, \bar{u}_z$	Laplace transforms of displacement components
v	rupture velocity
v_p, v_s	P- and S-wave velocities, respectively
W	fault width
x, y, z	coordinates of global system (half-space)
x', y', z'	coordinates of local system (fault)
$x_{G1,2}, y_{G1,2}$	axial and transverse ground motions at supports, respectively
$x_{1,2}, y_{1,2}$	axial and transverse displacements of pipe segments, respectively
z_0	depth of shallowest edge of a fault
z_1, z_2, z_3	generalized displacements in discrete pipeline system
$\Delta d, \Delta v, \Delta a$	differential ground displacement, velocity, and acceleration, respectively
$\Delta x, \Delta y$	differential axial and transverse displacements between pipe segments, respectively
δ	dip angle

λ	ratio of k_p to k_g (also c_p to c_g)
$\mu_{\Delta u_m}, \sigma_{\Delta u_m}$	mean value and standard deviation of maximum differential displacement between pipe segments, respectively
$\omega_{0, 1, 2, 3}$	natural frequencies in discrete pipeline system
ω_*, ω^*	natural frequencies in multi-degree-of-freedom system
ϕ, χ, ψ	1. Lamé potential functions
ψ	2. spatio-temporal autocorrelation function of dislocation velocity
$\phi_{1, 2}$	elements in modal shape vectors
ϕ_*, ϕ^*	participation factors in multi-degree-of-freedom system
Σ_{\pm}	Cagniard paths in the complex σ -plane
σ_1, σ_2	poles in the complex σ -plane
θ	1. argument of position vector in xy plane 2. rotation of pipe segment
ξ, η, ξ_p, ξ_s	global Fourier transform parameters
$\xi', \eta', \xi'_p, \xi'_s$	local Fourier transform parameters
$\xi_{0, 1, 2, 3}$	damping ratios in discrete pipeline system
ξ_*, ξ^*	damping ratios in multi-degree-of-freedom system
$[C]$	damping matrix
$[D], [D']$	global and local receiver function matrices, respectively
$[D^*]$	modified receiver function matrix
$[K]$	stiffness matrix

- $[M]$ mass matrix
- $[T]$ coordinate transformation matrix
- $\{F\}$ ground excitations to pipelines
- $\{\Phi_{1, 2, 3}\}$ modal shapes
-
- f^F Fourier transform of a function f
- f^{FF} double Fourier transform of a function f
- \bar{f} one-sided Laplace transform of a function f

SECTION 2

ANALYTICAL GROUND MOTIONS IN TRANSFORM DOMAIN

2.1 Review of Earthquake Source Models

Seismologists generally agree that earthquakes (particularly shallow earthquakes) are produced by a sudden rupture in the earth's crust caused by the release of accumulated strain initiated at a point on a geologic fault. The rupture spreads over the fault surface and shearing motions develop behind the rupture front. The rupture will eventually stop either because of a strong barrier or simply due to the lack of sufficient strain energy, and the ensuing shearing motions throughout the source region ceases. Another rupture might start again at some other point on the fault surface. To theoretically represent such an earthquake source mechanism, dislocation fault models, in which an earthquake is initiated by a discontinuous displacement on a fault plane, have been introduced. Such dislocation models may be divided into kinematic and dynamic models.

For fully dynamic dislocation models, the slip within a crack has to be estimated as a function of the stress drop (the pre-existing tectonic shear stress minus the dynamic frictional stress) and the velocity of the crack boundary is governed by a fracture criterion (stress-intensity factor, energy release rate, or maximum stress). In other words, the stress drop is considered as the driving force of an earthquake rupture and the motion of the rupture front is then determined by certain physical relations between stress concentration and material strength.

Because of the lack of information regarding stress drop and material strength, the slip has frequently been specified empirically. In kinematic dislocation models, the final slip is often assumed to be constant over a fault and the evolution of the rupture front is modeled as a unilateral or bilateral motion of a dislocation with a constant velocity.

There have been many investigations on determining the seismic source parameters from the analysis of observed records and the prediction of ground motions excited by a simplified source mechanism through an idealized medium. The analyses of seismic ground motions using various source models and the methods of solution can be classified as follows:

(1) Dislocation model

- (a) Type: strike-slip or dip-slip,
- (b) Length of fault: infinite, semi-infinite or finite,
- (c) Shape of rupture front: rectilinear or curvilinear,
- (d) Slip function: kinematic or dynamic.

(2) Medium

- (a) Dimensionality: 2-D anti-plane shear, 2-D plane strain or 3-D,
- (b) Region: full-space or half-space,
- (c) Property: uniform or layered.

(3) Method of solution

- (a) Green's function,
- (b) Equivalent body force,
- (c) Generalized ray theory,
- (d) Cagniard-de Hoop,
- (e) Self-similar potential,

- (f) Discrete wave number,
- (g) Mixed boundary integral equation,
- (h) Finite difference.

An extensive literature review can be found in Luco (1986).

Strictly speaking, the motions at the ground surface generated by an earthquake of fault rupture origin involve wave propagations in a three-dimensional half-space. The three-dimensional problem has been approximated by two-dimensional solutions; namely an anti-plane shear plus a plane-strain solution (*e.g.*, Seyyedien-Choobi and Robinson, 1975). The anti-plane shear model in a half-plane corresponds to a strike-slip rupture, whereas the plane-strain model leads to a dip-slip motion. In both models, the responses are independent of the coordinate in the out-of-plane direction. In other words, such an approximation implies the assumption that the rupture surface is infinitely long.

Comparisons of two- and three-dimensional solutions in infinite media have been presented by Boore and Zoback (1974) and Geller (1974). Boore and Zoback (1974) compared the three-dimensional solution of Haskell (1969) for a vertical strike-slip fault with a solution for a two-dimensional gliding dislocation model of finite length and concluded that, for near-field stations, the wave forms may be insensitive to the rupture length, but the amplitudes of the motions are not. Geller (1974) conducted similar comparisons and found that both solutions are almost identical until the arrival of the P-wave from the edge of a three-dimensional rupture of finite length.

In earlier studies, the effects of the free surface were approximated by doubling the amplitudes resulting from the response of a full-space. Anderson (1976) found that this approximation is valid only for the case when the angle of

incidence at the station is less than a specified value. In addition to the above restriction for amplification of waves, the other major deviations arise from the appearance of the Rayleigh and head waves in a half-space.

As for the method of solution, the synthesis of Green's functions is the most common approach to evaluate the ground motions caused by a fault dislocation, because the formulation of the response is straightforward as long as the Green's functions are available. However, formidable numerical efforts are required in evaluating the Green's functions and the resulting convolution integrals. In general, the response obtained by this approach involves a spatial integral of the point source solution over the whole fault plane either directly in the time domain (Kawasaki, 1975; Anderson, 1976; Hartzell, *et al.*, 1978) or in the frequency domain followed by the necessary Fourier inverse transform (Levy and Mal, 1976). Luco and Anderson (1983) adopted the equivalent body force representation to calculate the ground responses in the transform domain, in which the dislocation over a fault plane was converted to a set of equivalent body forces using the representation theorem introduced by Burridge and Knopoff (1964); the responses were then obtained by solving the inhomogeneous wave equations subject to the homogeneous boundary conditions at the free surface. A detailed review of the generalized ray theory can be found in Pao and Gajewski (1977). Basically, the Laplace transform response is expressed as the sum of several terms in this analysis. Each term represents the contribution from a particular ray and contains only the product of a source function, a receiver function, and a phase term. Chen (1981) used the generalized ray theory to analyze the ground responses induced by a non-propagating dislocation fault. Furthermore, each ray can be evaluated directly and exactly by applying the Cagniard-de Hoop technique (de Hoop, 1960)

to obtain the ground responses in the time domain. Madariaga (1978) proposed the same technique to invert the transform and found an exact solution of Haskell's model in an unbounded medium. The application of the generalized ray theory is as straightforward as that of the Green's functions; moreover, the application of the Cagniard-de Hoop technique reduces the computational efforts significantly.

There were also approaches to analyze the wave field induced by an extended fault embedded in a layered half-space. One of these is to represent the response in the frequency domain as a double integral over the two horizontal components of the wave number. Bouchon (1979) introduced the discretization over the two wave numbers in an elastic wave field.

For dynamic dislocation models, Das (1980) presented a method of mixed boundary integral equation to determine the displacements and stresses on the crack plane for a three-dimensional dynamic shear crack of arbitrary shape propagating in an infinite medium. A finite difference technique developed by Virieux and Madariaga (1982) was adopted for dynamic shear cracks and a maximum stress criterion was used to determine the rupture propagation. Achenbach and Harris (1987) applied dynamic fracture mechanics to analyze the strong ground motion excited by subsurface sliding cracks.

A three-dimensional kinematic dislocation model in an elastic half-space will be presented in this study to simulate an earthquake and the resulting ground motions. Similar models were proposed by Chen (1981) as well as Luco and Anderson (1983). Chen (1981) considered the rupture velocity to be infinite, whereas, in Luco and Anderson (1983), the rupture front is initiated at infinity so that the results are applicable only for near-field ground motions. To be more

realistic for determining the spatial variability of ground motions, the source mechanism of an earthquake is modeled by a shear fault of the Haskell type (Haskell, 1964) with finite length and finite rupture velocity.

2.2 The Haskell Model

The Haskell model is the earthquake source model most widely used for simulating seismic observations (Haskell, 1964, 1969; Aki, 1967, 1968; Kawasaki, 1975; Anderson, 1976; Geller, 1976; Israel and Kovach, 1977; Madariaga, 1978; Bouchon, 1979; Tanimoto, 1982; Yeh, *et al.*, 1988). This model assumes a rectangular fault of length L and width W as shown in Fig. 2.1. A dislocation line over the width W appears at one edge of the fault plane and propagates at a constant rupture velocity v until it suddenly stops at the other edge. The slip may be longitudinal (along the direction of rupture propagation) for the case of a strike-slip fault or transverse (normal to the direction of rupture propagation) for the case of a dip-slip fault. The dislocation amplitudes are assumed to be identical across the width in both cases. At the end of the rupture process, a constant dislocation remains on the source area. The Haskell model is also adopted in the present study. First, the analytical ground motions in the Laplace transform domain excited by a horizontal Haskell fault are obtained. Then the results are extended to the case of a general fault with an arbitrary dip angle. The resulting ground motions in the time domain are discussed in Section 3.

2.2.1 Horizontal Fault

Assume a horizontal fault at a depth of $z = z_0$. For the case of a strike-slip fault, the boundary conditions on the fault plane are

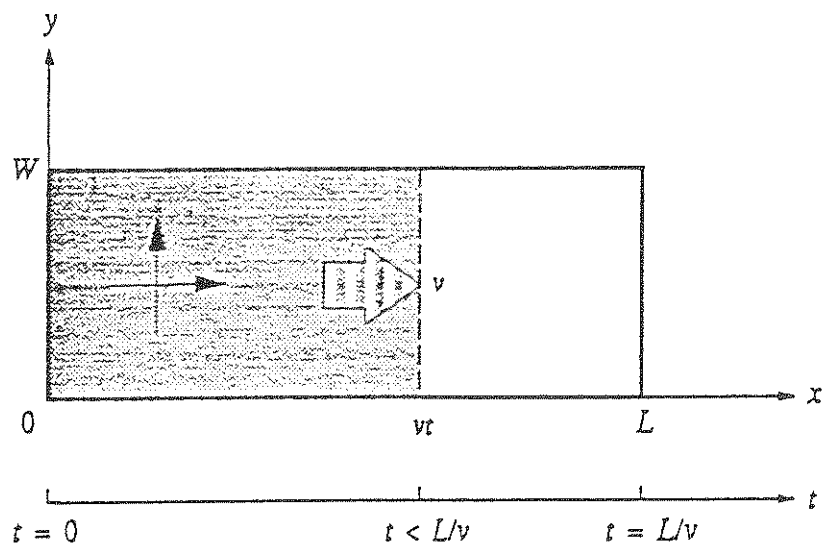


Figure 2.1 Shear Dislocation in a Rectangular Fault

$$u_x(x, y, z, t) = \frac{D_0}{2} \operatorname{sgn}(z - z_0) f(t) [H(y) - H(y - W)] \\ \cdot [H(x) - \{H(T_0 - t) H(x - vt) + H(t - T_0) H(x - L)\}], \quad (2.1)$$

$$u_y(x, y, z, t) = 0, \quad (2.2)$$

$$\tau_{zz}(x, y, z, t) = 0; \quad (2.3)$$

whereas for a dip-slip fault,

$$u_x(x, y, z, t) = 0, \quad (2.4)$$

$$u_y(x, y, z, t) = \frac{D_0}{2} \operatorname{sgn}(z - z_0) f(t) [H(y) - H(y - W)] \\ \cdot [H(x) - \{H(T_0 - t) H(x - vt) + H(t - T_0) H(x - L)\}], \quad (2.5)$$

$$\tau_{zz}(x, y, z, t) = 0. \quad (2.6)$$

In the foregoing equations,

D_0 = the magnitude of the dislocation,

sgn = the sigma function,

f = the source time function,

H = the Heaviside step function,

$T_0 = L / v$ = the duration of the spreading rupture.

In the following sections, the ground motions excited by a strike-slip fault are described in detail. Results for a dip-slip fault are listed, where necessary, for reference.

After expanding Eq. (2.1), *i.e.*,

$$\begin{aligned}
& H(x) - \{H(T_0 - t) H(x - vt) + H(t - T_0) H(x - L)\} \\
& = \{H(x) - H(x - vt)\} - H(t - T_0) \{H(x - L) - H(x - vt)\}, \tag{2.7}
\end{aligned}$$

the total field response (f^T) may be written as the superposition of the field response (f^Q) for four identical quadrantal dislocations shifted in space and time, as shown in Fig. 2.2, *i.e.*,

$$\begin{aligned}
f^T(x, y, z, t) & = f^Q(x, y, z, t) - f^Q(x, y - W, z, t) - H(t - T_0) f^Q(x - L, y, z, t - T_0) \\
& \quad + H(t - T_0) f^Q(x - L, y - W, z, t - T_0), \tag{2.8}
\end{aligned}$$

where f^Q is the response subject to boundary conditions (2.2), (2.3), and

$$\begin{aligned}
u_x(x, y, z, t) & = \frac{D_0}{2} \operatorname{sgn}(z - z_0) f(t) H(y) [H(x) - H(x - vt)] \\
& = \frac{D_0}{2} \operatorname{sgn}(z - z_0) f(t) H(x) H(y) H\left(t - \frac{x}{v}\right). \tag{2.9}
\end{aligned}$$

By applying the Helmholtz decomposition, the wave equations are

$$v_p^2 \nabla^2 \phi = \ddot{\phi}, \tag{2.10}$$

$$v_s^2 \nabla^2 \chi = \ddot{\chi}, \tag{2.11}$$

$$v_s^2 \nabla^2 \psi = \ddot{\psi}, \tag{2.12}$$

where ϕ , χ and ψ are the potential functions corresponding to P-, SH- and SV-wave, respectively; v_p and v_s are the P- and S-wave velocities, respectively.

In order to solve the wave equation, *e.g.*, Eq. (2.10), the one-sided Laplace transform over t and the double Fourier transform over x and y are employed. The corresponding transform pairs are

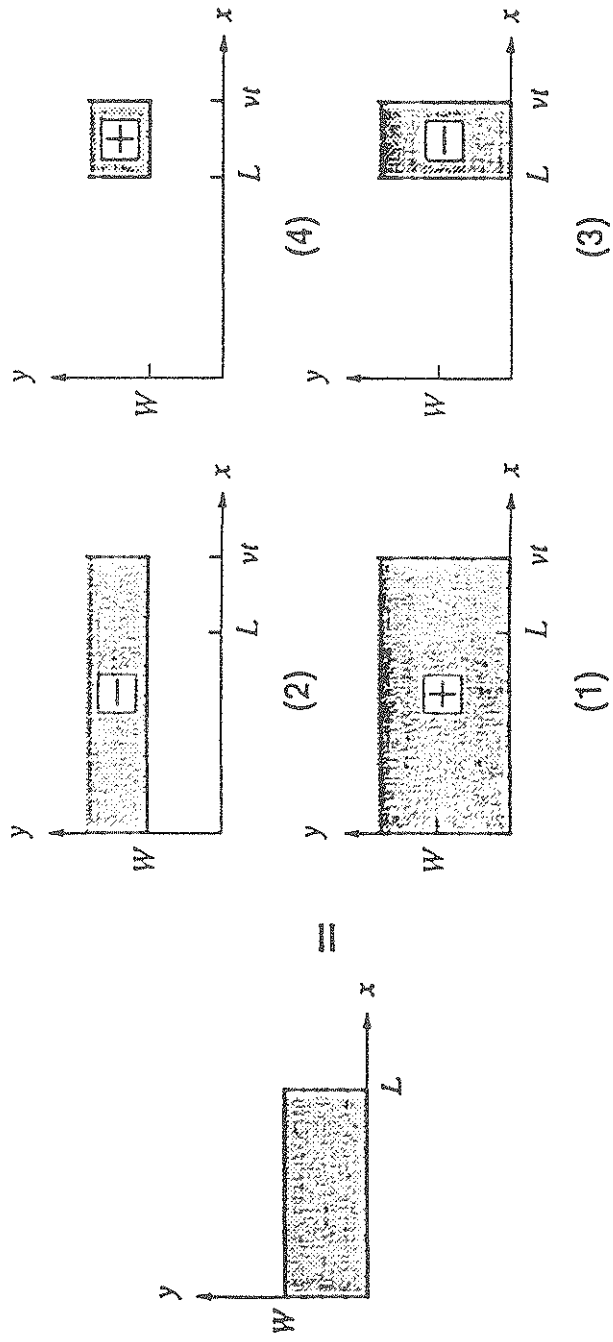


Figure 2.2 Schematic Diagrams of Superposition of Four Quadrantal Dislocations

$$\bar{\phi}(x, y, z, s) = \int_0^{\infty} \phi(x, y, z, t) e^{-st} dt, \quad (2.13)$$

$$\phi(x, y, z, t) = \frac{1}{2\pi i} \int_{B_r} \bar{\phi}(x, y, z, s) e^{st} ds, \quad (2.14)$$

and

$$\bar{\phi}^{FF}(\xi, \eta, z, s) = \int_{-\infty}^{\infty} \int_{-\infty}^{\infty} \bar{\phi}(x, y, z, s) e^{-s(i\xi x + i\eta y)} dx dy, \quad (2.15)$$

$$\bar{\phi}(x, y, z, s) = \frac{s^2}{4\pi^2} \int_{-\infty}^{\infty} \int_{-\infty}^{\infty} \bar{\phi}^{FF}(\xi, \eta, z, s) e^{s(i\xi x + i\eta y)} d\xi d\eta; \quad (2.16)$$

where:

s = the Laplace transform parameter,

B_r = the infinite Bromwich line,

ξ, η = the Fourier transform parameters.

By solving the transformed wave equations with the quiescent initial conditions, the radiation conditions at infinity and the boundary conditions on the fault plane, the transformed potential functions are

$$\bar{\phi}(x, y, z, s) = \frac{D\bar{f}(s)}{8\pi^2 b_s^2} \int_{-\infty}^{\infty} \int_{-\infty}^{\infty} S_p(\xi, \eta, s) e^{-s(\xi\rho|x-z_0|-i\xi x - i\eta y)} d\xi d\eta, \quad (2.17)$$

$$\bar{\chi}(x, y, z, s) = \frac{D_0 \bar{f}(s)}{8\pi^2 b_j^2 s} \int_{-\infty}^{\infty} \int_{-\infty}^{\infty} S_H(\xi, \eta, s) e^{-s(\xi_s |z-z_0| - i\xi x - i\eta y)} d\xi d\eta, \quad (2.18)$$

$$\bar{\psi}(x, y, z, s) = \frac{D_0 \bar{f}(s)}{8\pi^2 b_j^2 s^2} \int_{-\infty}^{\infty} \int_{-\infty}^{\infty} S_V(\xi, \eta, s) e^{-s(\xi_s |z-z_0| - i\xi x - i\eta y)} d\xi d\eta, \quad (2.19)$$

where:

$\bar{f}(s)$ = the Laplace transform of the source time function $f(t)$,

$$\xi_j^2 = b_j^2 + \xi^2 + \eta^2, \quad j = p, s,$$

$$b_j = 1/v_j, \quad j = p, s.$$

The three source functions S_P , S_V and S_H , which are related to the transformed Lamé potential functions in a full-space as shown in the preceding equations, are completely determined by the specified source mechanism, *i.e.*, the boundary conditions on the fault plane, and can be expressed as

$$\begin{pmatrix} S_P(\xi, \eta, s) \\ S_V(\xi, \eta, s) \\ S_H(\xi, \eta, s) \end{pmatrix} = \frac{1}{i\eta(i\xi + b)} \begin{pmatrix} 2i\xi \\ \frac{-i\xi(\xi_s^2 + \xi^2 + \eta^2)}{\epsilon\xi_s(\xi^2 + \eta^2)} \\ \frac{-ib_j^2\eta}{\xi^2 + \eta^2} \end{pmatrix}, \quad (2.20)$$

for a strike-slip fault, and

$$\begin{pmatrix} S_P(\xi, \eta, s) \\ S_V(\xi, \eta, s) \\ S_H(\xi, \eta, s) \end{pmatrix} = \frac{1}{i\eta(i\xi + b)} \begin{pmatrix} 2i\eta \\ \frac{-i\eta(\xi^2 + \xi^2 + \eta^2)}{\epsilon \xi_s(\xi^2 + \eta^2)} \\ \frac{ib_s^2 \xi}{\xi^2 + \eta^2} \end{pmatrix}, \quad (2.21)$$

for a dip-slip fault, in which $b = 1/v$ and $\epsilon = -\text{sgn}(z - z_0)$.

The displacement components are the spatial derivatives of the potential functions, *i.e.*,

$$u_x = \frac{\partial \phi}{\partial x} + \frac{\partial \chi}{\partial y} + \frac{\partial^2 \psi}{\partial x \partial z}, \quad (2.22)$$

$$u_y = \frac{\partial \phi}{\partial y} - \frac{\partial \chi}{\partial x} + \frac{\partial^2 \psi}{\partial y \partial z}, \quad (2.23)$$

$$u_z = \frac{\partial \phi}{\partial z} - \frac{\partial^2 \psi}{\partial x^2} - \frac{\partial^2 \psi}{\partial y^2}. \quad (2.24)$$

With Eqs. (2.17) through (2.19) and (2.22) through (2.24), the transformed displacement is

$$\begin{aligned} \bar{u}_i(x, y, z, s) = \frac{D_0 \bar{f}(s)}{8\pi^2 b_s^2} \int_{-\infty}^{\infty} \int_{-\infty}^{\infty} \left[S_P D_{u_i P} e^{-s\xi p} \right. \\ \left. + (S_V D_{u_i V} + S_H D_{u_i H}) e^{-s\xi z} \right] d\xi d\eta, \end{aligned} \quad (2.25)$$

where:

subscript $i = x, y$ or z ,

$D_{u_i J}$ = the receiver function, $J = P, V, H$,

$$g_j = \zeta_j |z - z_0| - i\xi x - i\eta y, \quad j = p, s.$$

The receiver functions relate the Lamé potentials to the desired responses at the field point in the full-space. The physical interpretation of Eq. (2.25) is that the transformed displacement at a receiver contains the three types of waves generated at the source multiplied by the corresponding receiver functions, which account for the wave propagation effects in the Fourier transform domain. The matrix form of Eq. (2.25) is

$$\begin{Bmatrix} \bar{u}_x(x, y, z, s) \\ \bar{u}_y(x, y, z, s) \\ \bar{u}_z(x, y, z, s) \end{Bmatrix} = \frac{D_0 \tilde{f}(s)}{8\pi^2 b_s^3} \int_{-\infty}^{\infty} \int_{-\infty}^{\infty} [D] \begin{Bmatrix} S_p(\xi, \eta, s) e^{-s g_p} \\ S_v(\xi, \eta, s) e^{-s g_s} \\ S_H(\xi, \eta, s) e^{-s g_s} \end{Bmatrix} d\xi d\eta, \quad (2.26)$$

in which the source functions are given in Eq. (2.20) or (2.21), and the receiver function matrix is

$$[D] = \begin{bmatrix} i\xi & i\xi \epsilon \zeta_s & i\eta \\ i\eta & i\eta \epsilon \zeta_s & -i\xi \\ \epsilon \zeta_p & \xi^2 + \eta^2 & 0 \end{bmatrix}. \quad (2.27)$$

2.2.2 Oblique Fault

In the above section, the source functions are obtained for a horizontal fault plane and the receiver functions are valid for waves propagating through an infinite medium. For waves propagating in a half-space, the free surface effect of the ground should be considered. If the ground surface is taken as horizontal, the source functions for an oblique fault is also needed.

Fig. 2.3 shows the coordinate system of the half-space, *i.e.*, (x, y, z) , and the

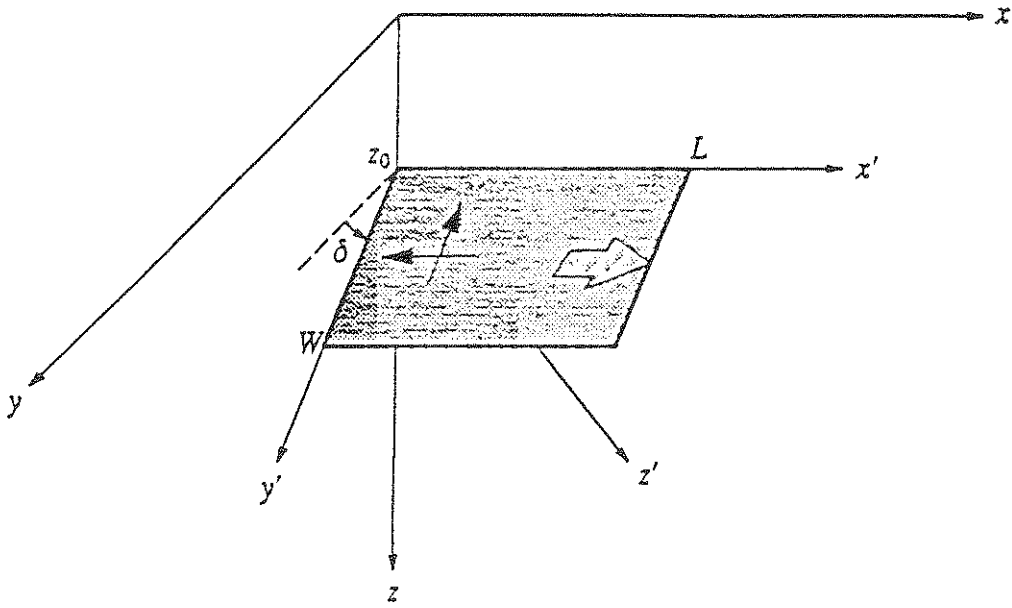


Figure 2.3 Coordinate Systems of Half-Space and Fault

fault, *i.e.*, (x', y', z') . The fault strikes in the x' -direction, and the dip angle δ is measured from the horizontal plane. The slips in the x' - and y' -directions represent the strike-slip and dip-slip motions, respectively.

The local coordinate system (x', y', z') can be transformed to the global coordinate system (x, y, z) through the following relation,

$$\begin{Bmatrix} x \\ y \\ z - z_0 \end{Bmatrix} = [T] \begin{Bmatrix} x' \\ y' \\ z' \end{Bmatrix}, \quad (2.28)$$

in which the coordinate transformation matrix $[T]$ is defined as

$$[T] = \begin{bmatrix} 1 & 0 & 0 \\ 0 & \cos \delta & -\sin \delta \\ 0 & \sin \delta & \cos \delta \end{bmatrix}. \quad (2.29)$$

The transforms for the displacements, in the global coordinates, are shown in Eq. (2.26). In the present case, however, the source functions are unknown.

The transforms for the ground motions, in terms of the local coordinates, are similar to Eq. (2.26), and may be expressed as follows,

$$\begin{Bmatrix} \bar{u}_x(x', y', z', s) \\ \bar{u}_y(x', y', z', s) \\ \bar{u}_z(x', y', z', s) \end{Bmatrix} = \frac{D_0 \bar{f}(s)}{8\pi^2 b_s^2} \int_{-\infty}^{\infty} \int_{-\infty}^{\infty} [D'] \begin{Bmatrix} S'_{p'}(\xi', \eta', s) e^{-i g'_p s} \\ S'_{v'}(\xi', \eta', s) e^{-i g'_s s} \\ S'_{H'}(\xi', \eta', s) e^{-i g'_s s} \end{Bmatrix} d\xi' d\eta', \quad (2.30)$$

in which $g'_j = \xi'_j |z'| - i \xi' x' - i \eta' y'$, $j = p, s$. The source and receiver functions are given in Eqs. (2.20) (or (2.21)) and (2.27), respectively, but with the global

coordinates (x, y, z) replaced by the local coordinates (x', y', z') , the global transform parameters (ξ, η, ζ) replaced by the local transform parameters (ξ', η', ζ') , and $\epsilon' = -\text{sgn}(z')$.

With the equivalent phase functions, *i.e.*, $g'_j = g_j$, $j = p, s$, the transform parameters are related also by

$$\begin{Bmatrix} i\xi \\ i\eta \\ \epsilon\zeta_j \end{Bmatrix} = [T] \begin{Bmatrix} i\xi' \\ i\eta' \\ \epsilon\zeta'_j \end{Bmatrix}. \quad (2.31)$$

The coordinate transformation matrix $[T]$ also gives

$$\begin{Bmatrix} \bar{u}_x \\ \bar{u}_y \\ \bar{u}_z \end{Bmatrix} = [T] \begin{Bmatrix} \bar{u}_{x'} \\ \bar{u}_{y'} \\ \bar{u}_{z'} \end{Bmatrix}. \quad (2.32)$$

Substituting Eqs. (2.26) and (2.30) into Eq. (2.32), the source functions corresponding to a general fault with an arbitrary dip angle δ are determined by

$$[D] \begin{Bmatrix} S_P e^{-s\delta p} \\ S_V e^{-s\delta s} \\ S_H e^{-s\delta s} \end{Bmatrix} = [T] [D'] \begin{Bmatrix} S'_P e^{-s\delta' p} J_p \\ S'_V e^{-s\delta' s} J_s \\ S'_H e^{-s\delta' s} J_s \end{Bmatrix}, \quad (2.33)$$

in which J_j is the Jacobian

$$J_j(\xi', \eta'; \xi, \eta) = \begin{vmatrix} \frac{\partial \xi'}{\partial \xi} & \frac{\partial \xi'}{\partial \eta} \\ \frac{\partial \eta'}{\partial \xi} & \frac{\partial \eta'}{\partial \eta} \end{vmatrix} = \frac{\epsilon' \zeta'_j}{\epsilon \zeta_j}. \quad (2.34)$$

After lengthy manipulation of Eq. (2.33), the source functions for an oblique Haskell fault can be given as follows:

$$\begin{pmatrix} S_P \\ S_V \\ S_H \end{pmatrix} = \frac{1}{i\eta'(i\xi' + b)} \left[\begin{pmatrix} \frac{2\xi\eta}{\epsilon\zeta_p} \\ \frac{-2\xi\eta}{\xi^2 + \eta^2} \\ \frac{b_i^2(\xi^2 - \eta^2)}{\epsilon\zeta_s(\xi^2 + \eta^2)} \end{pmatrix} \sin \delta + \begin{pmatrix} 2i\xi \\ \frac{-i\xi(\zeta_s^2 + \xi^2 + \eta^2)}{\epsilon\zeta_s(\xi^2 + \eta^2)} \\ \frac{-ib_i^2\eta}{\xi^2 + \eta^2} \end{pmatrix} \cos \delta \right], \quad (2.35)$$

for a strike-slip fault; and

$$\begin{pmatrix} S_P \\ S_V \\ S_H \end{pmatrix} = \frac{1}{i\eta'(i\xi' + b)} \left[\begin{pmatrix} \frac{\zeta_p^2 + \eta^2}{\epsilon\zeta_p} \\ \frac{\xi^2 + 2\eta^2}{\xi^2 + \eta^2} \\ \frac{b_i^2\xi\eta}{\epsilon\zeta_s(\xi^2 + \eta^2)} \end{pmatrix} \sin 2\delta + \begin{pmatrix} 2i\eta \\ \frac{-i\eta(\zeta_s^2 + \xi^2 + \eta^2)}{\epsilon\zeta_s(\xi^2 + \eta^2)} \\ \frac{b_i^2\xi}{\xi^2 + \eta^2} \end{pmatrix} \cos 2\delta \right], \quad (2.36)$$

for a dip-slip fault.

To determine the ground motions excited by a wave propagating through a half-space, the boundary conditions at the free surface, *i.e.*, $\tau_{zx} = \tau_{zy} = \tau_{zz} = 0$ at $z = 0$, should be considered in determining the receiver functions. The resulting receiver function matrix is modified as

$$[D^*] = \begin{bmatrix} i\xi + i\xi R^{PP} - i\xi\zeta_s R^{PV} & i\xi\zeta_s - i\xi\zeta_s R^{VV} + i\xi R^{VP} & 2i\eta \\ i\eta + i\eta R^{PP} - i\eta\zeta_s R^{PV} & i\eta\zeta_s - i\eta\zeta_s R^{VV} + i\eta R^{VP} & -2i\xi \\ \zeta_p - \zeta_p R^{PP} + (\xi^2 + \eta^2) R^{PV} & (\xi^2 + \eta^2) + (\xi^2 + \eta^2) R^{VV} - \zeta_p R^{VP} & 0 \end{bmatrix}, \quad (2.37)$$

in which R^{PP} , R^{PV} , R^{VP} , and R^{VV} are the reflection coefficients, which represent

the ratios of the amplitudes of the reflected waves to those of the respective incident waves.

In Eq. (2.37), each element in the receiver function matrix contains contributions from both the incident and reflected waves. For example, as shown in Fig. 2.4, when a P-wave is generated at the source, the incident P-wave, the reflected P-wave and the reflected SV-wave are all detected at the receiver, and assembled in the first element in Eq. (2.37). For the reflected waves, the degree of contribution to the displacement component at the receiver is determined by the reflection coefficients and the original receiver functions, *i.e.*, Eq. (2.27), which are associated with the type of wave arriving at the receiver. By substituting the reflection coefficients in terms of the transform parameters, the modified receiver function matrix is then expressed as

$$[D^*] = \frac{1}{R} \begin{bmatrix} -4ib_s^2 \xi \zeta_p \zeta_s & -2ib_s^2 \xi \zeta_s (\zeta_s^2 + \xi^2 + \eta^2) & 2i\eta R \\ -4ib_s^2 \eta \zeta_p \zeta_s & -2ib_s^2 \eta \zeta_s (\zeta_s^2 + \xi^2 + \eta^2) & -2i\xi R \\ -2b_s^2 \zeta_p (\zeta_s^2 + \xi^2 + \eta^2) & -4b_s^2 \zeta_p \zeta_s (\xi^2 + \eta^2) & 0 \end{bmatrix}, \quad (2.38)$$

where the Rayleigh function is

$$R = 4\zeta_p \zeta_s (\xi^2 + \eta^2) - (\zeta_s^2 + \xi^2 + \eta^2)^2. \quad (2.39)$$

Finally, the transforms for the ground motions excited by an oblique dislocation fault are

$$\begin{Bmatrix} \bar{u}_x(x, y, 0, s) \\ \bar{u}_y(x, y, 0, s) \\ \bar{u}_z(x, y, 0, s) \end{Bmatrix} = \frac{D_0 \tilde{f}(s)}{8\pi^2 b_s^2} \int_{-\infty}^{\infty} \int_{-\infty}^{\infty} [D^*] \begin{Bmatrix} S_P(\xi, \eta, s) e^{-s\beta p} \\ S_V(\xi, \eta, s) e^{-s\xi s} \\ S_H(\xi, \eta, s) e^{-s\xi s} \end{Bmatrix} d\xi d\eta. \quad (2.40)$$

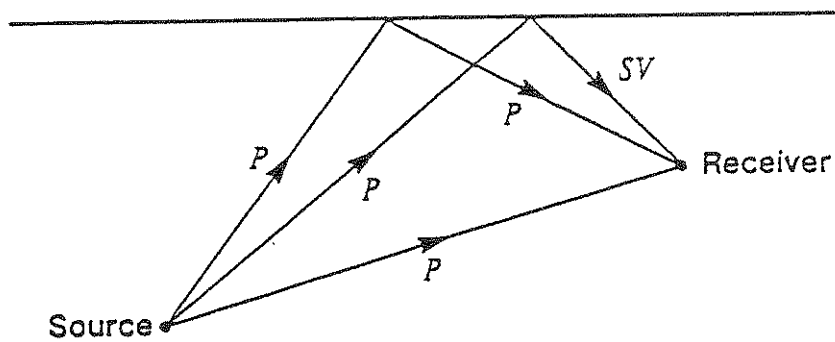


Figure 2.4 Incident and Reflected Waves at a Receiver

Substituting Eqs. (2.35), (2.36) and (2.38) into Eq. (2.40), the transforms for the displacements become

$$\{\bar{u}(x, y, 0, s)\} = \frac{D_0 \vec{f}(s)}{8\pi^2} \sum_{j=p, s} \int_{-\infty}^{\infty} \int_{-\infty}^{\infty} \{F_j\} \frac{e^{-s(\zeta_j z_0 - i\xi x - i\eta y)}}{(i\xi + b)(i\eta \cos \delta + \zeta_j \sin \delta)R} d\xi d\eta, \quad (2.41)$$

where the vectors $\{F_j\}$, $j = p, s$, are summarized in Appendix A.

Inversion of the Laplace transform, Eq. (2.41), is necessary to obtain the ground motions in the time domain.

SECTION 3

ANALYTICAL GROUND MOTIONS IN TIME DOMAIN

3.1 Introduction

In the previous Section, Eq. (2.41) gives the Laplace transform for the analytical ground motions. To obtain the responses in the time domain, a special inverse transform method is needed. An effective method for this purpose is the Cagniard technique (Cagniard, 1962). The main idea of the Cagniard technique is to assign the phase function in Eq. (2.41) to the time variable t and then invert the Laplace transform by direct inspection. A transformation was introduced by de Hoop (1960) to simplify the Cagniard technique when two transform parameters, *e.g.*, ξ and η in Eq. (2.41), are involved. In fact, the assignment of g_p or g_s to t represents a hyperbola, which is called the Cagniard path, in a complex plane after the de Hoop transformation has been employed, and constitutes a contour including the original integral path in Eq. (2.41). In addition to the Cagniard path, the contributions from the poles within the contour and from the branch cut should be included in evaluating the integral of Eq. (2.41) by the residue theorem. The exact inversion contains a sum of single integrals and algebraic terms. Each term contributing to the ground motion is identified as a specific wave.

Consider a general term in Eq. (2.41),

$$U(x, y, 0, s) = \frac{D_0}{8\pi^2} \sum_{j=p,s} \int_{-\infty}^{\infty} \int_{-\infty}^{\infty} \frac{F_j e^{-s(\zeta_j z - i\xi z - i\eta y)}}{(i\xi + b)(i\eta \cos \delta + \zeta_j \sin \delta)R} d\xi d\eta, \quad (3.1)$$

where F_j is one element in Appendix A and the Rayleigh function R is given in Eq. (2.39). After applying the de Hoop transformation,

$$\begin{cases} \xi = i\sigma \cos \theta - q \sin \theta, \\ \eta = i\sigma \sin \theta + q \cos \theta, \end{cases} \quad (3.2)$$

in which $\cos \theta = x/r$, $\sin \theta = y/r$, and $r^2 = x^2 + y^2$, Eq. (3.1) becomes

$$\bar{U}(x, y, 0, s) = \frac{D_0}{8\pi^2} \sum_{j=p,s} \int_{-\infty}^{\infty} \left[\int_{-i\infty}^{i\infty} \frac{(-i) F_j e^{-s(\zeta_j z_0 + \sigma r)}}{(i\xi + b)(i\eta \cos \delta + \zeta_j \sin \delta)R} d\sigma \right] dq. \quad (3.3)$$

The mapping of $\zeta_j z_0 + \sigma r$ to t represents the Cagniard paths $\Sigma_{\pm p}$ or $\Sigma_{\pm s}$ in the complex σ -plane, as shown in Fig. 3.1. Also shown in Fig. 3.1 are the branch cuts, the branch points, and the poles. By the residue theorem, the integration of Eq. (3.3), which is taken along the imaginary axis of the complex σ -plane, is replaced by the integration along the Cagniard path plus the contributions from any poles within the contour. No contributions from the circular paths $C_{\pm p}$ or $C_{\pm s}$ are included as their radii tend to infinity. Two possible poles, σ_1 and σ_2 in Fig. 3.1, are located inside the contour. They are the roots of $i\xi + 1/\nu = 0$ and $i\eta \cos \delta + \zeta_j \sin \delta = 0$, respectively.

3.2 Inverse Laplace Transform

3.2.1 Cagniard Path Contribution

Let $\bar{U}_1(x, y, 0, s)$ be the contribution from the Cagniard paths, *i.e.*,

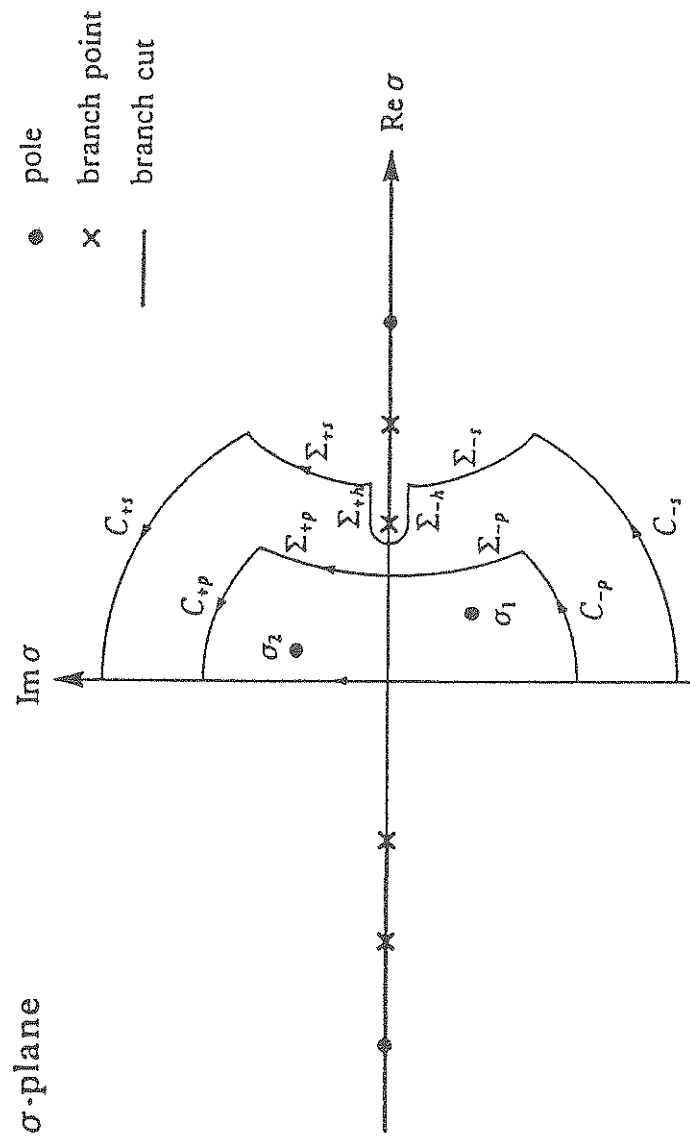


Figure 3.1 Poles and Cagniard Paths in Complex σ -Plane

$$\bar{U}_1(x, y, 0, s) = \frac{D_0}{8\pi^2} \sum_{j=p,s} \int_{-\infty}^{\infty} \left[\int_{\Sigma_{\pm j}} \frac{(-i) F_j \frac{d\sigma_j}{dt}}{(i\xi + b)(i\eta \cos \delta + \zeta_j \sin \delta)R} e^{-st} dt \right] dq. \quad (3.4)$$

After interchanging the order of integration, the inverse Laplace transform of \bar{U}_1 could be determined by directly inspecting the integrand. $U_1(x, y, 0, t)$ is a proper single integral with respect to q , and its exact formulation is listed in Eq. (B.1).

3.2.2 Branch Cut Contribution

If the vertex of the hyperbola, $\Sigma_{\pm s}$, is located on the right side of the branch point associated with the P-wave, the Cagniard path $\Sigma_{\pm s}$ must be indented around the branch cut, *i.e.*, $\Sigma_{\pm h}$, as shown in Fig. 3.1. This case occurs when $r/R_0 > b_p/b_s$, and constitutes the other type of wave, namely head wave or SP-wave. Let $\bar{U}_{1h}(x, y, 0, s)$ denote the contribution from this indented path, *i.e.*,

$$\bar{U}_{1h}(x, y, 0, s) = \frac{D_0}{8\pi^2} \sum_{j=p,s} \int_{-\infty}^{\infty} \left[\int_{\Sigma_{\pm h}} \frac{(-i) F_j \frac{d\sigma_h}{dt}}{(i\xi + b)(i\eta \cos \delta + \zeta_s \sin \delta)R} e^{-st} dt \right] dq. \quad (3.5)$$

The interchange of the order of the integration is also needed to take the inverse transform. The exact form of $U_{1h}(x, y, 0, t)$ is described in Eq. (B.2).

3.2.3 Pole Contribution

Let $\bar{U}'_2(x, y, 0, s)$ and $\bar{U}'_3(x, y, 0, s)$ be the contributions from the poles σ_1 and σ_2 , respectively. For the pole σ_1 being inside the contour shown in Fig. 3.1, it is required that $x > 0$ and $q^2 > q_{\sigma_1}^2$ in which

$$q_{\sigma_j} = \frac{z_0}{r\sqrt{y^2 + z_0^2}} \sqrt{\frac{R_0^2}{v^2} - x^2 b_j^2}, \quad R_0^2 = x^2 + y^2 + z_0^2.$$

Then, the contribution from the pole σ_1 is

$$\begin{aligned} \bar{U}'_2(x, y, 0, s) = \frac{D_0}{8\pi^2} H(x) \sum_{j=p,s} \left[\int_{-\infty}^{-q_{\sigma_j}} (-2\pi i) \frac{(-i) F_j e^{-s(\zeta_j z_0 + \sigma_1 r)}}{\left(\frac{-x}{r}\right)(i\eta \cos \delta + \zeta_j \sin \delta)R} dq \right. \\ \left. + \int_{q_{\sigma_j}}^{\infty} (-2\pi i) \frac{(-i) F_j e^{-s(\zeta_j z_0 + \sigma_1 r)}}{\left(\frac{-x}{r}\right)(i\eta \cos \delta + \zeta_j \sin \delta)R} dq \right]. \quad (3.6) \end{aligned}$$

Let $q = i\alpha$ and apply the Cagniard method again to obtain $U'_2(x, y, 0, t)$. Fig. 3.2 shows the Cagniard path $A_{\pm j}$ corresponding to the mapping of $\zeta_j z_0 + \sigma_1 r = t$, the associated poles, the branch points, and the branch cuts in the complex α -plane for $y > 0$ and $v < c_s$. For $y < 0$, the contours are located in the left-half of α -plane. In the case of the subsonic rupture, *i.e.*, $v < c_s$, no contributions from the poles and the branch cuts are involved when the integration paths of Eq. (3.6) is replaced by the Cagniard paths $A_{\pm j}$ because no poles are located inside the contour and no branch cuts intersect the Cagniard paths, as shown in Fig. 3.2. For the transonic and supersonic ruptures, the contributions from the branch cuts should be considered. The complete representation of $U_2(x, y, 0, t)$, *i.e.*, the contributions from the Cagniard paths $A_{\pm p}$ and $A_{\pm s}$, and $U_{2h}(x, y, 0, t)$, *i.e.*, the contributions from the branch cuts, are listed in Eqs. (B.3) and (B.4), respectively.

The necessary condition for the pole σ_2 lying within the contour shown in Fig. 3.1 is that $y > 0$ and $y' > 0$. Therefore, the contribution from the pole σ_2 is

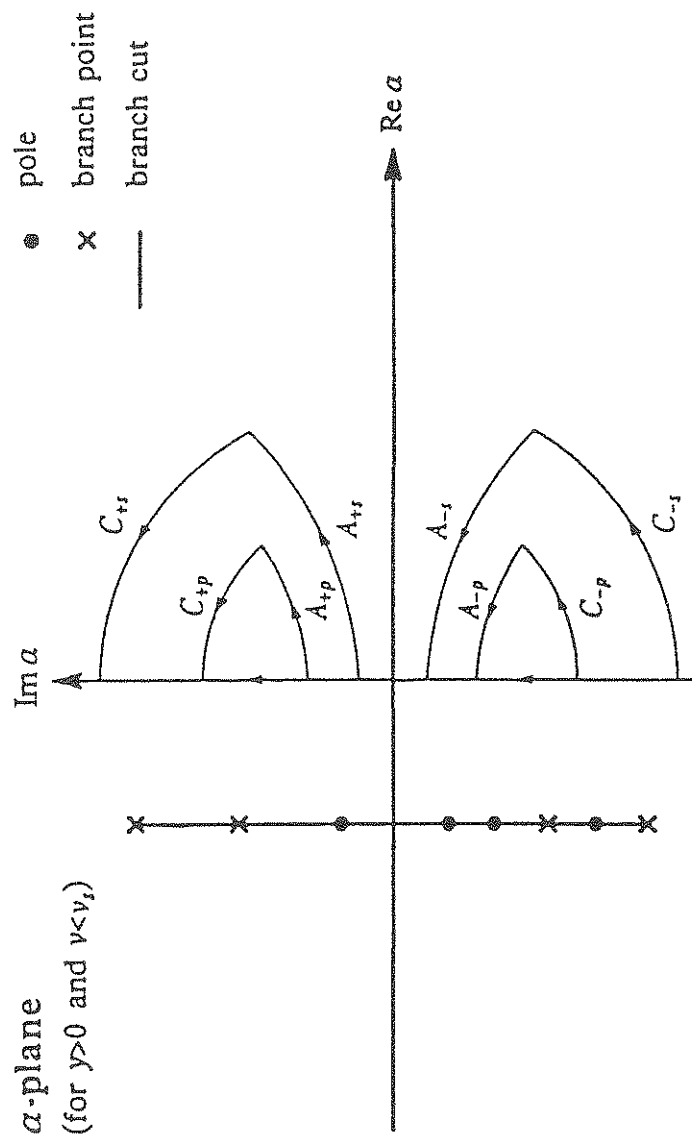


Figure 3.2 Poles and Cagniard Paths in Complex α -Plane

$$U_3'(x, y, 0, s) = \frac{D_0}{8\pi^2} H(y)H(y') \sum_{j=p, s}^{\infty} \int_{-\infty}^{\infty} (-2\pi i) \frac{(-i) F_j e^{-s(\xi_j z_0 + \sigma_2 r)}}{(i\xi_j + b) (-G_j) R} dq, \quad (3.7)$$

where

$$G_j = \frac{\sigma_2 \sin \delta + \xi_j \sin \theta \cos \delta}{\xi_j}.$$

Let $q = -i\beta$ and apply the Cagniard method once more. Fig. 3.3 shows the Cagniard paths $B_{\pm j}$ associated with the mapping of $\xi_j z_0 + \sigma_2 r = t$ in the complex β -plane for $x > 0$. The Cagniard path $B_{\pm r}$, the indented path $B_{\pm h}$, and the corresponding branch cuts are shown in Fig. 3.3(b) only for the case of $b_p/b_s > \sin \delta / \sqrt{1 - \cos^2 \theta \cos^2 \delta}$. The various contributions from the indented path $B_{\pm h}$ for other cases will be included in the final formulation. Let $U_3(x, y, 0, t)$ and $U_{3h}(x, y, 0, t)$ denote the ground motions from the Cagniard path $B_{\pm r}$ and the indented path $B_{\pm h}$, respectively. These formulations are listed in Eqs. (B.5) and (B.6), respectively.

3.3 Analytical Formulation

From the preceding sections, the ground displacement in a specific direction, *i.e.*, the inverse Laplace transform of Eq. (3.1), can be evaluated as

$$U(x, y, 0, t) = U_1 + U_{1h} + U_2 + U_{2h} + U_3 + U_{3h}. \quad (3.8)$$

Each term in Eq. (3.8) is expressed explicitly in Appendix B.

Similar results have also been obtained by Yeh, *et al.* (1988) and Wang (1988). Comparing Eq. (2.41) with Eq. (3.1), the transform for the ground

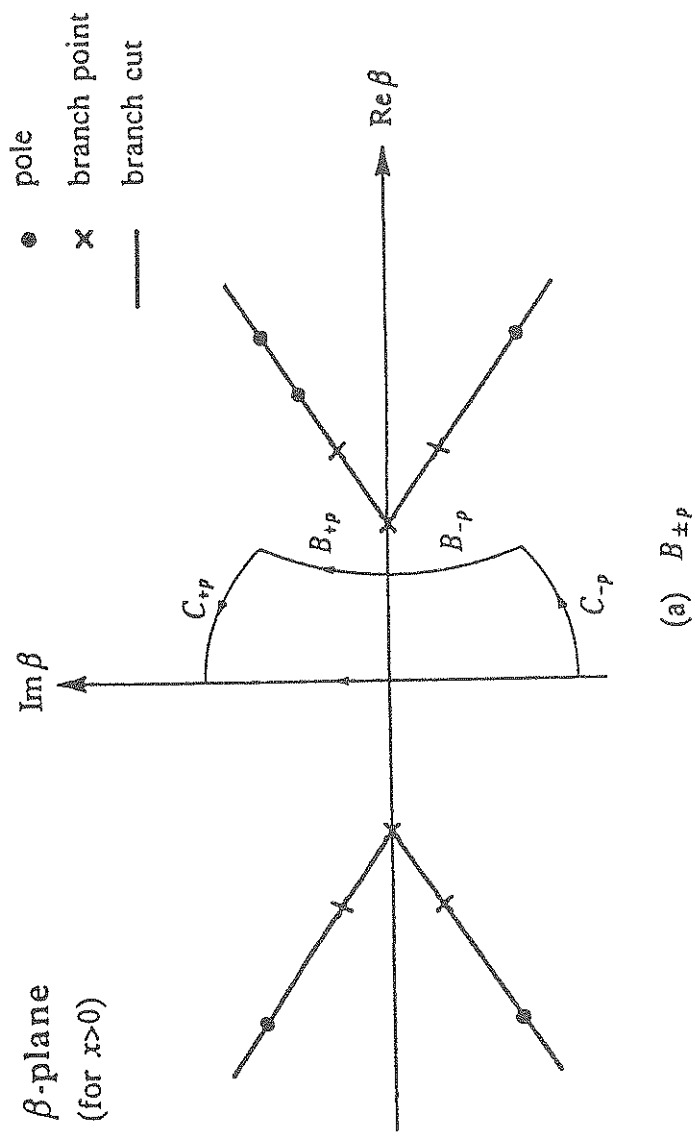
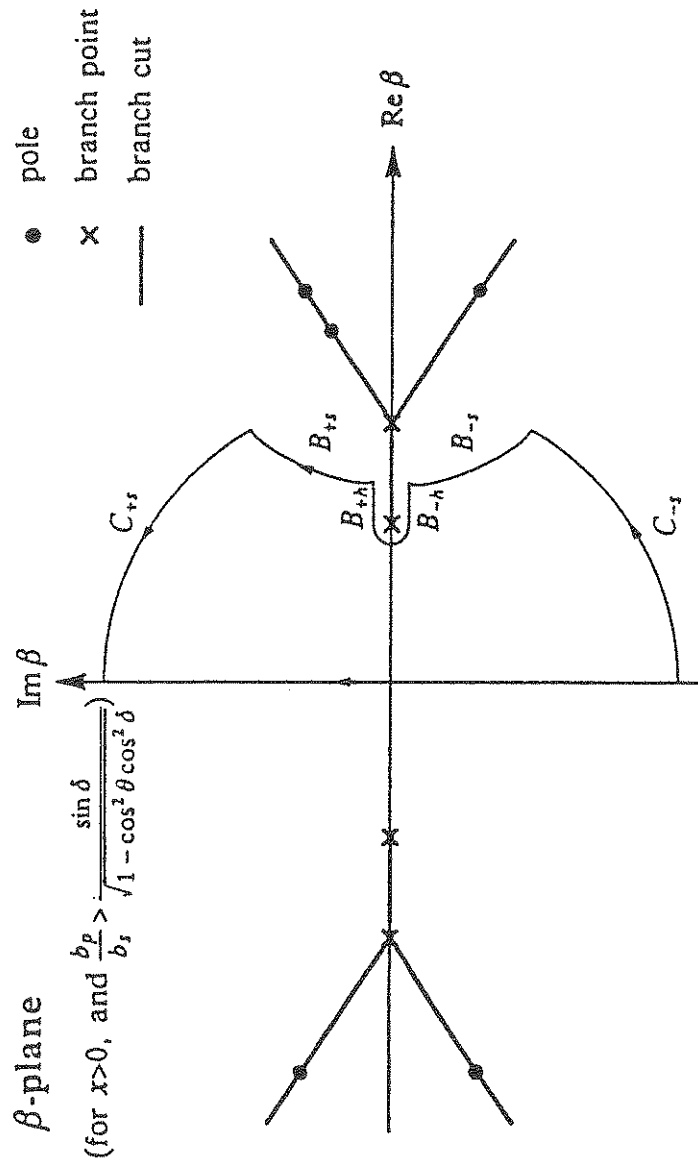


Figure 3.3 Poles and Cagniard Paths in Complex β -Plane



(b) $B_{\pm s}$ and $B_{\pm h}$

Figure 3.3 Poles and Cagniard Paths in Complex β -Plane

(cont'd)

displacement in the i -direction is given by

$$\bar{u}_i(x, y, 0, s) = \tilde{f}(s) \bar{U}(x, y, 0, s). \quad (3.9)$$

Therefore,

$$u_i(x, y, 0, t) = \int_0^t f(t - \tau) U(x, y, 0, \tau) d\tau, \quad (3.10)$$

in which $f(t - \tau)$ is the source time function and $U(x, y, 0, \tau)$ is given by Eq. (3.8). Two special cases of the source time function can be identified, for which the ground motions may be obtained directly from Eq. (3.8) without the convolution integral of Eq. (3.10).

(1) Step-time source function:

$$f(t) = H(t). \quad (3.11)$$

The Laplace transform of such a source time function is

$$\tilde{f}(s) = \frac{1}{s}, \quad (3.12)$$

Then, from Eq. (3.9),

$$\dot{u}_i(x, y, 0, t) = U(x, y, 0, t), \quad (3.13)$$

where $\dot{u}_i(x, y, 0, t)$ is the ground velocity in the i -direction.

(2) Linear ramp-time source function:

$$f(t) = \begin{cases} 0, & t \leq 0; \\ t/T_r, & 0 < t < T_r; \\ 1, & T_r \leq t; \end{cases} \quad (3.14)$$

in which T_r is the rise time. In this case,

$$\tilde{f}(s) = \frac{1 - e^{-sT_r}}{T_r s^2}, \quad (3.15)$$

and

$$\ddot{u}_i(x, y, 0, t) = \frac{U(x, y, 0, t) - H(t - T_r) U(x, y, 0, t - T_r)}{T_r}, \quad (3.16)$$

where $\ddot{u}_i(x, y, 0, t)$ is the ground acceleration in the i -direction.

Eq. (3.10) gives the ground motion only for one quadrantal dislocation, as shown in Fig. 2.2. The total ground motion generated by an oblique rectangular fault is given by

$$\begin{aligned} u_i^T(x, y, 0, t) = & u_i(x, y, 0, t; z_0) - u_i(x, y - W \cos \delta, 0, t; z_0 + W \sin \delta) \\ & - H(t - T_0) u_i(x - L, y, 0, t - T_0; z_0) \\ & + H(t - T_0) u_i(x - L, y - W \cos \delta, 0, t - T_0; z_0 + W \sin \delta), \end{aligned} \quad (3.17)$$

where $u_i^T(x, y, 0, t)$ is the total ground displacement in the i -direction and $u_i(x, y, 0, t; z_0)$ is given by Eq. (3.10).

The rupture is assumed to propagate unilaterally along the fault plane, as indicated in Eq. (3.17). However, the principle of superposition may be applied for the case of a bilaterally propagating rupture. Furthermore, the generalized ray theory can be extended systematically to analyze the ground responses excited by a

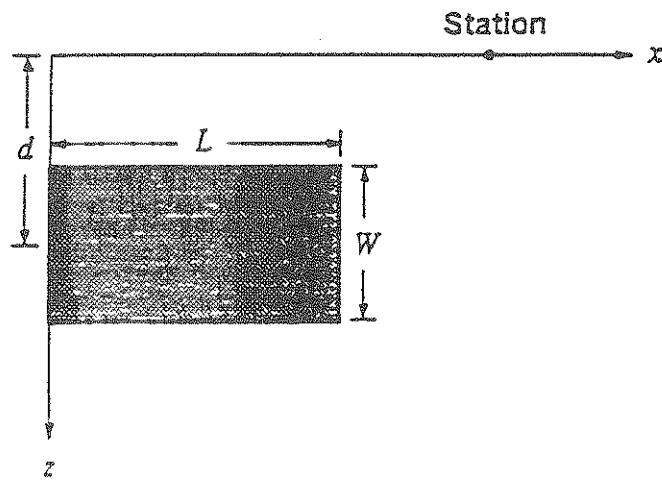
dislocation fault in a layered medium. The validity of the analytical ground motions is examined in the following case studies.

3.4 Case Studies

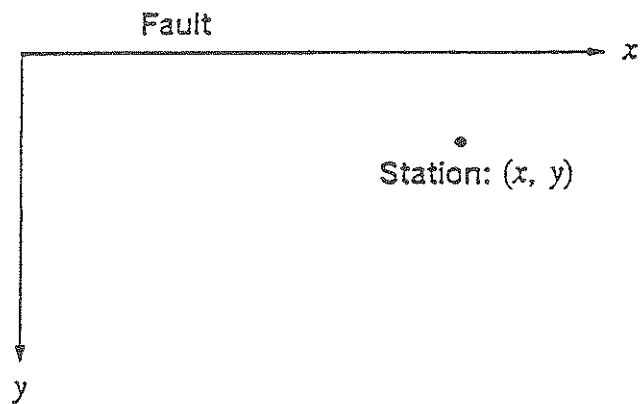
In order to investigate the difference between the ground motions obtained by the half- and full-space models, Anderson (1976) examined the ground displacements induced by a shallow vertical fault with either a strike-slip or dip-slip rupture using the method of Green's function. With this method, a four-fold integral must be evaluated approximately by a numerical method. One integral is associated with the formulation of the Green's functions which are applicable to a point source as developed by Johnson (1974) with the Cagniard-de Hoop method. The other triple integration comes from the Knopoff-de Hoop representation theorem (Burridge and Knopoff, 1964) for evaluating the response through the convolution of the dislocation and the Green's functions with respect to one temporal variable and two spatial variables.

In Anderson's quadrature, several schemes were applied to reduce the random and systematic errors, that may be introduced from the multiple numerical integration. In contrast, only single integrals are needed in the current study, as shown in Eqs. (B.1) and (B.2). Therefore, the numerical evaluation in this study should greatly reduce the numerical work and increase the accuracy of the results relative to those of Anderson (1976). Moreover, $U_{2h} = U_3 = U_{3h} = 0$ in Eq. (3.8) for the case of a vertical rupture with subsonic rupture motion.

To appraise the correctness of the analytic formulation developed in the present study, two cases from Anderson (1976) are used for comparison. The schematic diagram of the station and the fault is shown in Fig. 3.4. In each case,



(a) Side View



(b) Plan View

Figure 3.4 Vertical Fault and Ground Station

two sets of ground displacements are evaluated for strike-slip and dip-slip motions, respectively. Linear ramp-time source function and unilateral rupture are assumed in both cases. The common values of the parameters are as follows:

P-wave velocity	$v_p = 6$ km/sec,
S-wave velocity	$v_s = 3.4$ km/sec,
Fault length	$L = 5$ km,
Rupture velocity	$v = 3$ km/sec,
Final dislocation	$D_0 = 1$ cm,
Rise time	$T_r = 1$ sec,
Station	$(x, y) = (7.5$ km, 1.5 km).

Two different cases are examined with the following parameters:

Case I:

Fault width	$W = 3.3$ km,
Focal depth	$d = 3.8$ km,

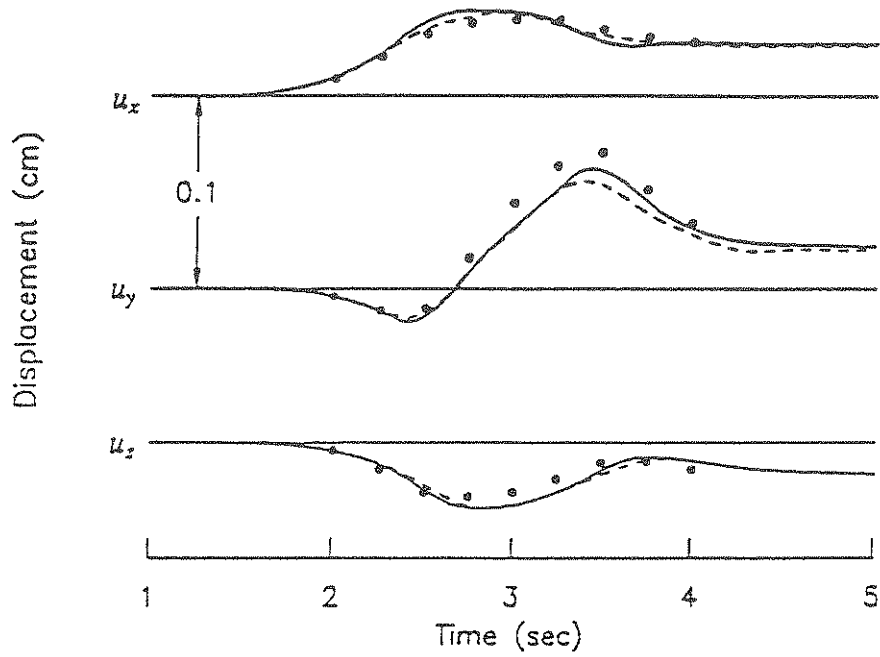
Case II:

Fault width	$W = 1.2$ km,
Focal depth	$d = 1.1$ km.

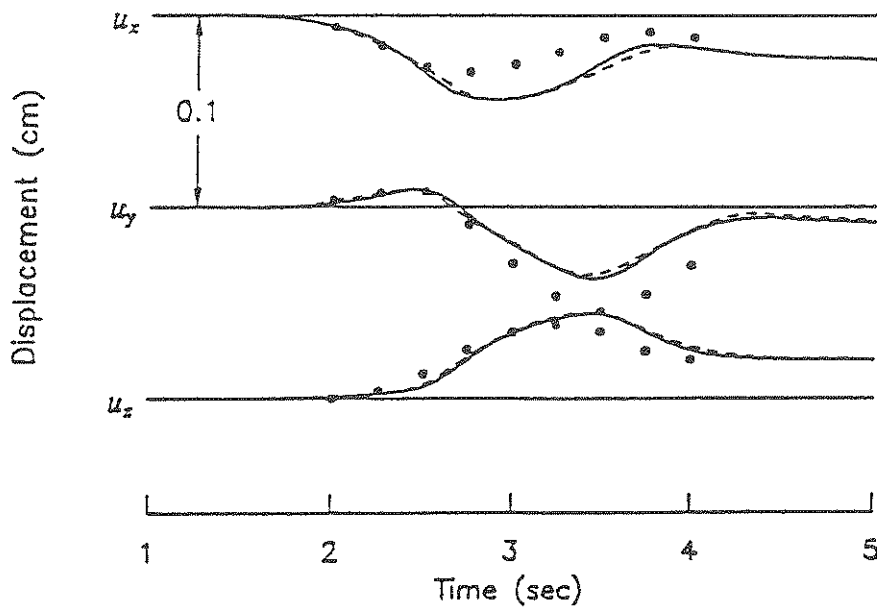
An epicentral distance of 7.65 km is the same in both cases, whereas Case II represents a shallow earthquake, in which the surface wave is dominant.

The comparisons are shown in Figs. 3.5 and 3.6, which demonstrate good agreement between the two studies for different response components, types of rupture, and fault locations. As mentioned in Section 2.1, the response of a full-space was doubled to approximately account for the free surface effect. This

• Anderson's Solution (doubled full-space)
 - - - Anderson's Solution (half-space) — Present Model



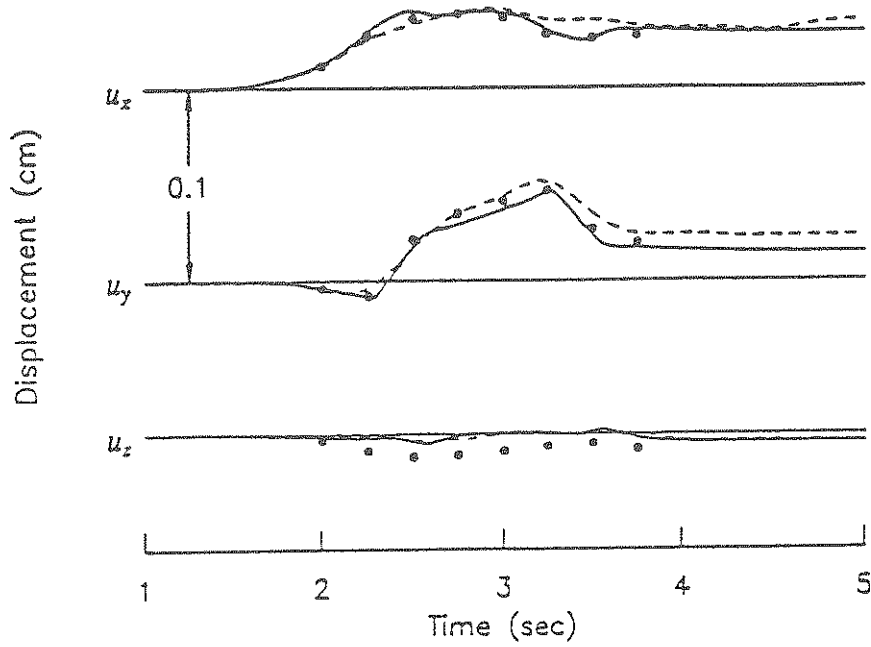
(a) Strike-slip Fault



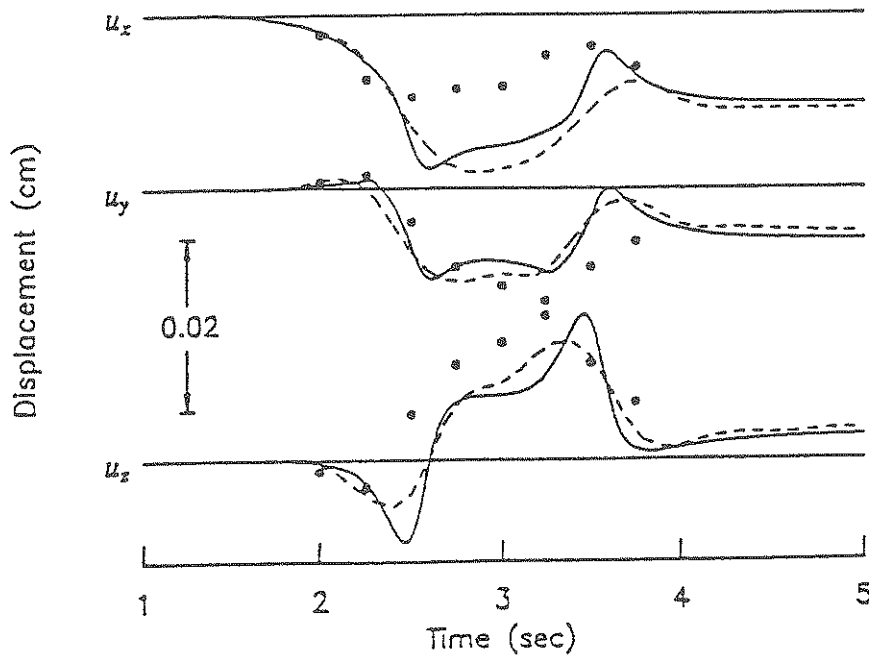
(b) Dip-slip Fault

Figure 3.5 Displacements in Case I

• Anderson's Solution (doubled full-space)
 - - - Anderson's Solution (half-space) — Present Model



(a) Strike-slip Fault

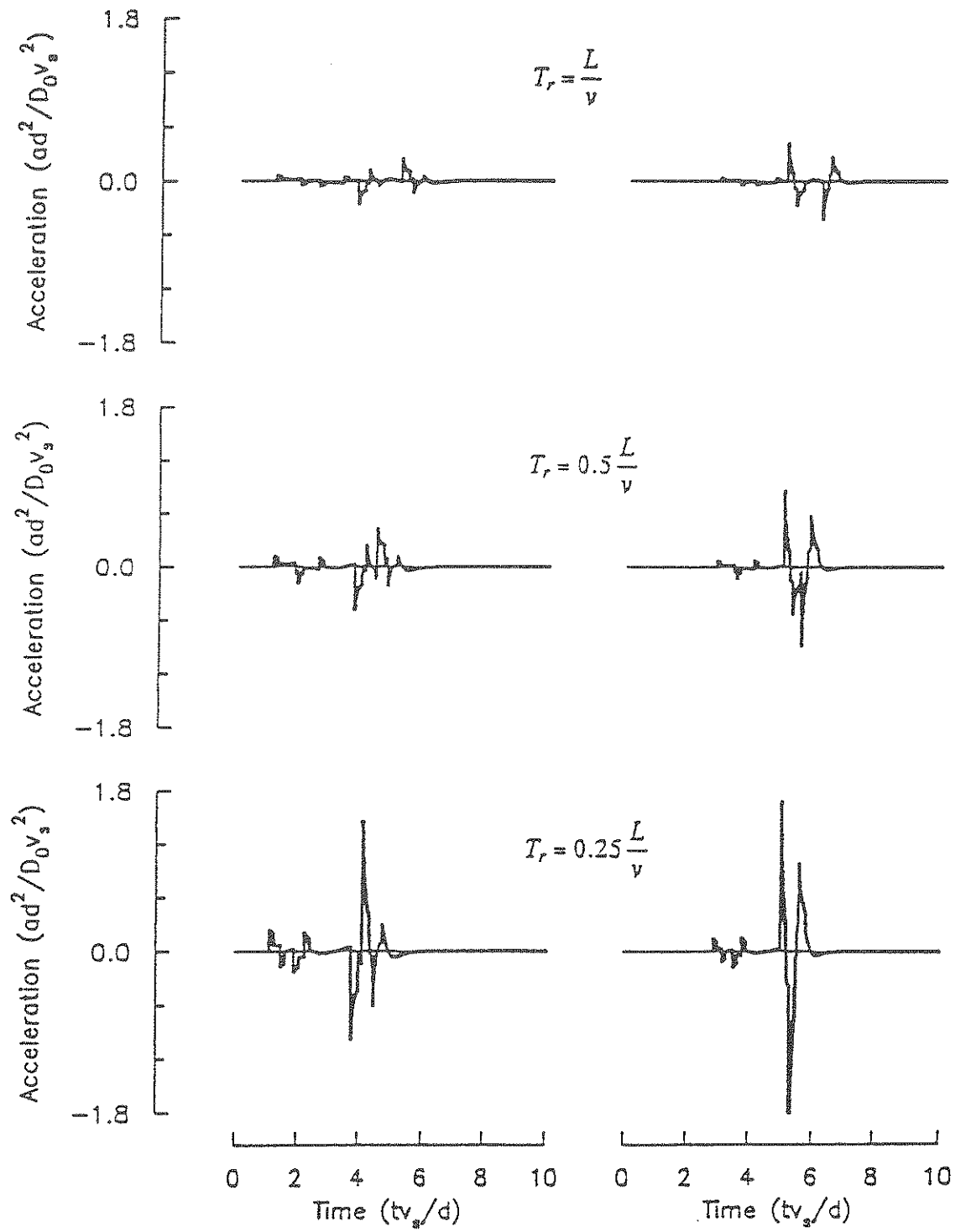


(b) Dip-slip Fault

Figure 3.6 Displacements in Case II

approximation is not valid especially for a shallow dip-slip fault, as shown in Figs. 3.5 and 3.6.

The effect of rise time — The rise time, T_r , to reach the final slip at each point in a fault plane during an earthquake is probably the parameter most difficult to estimate. To investigate its effect, consider a vertical square fault with strike-slip motion. For simplicity, the fault length L and width W are assumed to be equal to the focal depth d . A station is located at a distance of $5d$ from the epicenter, and the epicentral direction is 30° from the fault orientation. Three different values of the rise time, *i.e.*, $T_r = L/v$, $0.5L/v$ and $0.25L/v$, were examined. The P-wave velocity v_p is $\sqrt{3}v_s$, corresponding to Poisson's ratio of 0.25, and a rupture velocity of $v = 0.9v_s$ is assumed. The results are shown in Fig. 3.7, where the non-dimensional ground accelerations, $ad^2/D_0v_s^2$, along and normal to the strike direction versus the non-dimensional time, tv_s/d , are plotted, in which a is the ground acceleration and D_0 is the final slip. From Fig. 3.7, it can be seen that as the rise time decreases, the duration also decreases whereas the peak acceleration increases. For the limit case of $T_r = 0$, *i.e.*, the case of step-time source function, large values of the ground acceleration occur when the dominant waves, usually the S-waves, arrive.



(a) Along Strike Direction (b) Normal to Strike Direction

Figure 3.7 Accelerations for Different Rise Times

SECTION 4

ANALYSIS OF SEISMIC GROUND MOTIONS

4.1 Deterministic Analysis

4.1.1 The Event 5

On January 29, 1981 a large earthquake occurred off the northeastern coast of Taiwan. This event, cataloged as Event 5, was felt throughout Taiwan and triggered all 27 strong motion recorders in the SMART-1 array located 30.2 km NNW of the epicenter. The peak acceleration of 0.24 g is the largest acceleration recorded by the array during its first four years of operation. This event was selected for comparison because its focal mechanism has been well described (*e.g.*, Abrahamson, 1985). It is probably the event, among other events in the SMART-1 array, in which most information at the focus has been estimated. In fact, it is also the event whose recordings have most frequently been analyzed by other investigators.

The seismic source of Event 5, at a depth of 25.2 km, had a reverse mechanism with unilateral rupture propagating almost from east to west. The local magnitude was estimated by the Institute of Earth Sciences to be $M_L = 6.3$, whereas Abrahamson (1985) corrected it to $M_L = 6.7$ by using the Taiwan attenuation curve, instead of Richter's attenuation curve for Southern California.

Among the 27 stations, the recordings of 7 stations, whose alignment (N17.5°W) is closest to the epicentral direction (N26.2°W) to the central station

C00, will be used for analysis. Fig. 4.1 shows these seven stations in the array. The accelerograms at these stations along and normal to the epicentral direction are plotted in Figs. 4.2 and 4.3, respectively, and are aligned according to increasing epicentral distance and absolute time for these seven stations. By investigating the recordings in Figs. 4.2 and 4.3, no obvious attenuating phenomenon across these stations is observed and the oscillating patterns of these recordings are quite different, from which it is indicated that the local soil effect (*i.e.*, soil amplification) plays an important role on the measured ground accelerations.

4.1.2 Model Parameters

The parameters for this event were estimated primarily based on the study of Abrahamson (1985), supplemented by other empirical relations as necessary.

Velocity structure — The S-wave velocity is approximately 3.5 km/sec in the source region (Abrahamson, 1985). No estimate of the P-wave velocity at the source is available. However, with the assumption of equal Lamé constants, it is suggested that

$$v_p = \sqrt{3} v_s = 6.1 \text{ km/sec.}$$

This value is slightly less than that determined by Roecker, *et al.* (1987) based on a set of 1600 events dispersed throughout the island of Taiwan.

Fault plane orientation — Based on the first motion data of the mainshock and 18 aftershocks to form the group focal plane solutions, Abrahamson (1985) concluded that the nodal plane with mean strike of N71.2°W and mean dip of

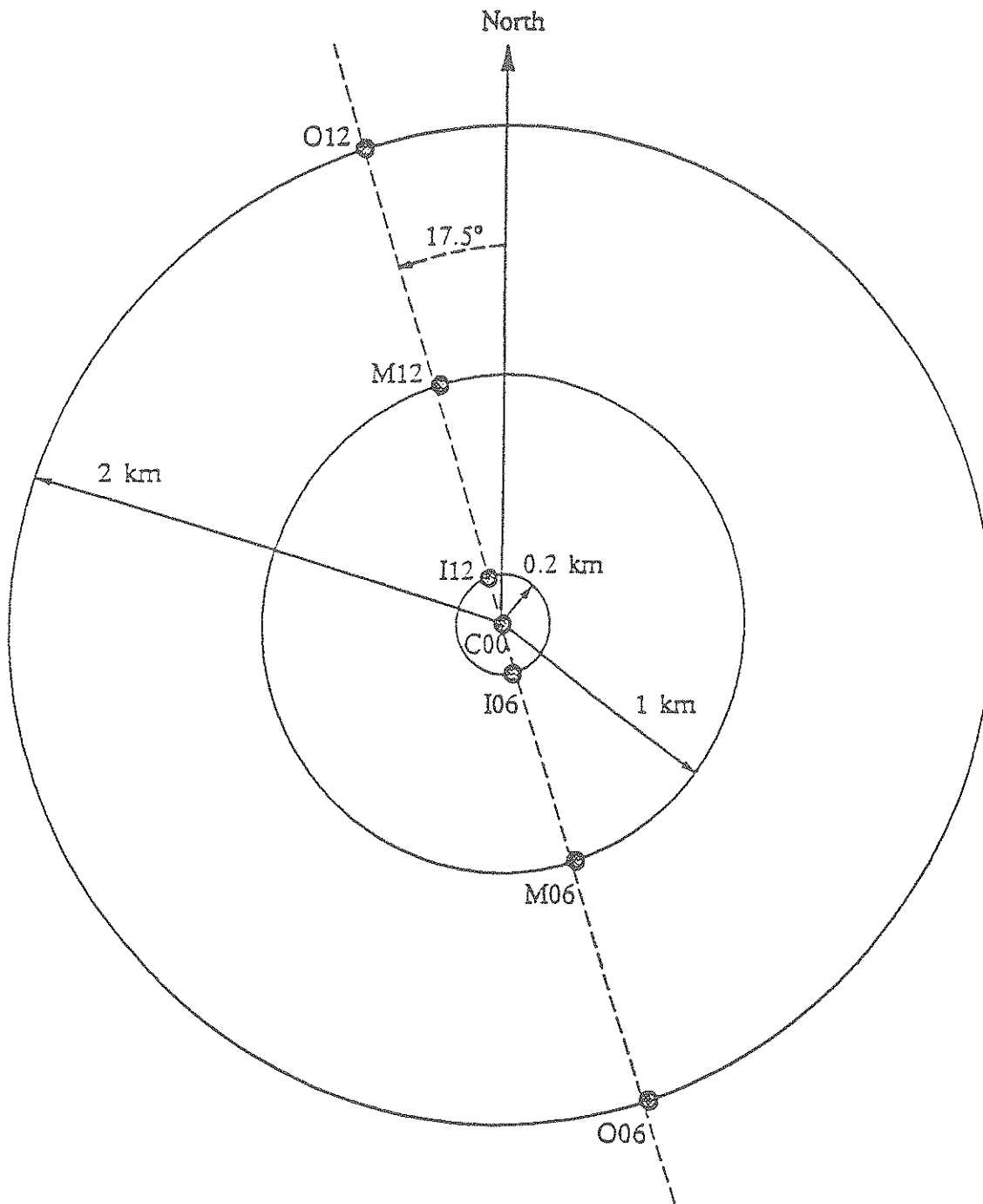


Figure 4.1 Seven Stations in the SMART-1 Array

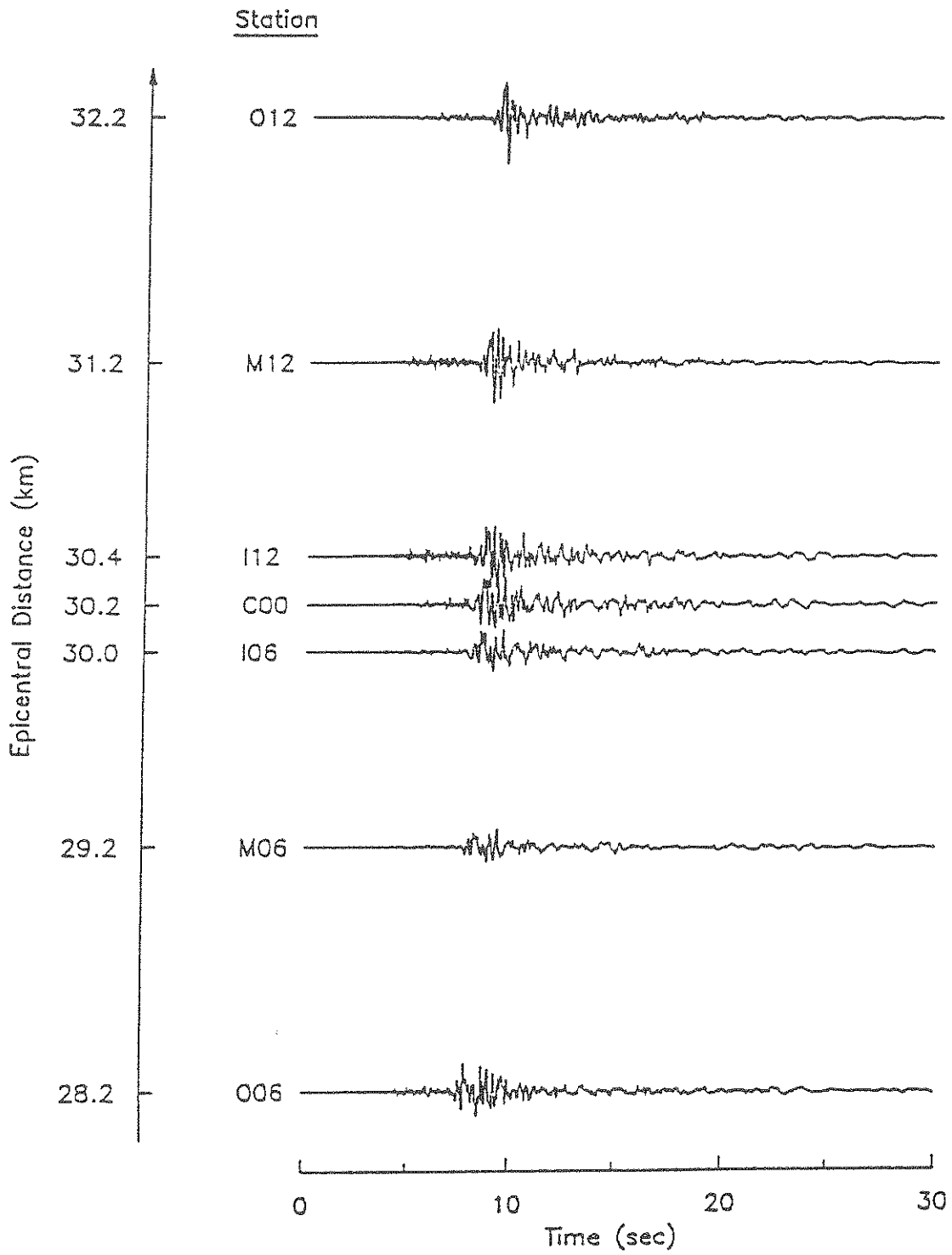


Figure 4.2 Accelerograms along Epical Direction

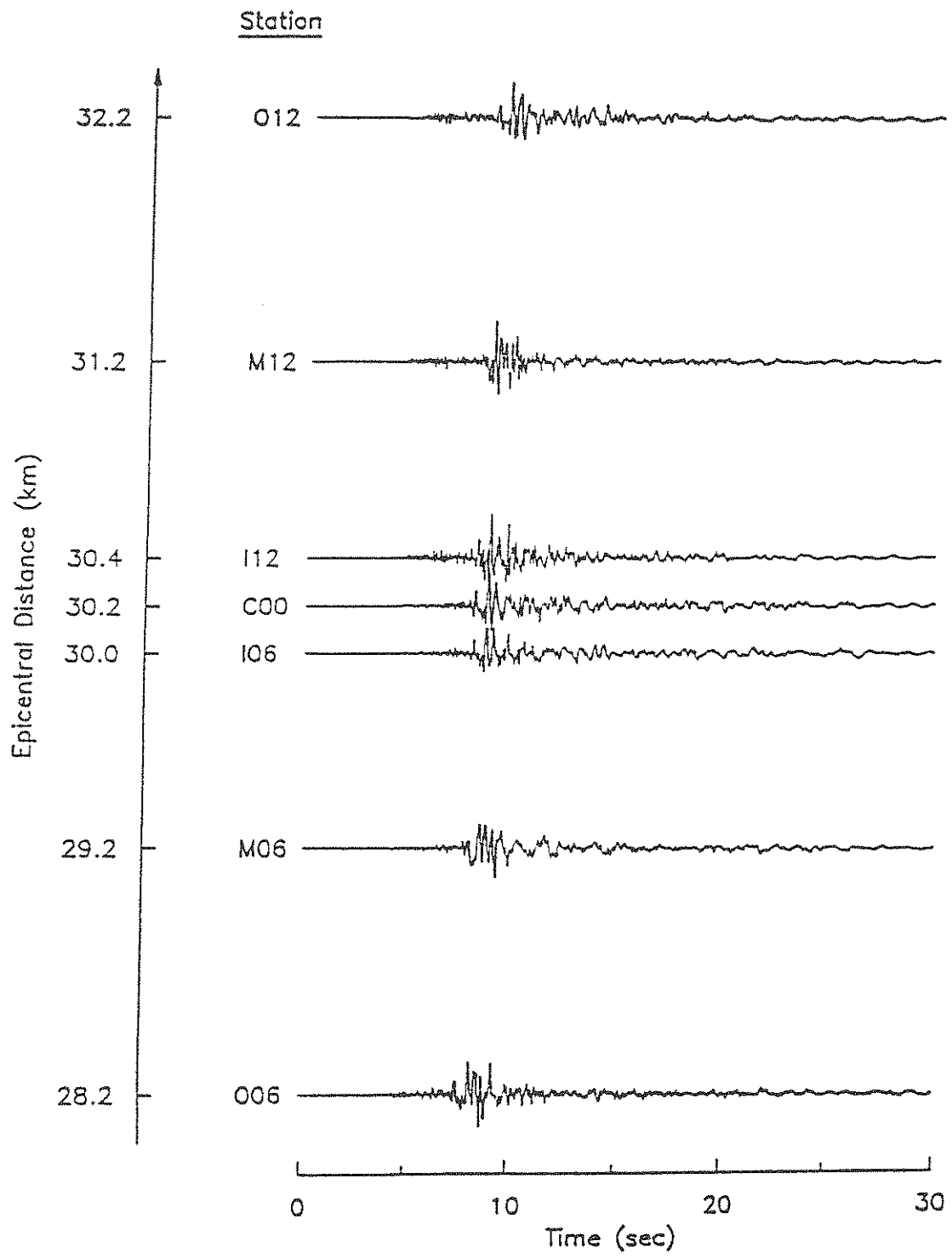


Figure 4.3 Accelerograms Normal to Epicentral Direction

60.7°SE may be chosen as the fault plane of the mainshock. This estimate of the fault plane orientation is consistent with the distribution of the mainshock and aftershock hypocenters.

Rupture velocity — By using the frequency-wavenumber analysis to measure the phasing of wave fronts of coherent S waves across the SMART-1 array, Abrahamson (1985) obtained the time-dependent rupture velocity, which is shown in Fig. 4.4. The inferred rupture speed shown in Fig. 4.4 covers the range of subsonic and transonic rupture velocities. Abrahamson suggested that two effects are responsible for the apparent super-shear rupture velocity; namely, the assumptions of a constant rupture direction and the laterally homogeneous velocity structure. Since the same assumptions are chosen in the 3-D wave propagation model of the current study, the rupture velocity in Fig. 4.4 will also be adapted. Moreover, the model assumes incrementally constant rupture velocities over short time increments, as shown in Fig. 4.4. The total rupture length obtained by integrating the rupture velocity is 17.15 km, and the duration of rupture is 5.75 sec, giving an average rupture velocity of 2.98 km/sec. This average rupture velocity is slightly less than the mean rupture velocity of 3.05 km/sec obtained by Abrahamson (1985).

Slip direction and amplitude — The rake of 64.3°UP was used in Abrahamson (1985) according to the focal distribution of the mainshock and aftershocks. No estimate of the fault offset of Event 5 is available. Some empirical formulas are listed as follows.

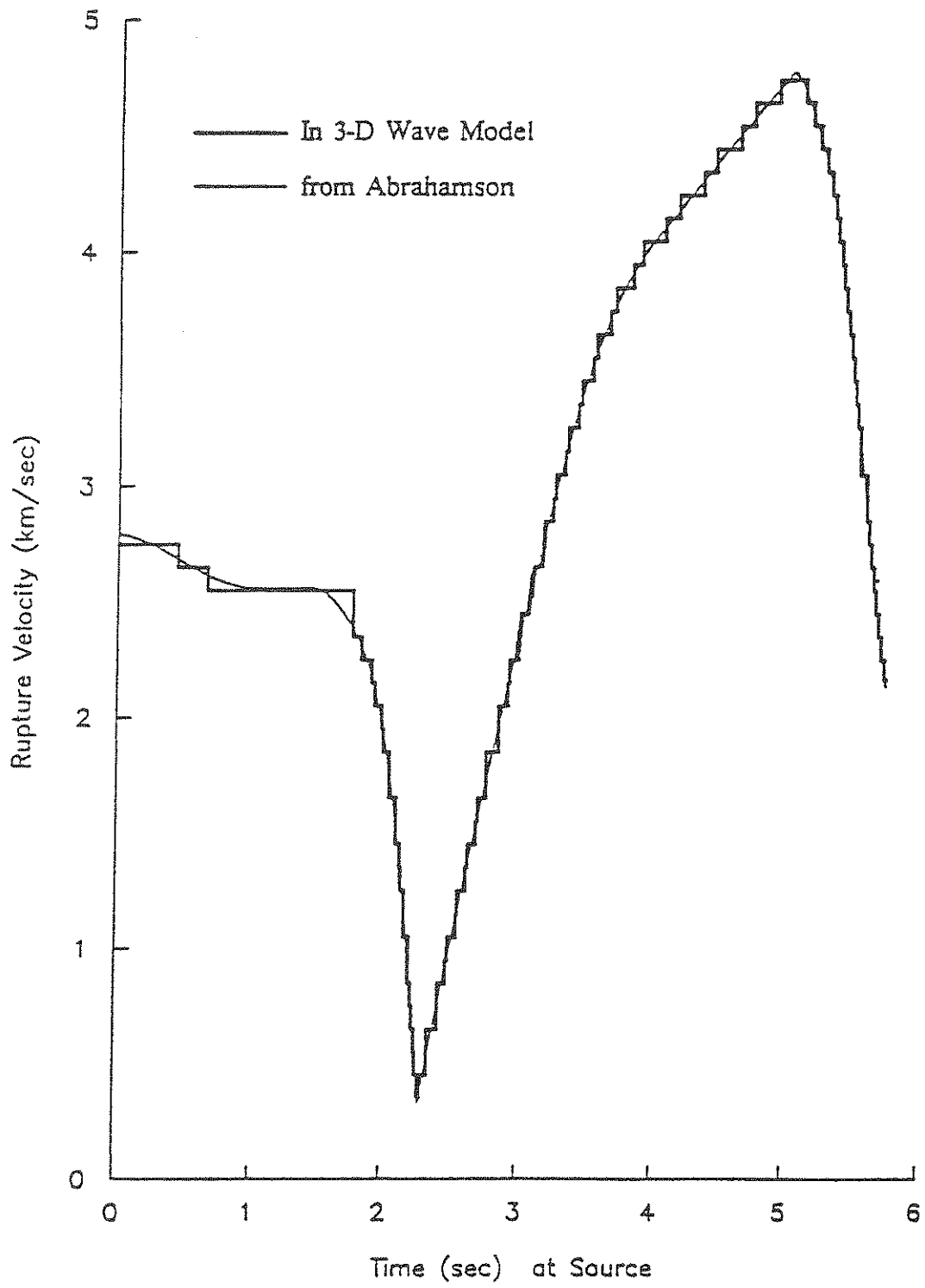


Figure 4.4 The Rupture Velocity

Iida (1965), world-wide data:

$$\log D_0 = 0.55 M_L - 1.71,$$

Bonilla (1970), USA data:

$$\log D_0 = 0.57 M_L - 1.91,$$

Matsuda (1975), Japan data:

$$\log D_0 = 0.6 M_L - 2.0,$$

King and Knopoff (1968), world-wide data:

$$\log LD_0^2 = 2.24 M_L - 4.99,$$

where D_0 and L are in unit of cm. With $M_L = 6.7$ and $L = 17.15$ km, the above formulas give $D_0 = 94$ cm, 81 cm, 105 cm, and 78 cm, respectively. An average value of 90 cm is taken as the slip amplitude.

Fault plane dimensions — The fault length is determined to be 17.15 km by integrating the time-dependent rupture velocity shown in Fig. 4.4. This rupture length is less than the 25 km rupture length indicated by the aftershock distribution. It is recognized, however, that aftershocks tend to overestimate the mainshock fault area (Aki, 1968). Similarly, a value of 6.0 km is taken for the fault width; the aftershock distribution would indicate a width of 7.9 km. One empirical formula in Mohammadi and Ang (1980) is

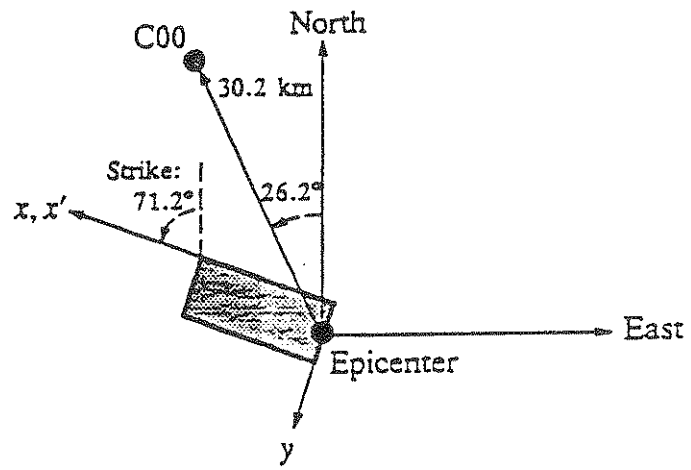
$$M_L = 0.932 \log D_0 \sqrt{W} + 6.456$$

which would give $W = 4.1$ km corresponding to $M_L = 6.7$ and $D_0 = 0.9$ m.

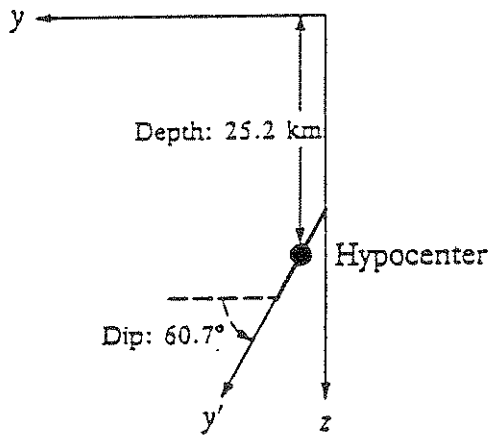
According to the above estimation, the focal mechanisms and the associated parameters for Event 5 are shown in Fig. 4.5. Fig. 4.6 shows typical analytic velocity time histories (at station C00) along and normal to the epicentral directions obtained through the 3-D wave model for the above parameters and the assumption of a step-time source function. The arrival of the P- and S-waves from the corners and the edges of the fault results in several abrupt changes of the analytic velocities in Fig. 4.6, which imply relatively high accelerations.

No empirical formulations were available to evaluate the rise time. Hence, three values of the rise time, *i.e.*, $T_r = 0.15$ sec, 0.10 sec, and 0.05 sec, were examined, and the resulting analytic ground accelerations are shown in Fig. 4.7. As shown in Fig. 4.7 and discussed in Section 3, the shorter rise times will induce higher peak accelerations. Since the peak accelerations obtained at station C00 in both directions are about 100 cm/sec^2 , a very short rise time would be required in the analytic model. Moreover, the integration of the velocity time histories in Fig. 4.6 gives the peak displacement of about 1.5 cm, which is consistent with the peak ground displacement obtained by integrating the field accelerogram twice at the same station. Therefore, the assumption of a step-time source function is reasonable in the analytic 3-D model for this event.

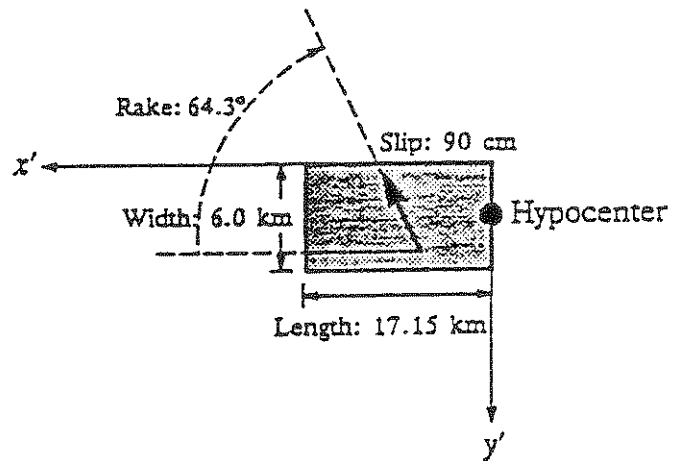
The velocity time histories shown in Fig. 4.6 do not contain as many oscillations as the field recordings. This may be attributed to the assumption of a coherent rupture at the source and of the homogeneous half-space medium. In studies concerned primarily with the spatial displacements, however, the effect of the high-frequency content is not very significant such that the simple source



(a) Plan View

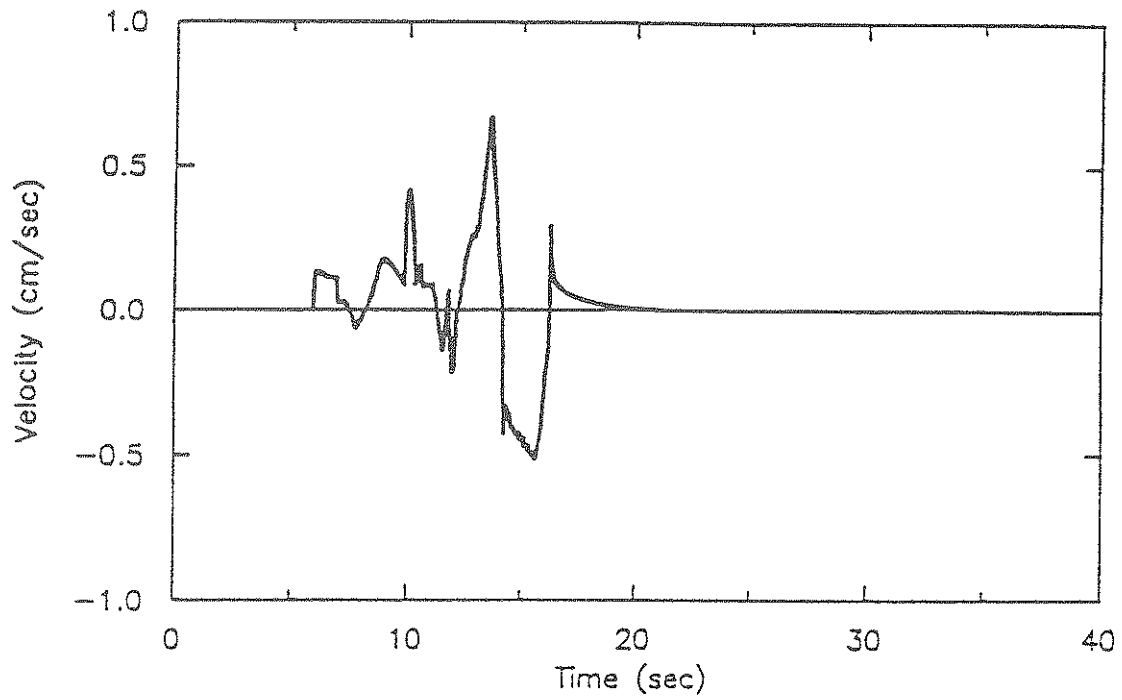


(b) Side View

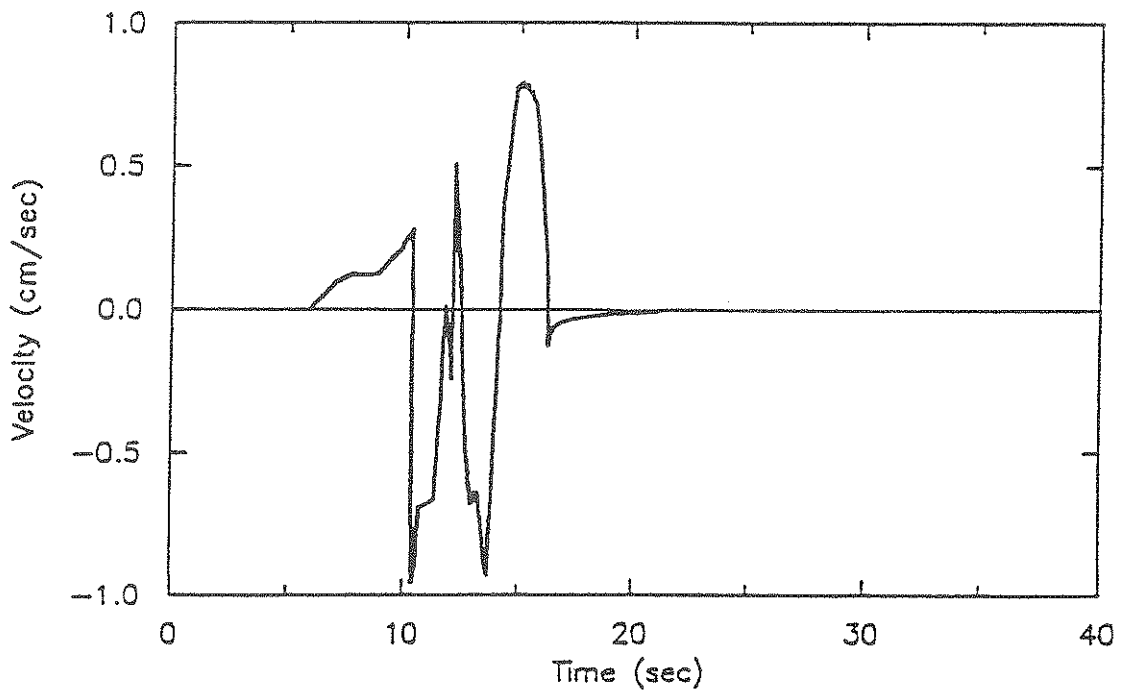


(c) Fault Plane

Figure 4.5 Focal Mechanisms of Event 5

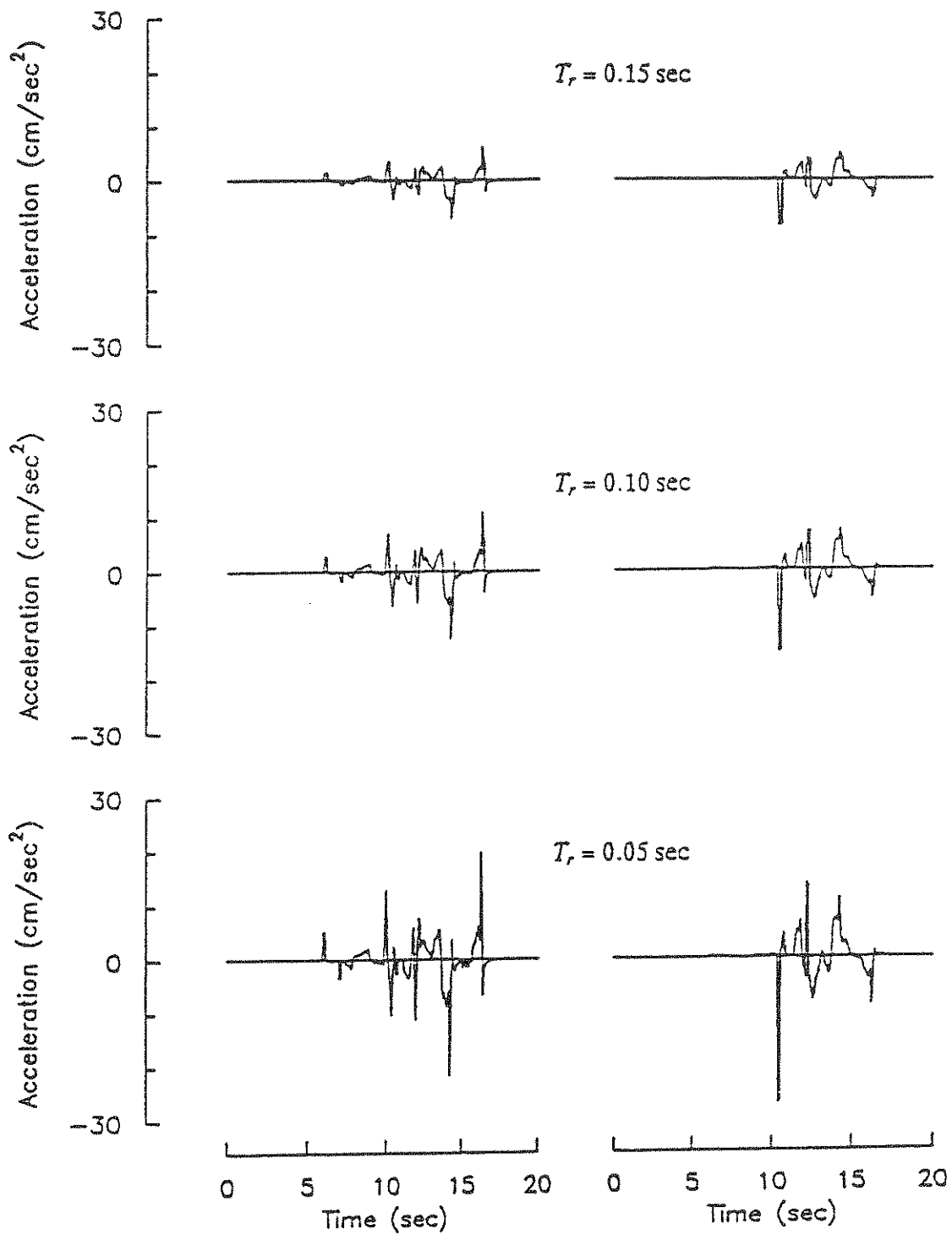


(a) Along Epicentral Direction



(b) Normal to Epicentral Direction

Figure 4.6 Analytic Velocities at Station C00 with $T_r = 0$ sec



(a) Along Epicentral Direction (b) Normal to Epicentral Direction

Figure 4.7 Accelerations for Different Rise Times at Station C00

models may be used to reproduce the displacement time histories. As a matter of fact, the response of pipelines derives primarily from the region of low frequencies. Therefore, the results should be acceptable for the analysis of pipeline systems. A stochastic approach is considered in the following section to partially account for the incoherence in the rupture process.

4.2 Stochastic Analysis

The spatial and temporal variation of a fault dislocation is too complex to be represented by any simple mathematical function such as Eq. (2.1). In general, strong ground motions are characterized by a high-frequency content which is strongly related to the details of faulting. These details arise from the nonuniform distribution of various physical properties on the fault plane, including the rupture velocity, the slip magnitude, the direction of rupture, *etc.* Therefore, strong ground motions are too complicated to be simulated by a purely deterministic model because they are affected by numerous small-scale heterogeneities of the fault plane. To avoid this difficulty, several attempts have been made to introduce hybrid deterministic and stochastic models, in which the gross features of the rupture propagation are defined deterministically but the details of the rupture are represented by a stochastic process (Boore and Joyner, 1978; Andrews, 1980, 1981; Boatwright, 1982; Papageorgiou and Aki, 1983a, 1983b).

For the purpose of modeling long-period seismic waves, the kinematic dislocation model is a good approximation to explain the radiation of seismic waves. A major shortcoming with the kinematic models is that a constant slip is inadmissible from a purely continuum mechanical point of view, as well as from many practical investigations. Nonuniform fault slip over a fault plane has been

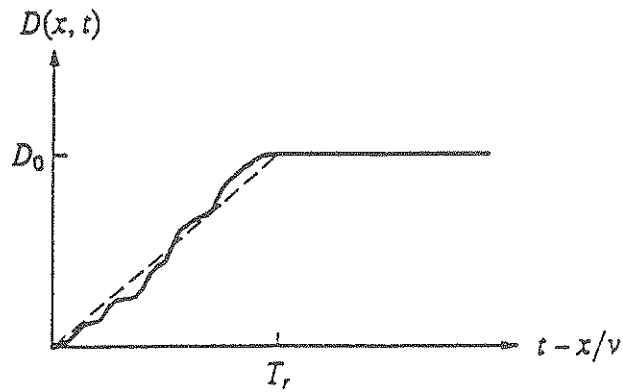
found for several earthquakes by various seismologists, and also from the analysis of teleseismic body wave data for many earthquakes (Aki, 1982). Based on the above considerations, an effective way to describe the rupture process is through a stochastic approach.

4.2.1 Randomness of Earthquake Source

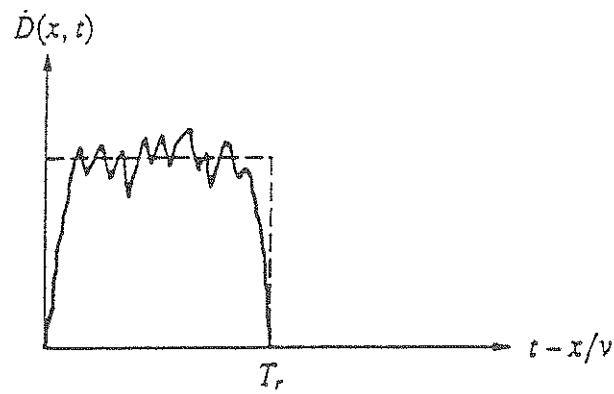
To account for an incoherent slip, Haskell (1966) postulated the rupture mechanism as a random process with a specified spatio-temporal autocorrelation for the dislocation acceleration, whereas Aki (1967) introduced the spatio-temporal autocorrelation of the dislocation velocity at the source. In both models, the random dislocation spreads at a constant rupture velocity.

In Haskell's statistical model, the Fourier transform source factor of the far-field response decreases with ω^{-3} for large ω , whereas it is inversely proportional to ω^{-2} in Aki's model. Hence, these have been referred to as the " ω -cube model" and " ω -square model", respectively. Under the assumption of similarity, it has been shown that the ω -square model compares better with observations than the ω -cube model. Therefore, the ω -square model will be adopted in this study to represent the randomness at the source. The physical interpretation of this model is discussed in the following.

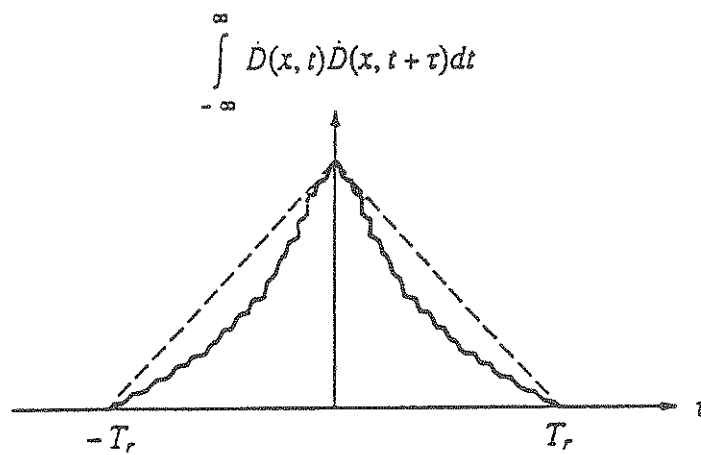
Since an earthquake is essentially a transient phenomenon, the spatio-temporal autocorrelation function introduced at the source should be different from those for a stationary time series. Fig. 4.8 will schematically illustrate what form may be expected for the autocorrelation function of the dislocation process at an earthquake source. Let the dislocation start at $x = 0$ and propagate along the x



(a) Dislocation



(b) Dislocation Velocity



(c) Autocorrelation Function of Dislocation Velocity

Figure 4.8 Schematic Diagrams of Dislocation and Its Autocorrelation Function

axis at a constant rupture velocity v ; then the dislocation at a given point x will be zero for $t < x/v$ and increase up to a final value D_0 for $t > T_r + x/v$, in which T_r is the rise time. The actual dislocation at the transition time, *i.e.*, $x/v < t < T_r + x/v$, is unknown. In Fig. 4.8, the dashed lines are for the case of an idealized linear ramp-time source function. Fig. 4.8(a) and (b) show the corresponding dislocation and its velocity functions, respectively. The autocorrelation function of dislocation velocity is also shown in Fig. 4.8(c). Based on Fig. 4.8(c), the suitable form for the temporal autocorrelation function of dislocation velocity will be a negative exponential function.

Assume first that the temporal autocorrelation function of dislocation velocity at the point x decreases exponentially with the time lag τ , *i.e.*,

$$\int_{-\infty}^{\infty} \dot{D}(x, t) \dot{D}(x, t + \tau) dt = \psi_1 e^{-k_T |\tau|}, \quad (4.1)$$

where:

$\dot{D}(x, t)$ = the dislocation velocity at a point x and time t ,

τ = the temporal separation,

ψ_1 = a constant,

k_T^{-1} = the correlation time.

Furthermore, since the spatial autocorrelation function between the dislocation velocity at (x, t) and that at $(x + \epsilon, t + \epsilon/v)$ will indicate the degree of persistency of offsetting and this persistency decreases with the separation distance ϵ between the two points, a similar exponential form may be adopted also for the spatial autocorrelation function, *i.e.*,

$$\int_{-\infty}^{\infty} \dot{D}(x, t) \dot{D}(x + \epsilon, t + \epsilon/v) dx = \psi_2 e^{-k_L |\epsilon|}, \quad (4.2)$$

where:

ϵ = the spatial separation,

ψ_2 = a constant,

k_L^{-1} = the correlation length,

v = the rupture velocity.

Then, the temporal and spatial autocorrelation functions can be expressed in a single form as

$$\int_{-\infty}^{\infty} \int_{-\infty}^{\infty} \dot{D}(x, t) \dot{D}(x + \epsilon, t + \tau) dx dt = \psi_0 e^{-k_L |\epsilon|} e^{-k_T |\tau - \epsilon/v|}. \quad (4.3)$$

In Eq. (4.3), the constant ψ_0 is related to the final slip D_0 , as shown in Eq. (C.12); k_T is the corner frequency; and $vk_L = k_T$ is assumed for simplicity (Aki, 1967). For example, the corner frequency for Event 5 of the SMART-1 array was estimated by Abrahamson (1985) to be 0.7 Hz.

The introduction of randomness at the source, as indicated in Eq. (4.3), should partially account for the nonuniformness of the fault slip over a fault plane. Eq. (4.3) can be interpreted as follows: a rupture breaks evenly across the fault width but coherently only for short distances along the fault, compared to the total fault length, and only over a short time relative to the total fracture time. In other words, $(vk_L)^{-1}$ is related to the time required for propagation of fracture along the length of the fault, whereas k_T^{-1} is associated with the time required for formation of fracture across the fault width.

Although the randomness of an earthquake source has been developed as described above, the path effect representing the wave propagation between the source and the ground stations is still needed for a stochastic analysis. This path effect has been approximately separated from the source effect for the far-field responses in a full-space, in which the fault is treated as a point source (*e.g.*, Aki, 1967). Such a simple isolation is not permitted if the fault dimension in the half-space is accounted. The alternative way is to search a substitute system with equivalent transmission effect.

4.2.2 The Substitute System

The deterministic 3-D wave propagation model yields the ground response time histories at various stations excited by a fault rupture in a half-space. In order to facilitate the evaluation of the randomness of the source on the ground motions, a "substitute system" is introduced to represent the path effect. To ensure an almost identical transmission effect, the substitute system should be subjected to the "same" excitation and reproduce the "equivalent" response for each station and in each direction. The "same" excitation can be achieved simply by transforming the rupture into a support motion suitable for the substitute system, whereas the "equivalent" response is obtained by minimizing the error function defined as the differences between the responses of the analytic model and the substitute system. It is difficult to find such a substitute system that satisfies the above requirements for all stations and directions. Hence, one substitute system is required for each station and each direction in order to neglect the spatial and directional parameters in the substitute system. Furthermore,

identical form of the substitute system is used for all stations but with different parameters.

An ordinary single-degree-of-freedom system may be adequate to simulate the medium transition effect from the fault to the free surface because the behavior of the negative exponential term and the sinusoidal term in the response of such a system is consistent with observed displacement time histories from an earthquake. Hence, a linear multi-degree-of-freedom system is adopted as the substitute system. The appropriate parameters for the different stations are evaluated through system identification.

In the analytic model, the source mechanism is a series of dislocations propagating along the fault length, whereas the excitation to the multi-degree-of-freedom should be a point motion. Therefore, the equivalent point base excitation of the substitute system may be assumed to be the average dislocation over the length of the fault, or

$$B(t) = \frac{1}{L} \int_0^L D(x, t) dx . \quad (4.4)$$

Because Eq. (4.3) defines the autocorrelation function for a transient random process, the power spectral density of the faulting motion can not be obtained directly from the Fourier transform of the autocorrelation function specified in Eq. (4.3), such as the case for a stationary random process. However, with the autocorrelation function defined in Eq. (4.3) and the equivalent point base motion defined in Eq. (4.4), the power spectral density of the base velocity of the substitute system can be estimated as

$$S_{\ddot{B}\ddot{B}}(\omega) = \frac{2\pi}{T_0} \frac{D_0^2}{\left(1 + \frac{\omega^2}{k_T^2}\right)\left(1 + \frac{\omega^2}{k_L^2 v^2}\right)}, \quad (4.5)$$

in which D_0 is the final dislocation and $T_0 = L / v$ is the duration of faulting. The derivation of Eq. (4.5) is described in Appendix C. Eq. (4.5) represents the stochastic excitation of the substitute system, and is useful when the spatial variation of ground motions is evaluated.

In the multi-degree-of-freedom system, the impulse response function for each mode is

$$h_j(t) = \frac{\phi_j}{\omega_j \sqrt{1 - \xi_j^2}} e^{-\xi_j \omega_j t} \sin(\omega_j \sqrt{1 - \xi_j^2} t), \quad (4.6)$$

where:

ϕ_j = the participation factors, $j = 1, 2, \dots, N$,

ω_j = the natural frequencies, $j = 1, 2, \dots, N$,

ξ_j = the damping coefficients, $j = 1, 2, \dots, N$,

N = the number of modes.

With the base motion specified in Eq. (4.4) and the impulse response function shown in Eq. (4.6), the displacement response of the substitute system can be obtained by using the Duhamel integral and the modal superposition, *i.e.*,

$$\begin{aligned}
d(t) &= \sum_{j=1}^N \phi_j \int_0^t h_j(t-\tau) [2\xi_j \omega_j \dot{B}(\tau) + \omega_j^2 B(\tau)] d\tau \\
&= \frac{D_0}{T_0} \sum_{j=1}^N \phi_j [\tau - h_j(\tau)] \Big|_{\tau=t'}^{\tau=t}, \tag{4.7}
\end{aligned}$$

in which $t' = \max(0, t-T_0)$.

System Identification — An error function E , for determining the parameters of the substitute system, is defined as the sum of squares of the differences between the responses of the substitute system and the 3-D analytical solutions over the whole record. Since the velocity time history is the direct solution obtained in the 3-D wave propagation model, it will be adopted to define the necessary error function. Therefore, the form of the error function will be

$$E(\phi_j; \omega_j; \xi_j) = \int_{t_i}^{t_f} [\dot{u}(t) - \dot{d}(t-t_i)]^2 dt, \tag{4.8}$$

where:

- ϕ_j, ω_j, ξ_j = the parameters of the substitute system, $j = 1, 2, \dots, N$,
- t_i = the initial time of the record,
- t_f = the final time of the record,
- \dot{u} = the ground velocity obtained in the wave propagation model,
- \dot{d} = the velocity response of the substitute system.

Observe that the time variable in the response of the substitute system is shifted by t_i , the first arrival time of the propagating waves. This is because there is a time

lag for the response associated with the wave propagating from the source to the station. No response will occur in the substitute system for $t \leq t_i$; the quiescent initial conditions must be specified at $t = t_i$, instead of at $t = 0$.

$\dot{d}(t)$ in Eq. (4.8) is the time derivative of Eq. (4.7), *i.e.*,

$$\dot{d}(t) = \frac{D_0}{T_0} \sum_{j=1}^N \frac{\phi_j}{\sqrt{1-\xi_j^2}} \left\{ e^{-\xi_j \omega_j \tau} \left[\xi_j \sin(\omega_j \sqrt{1-\xi_j^2} \tau) - \sqrt{1-\xi_j^2} \cos(\omega_j \sqrt{1-\xi_j^2} \tau) \right] \right\} \Big|_{\tau=t'}^{\tau=t}, \quad (4.9)$$

in which $t' = \max(0, t-T_0)$.

The parameters of the substitute system are estimated by minimizing the error function of Eq. (4.8). The system identification used here is an extension of the modal minimization method for multi-degree-of-freedom linear models in Beck (1978). It includes one-dimensional minimization, single-mode minimization, modal sweeps, and addition of new modes.

Each time when a new mode is needed, initial estimates are made for its parameters. The modal sweep then starts from the first mode. During the single-mode minimization, the parameters of the first mode are sequentially optimized, whereas the parameters of the other modes are held constant. Since $\dot{d}(t)$ is a linear function of ϕ_j , the optimized participation factor in each mode can be obtained, as long as the other parameters are given, by equating the derivative of the error function with respect to the participation factor to zero, *i.e.*,

$$\phi_j = \frac{\int_{t_i}^{t_f} \left[\dot{u}(t) - \sum_{\substack{k=1 \\ k \neq j}}^N \phi_k f_k(t) \right] f_j(t) dt}{\int_{t_i}^{t_f} f_j^2(t) dt}, \quad (4.10)$$

where $f_k(t)$ is the unit impulse response (velocity) function for the k th mode of the substitute system, or

$$\dot{d}(t) = \sum_{k=1}^N \phi_k f_k(t). \quad (4.11)$$

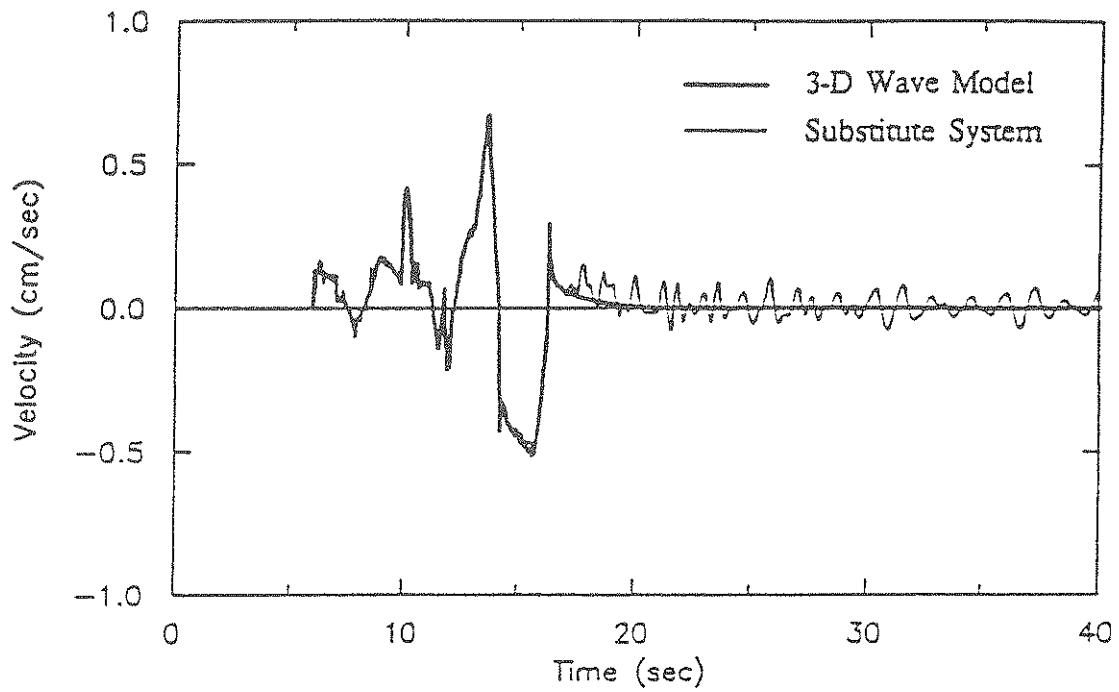
Therefore, a series of 1-D minimizations are taken by minimizing E alternately only with respect to ω_j and ξ_j in the single-mode minimization. This process is continued until a consecutive pair of 1-D minimizations results in a fractional decrease in E of less than a specified value. Then, the single-mode minimization is continued for the next mode, and so on. After convergence for the last mode is achieved, the sweep over all modes may start again if total convergence, which is compared to the last modal sweep, has not been achieved; otherwise, a new mode is added. The addition of a new mode will be stopped if its contribution is less than a specified tolerance.

The advantage of the procedure described above is to keep the number of mode in the substitute system to a minimum. The criterion for convergence in terms of the relative change in E is chosen instead of the change in the estimates of the parameters because the latter can cause difficulties with the higher modes (Beck, 1978).

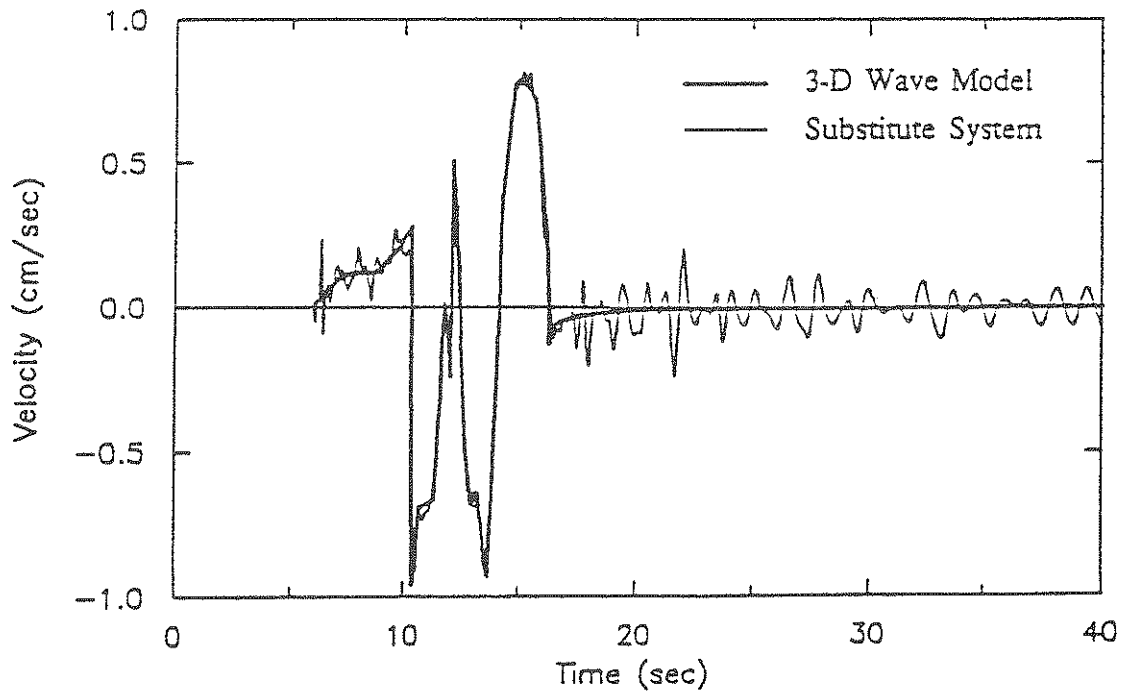
Since the error function E is a highly non-linear function of ω_j and ξ_j , the final optimized parameters will strongly depend on the initial guesses, especially for the case of ω_j , which was found in the sensitivity study with respect to the initial estimates of the parameters. To find the best initial value of ω_j , that will give the error function an absolute minimum, a sweep over an adequate range of modal frequencies was performed each time a new mode is added.

There are two constraints to the modal natural frequencies and modal dampings. In the analytic velocity time histories, the results were obtained at every 0.05 sec, so the maximum natural frequency for each mode was set at 10 Hz corresponding to the resolution of the responses in the deterministic model. This range of frequency also covers the frequencies of engineering interest. Furthermore, the damping coefficient for an underdamped system is between 0 and 1. The response of such a system will decay slowly as the damping ratio decreases. Since only finite record is used in the system identification, the lower limit of the damping ratio should be specified to produce the quiescent response when the time variable approach infinity. To investigate the effect of this lower limit, three different values, *i.e.*, 0.05, 0.1, and 0.2, were examined, and the results are shown in Figs. 4.9, 4.10, and 4.11, respectively. By comparing these figures, the lower limit of 0.1 was selected to ensure good results.

In addition to Fig. 4.10, Figs. 4.12 and 4.13 show the responses of the substitute system at the other two stations O06 and O12, respectively. The number of modes used in the analysis ranged from 44 to 60 corresponding to a tolerance of 0.0001. These figures show that the results of the substitute system closely resemble those of the corresponding analytical solutions at the selected stations.

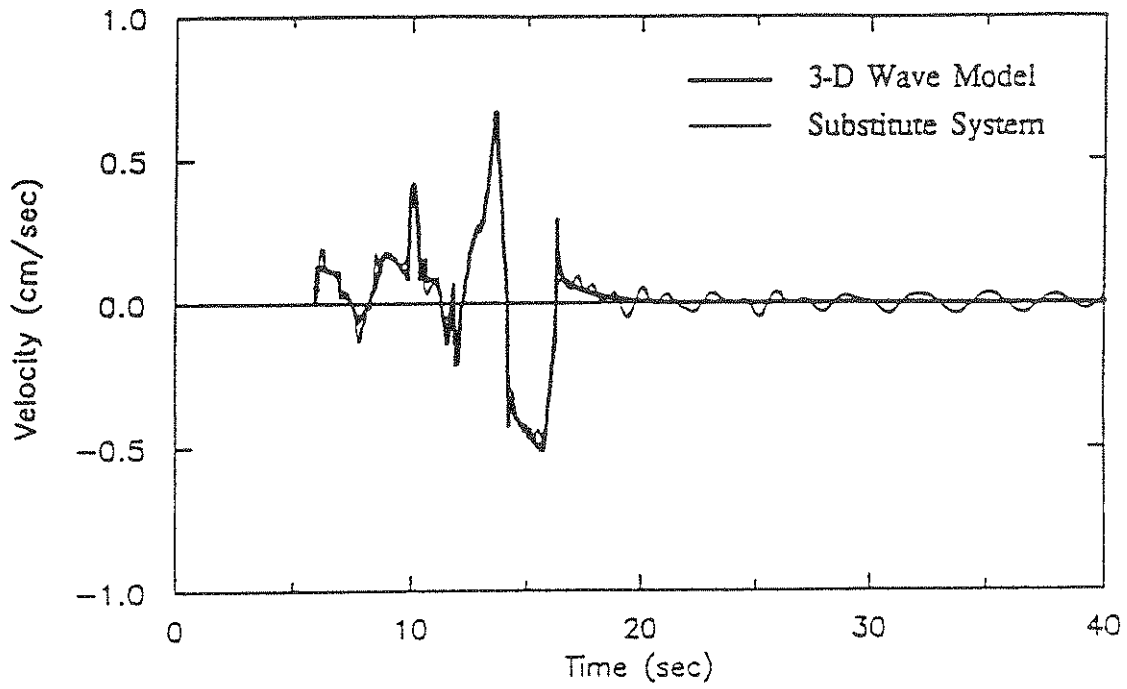


(a) Along Epicentral Direction

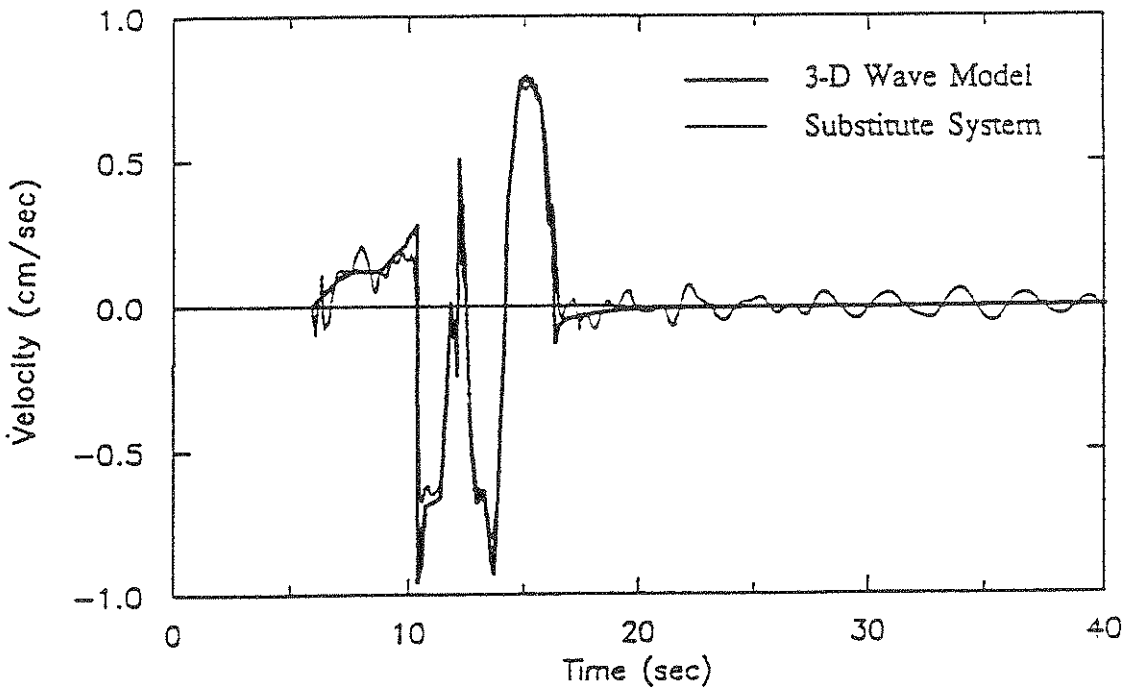


(b) Normal to Epicentral Direction

Figure 4.9 Velocities from Analytic Model and Substitute System at Station C00 ($0.05 < \xi_i < 1$)

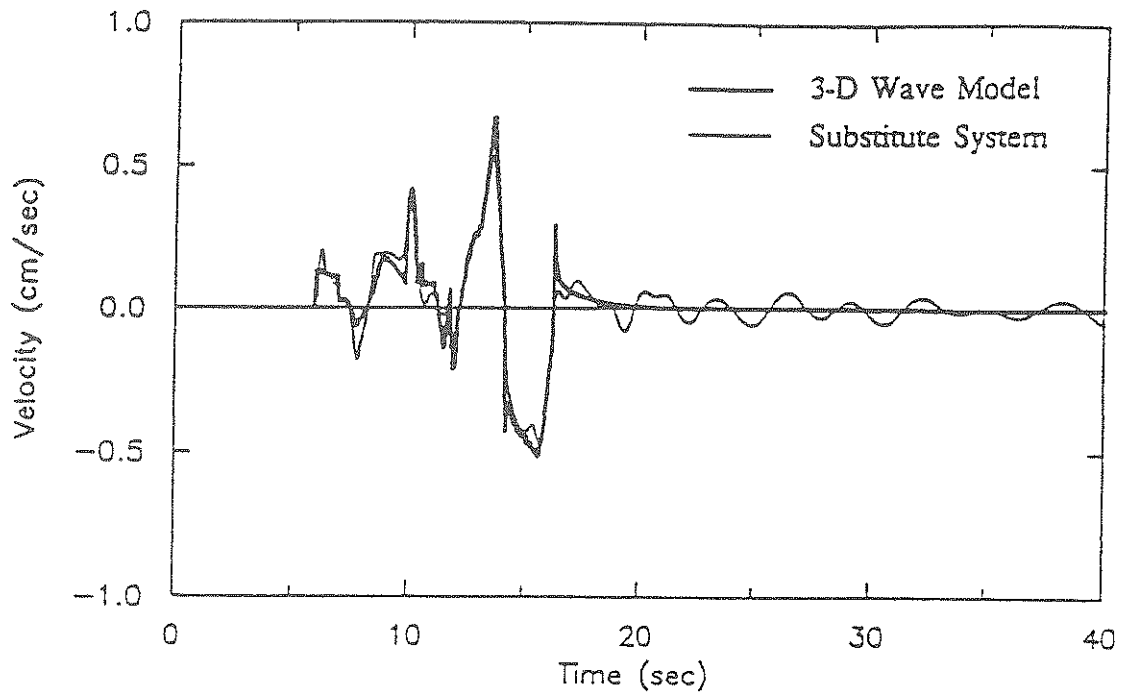


(a) Along Epicentral Direction

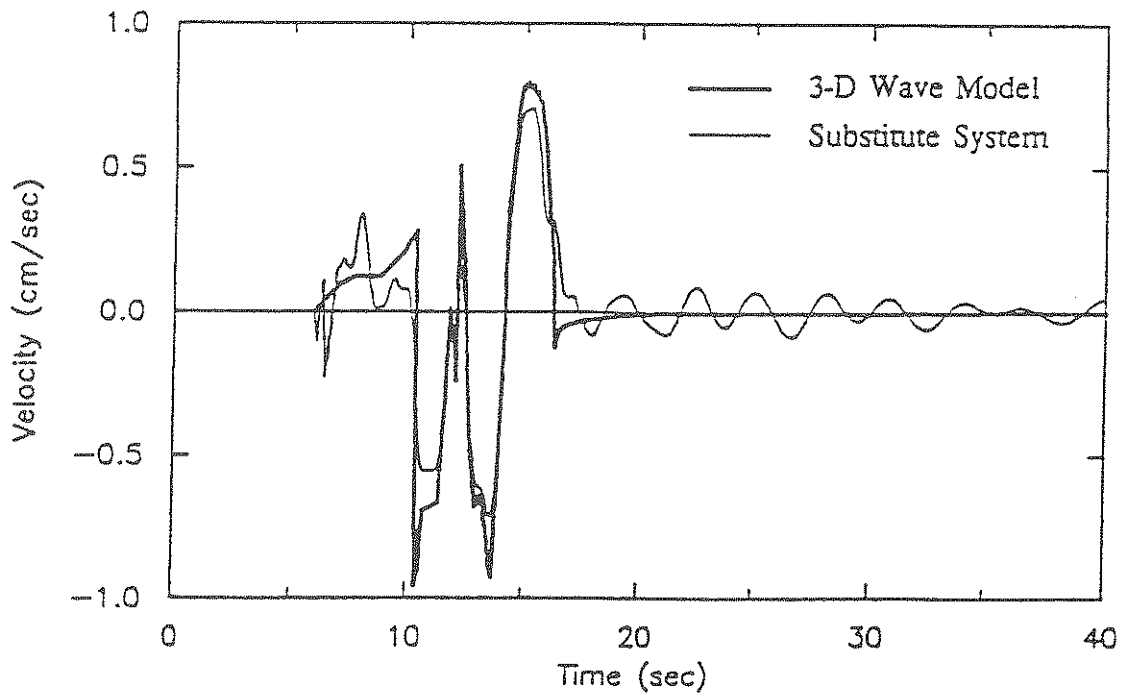


(b) Normal to Epicentral Direction

Figure 4.10 Velocities from Analytic Model and Substitute System at Station C00 ($0.1 < \xi_j < 1$)

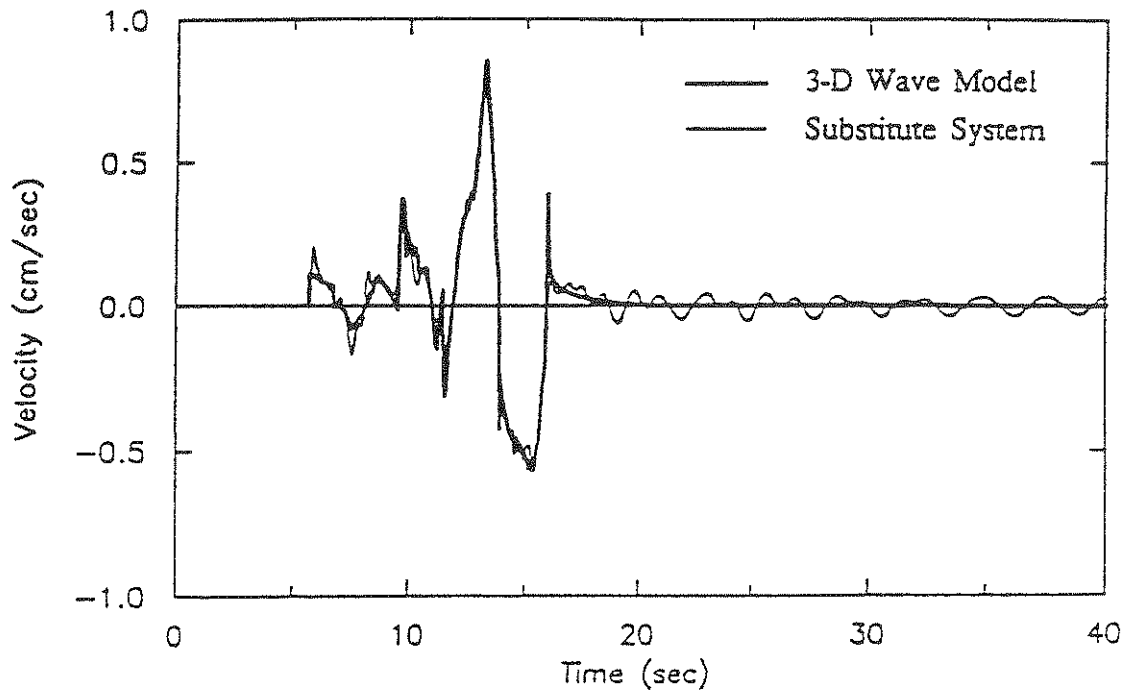


(a) Along Epicentral Direction

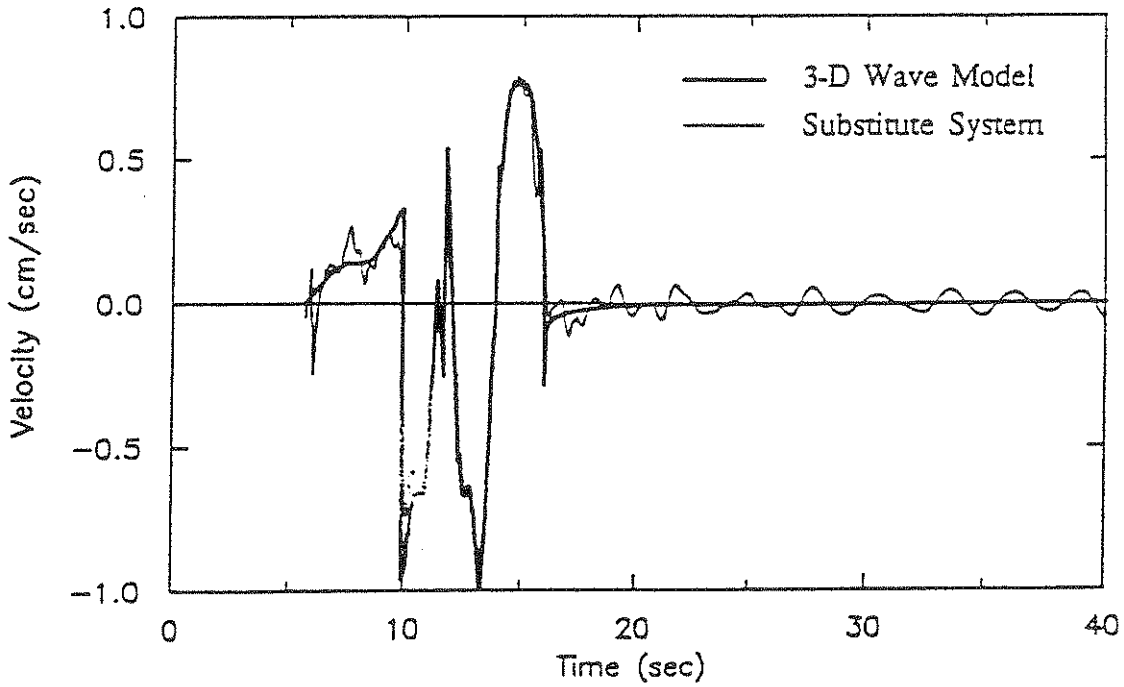


(b) Normal to Epicentral Direction

Figure 4.11 Velocities from Analytic Model and Substitute System at Station C00 ($0.2 < \xi_j < 1$)

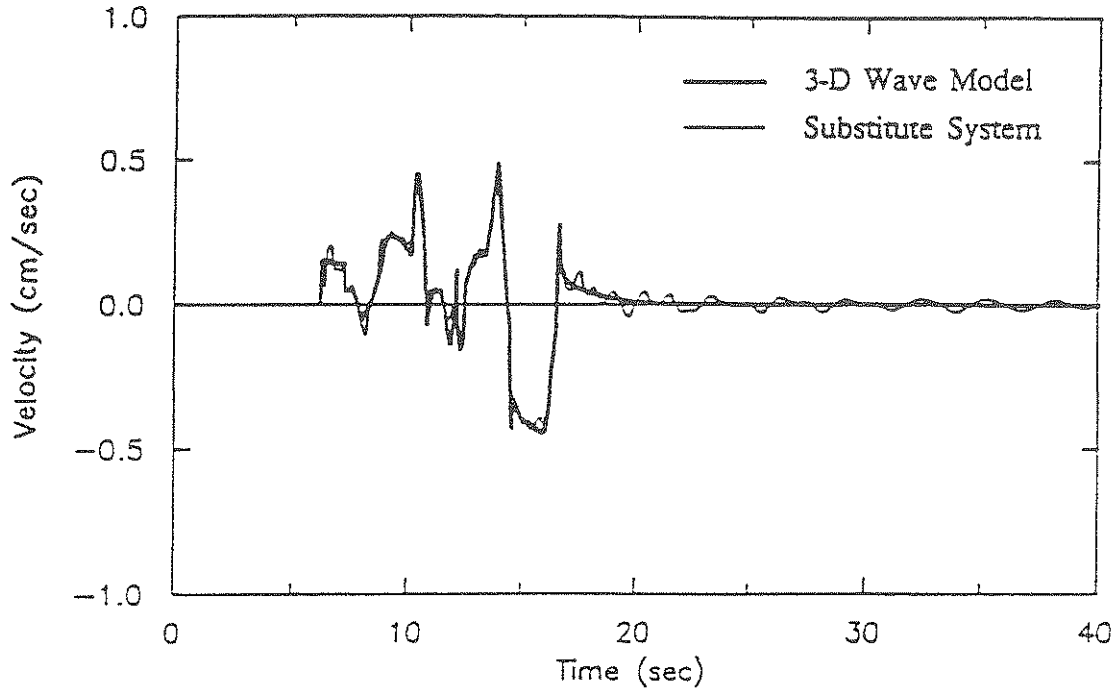


(a) Along Epicentral Direction

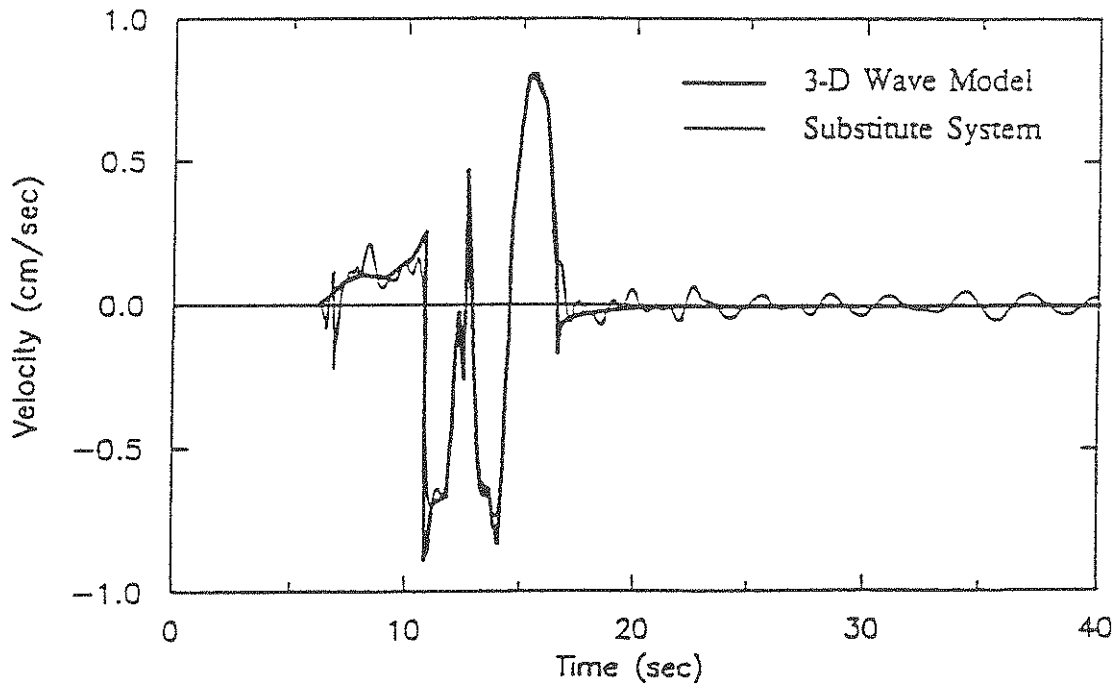


(b) Normal to Epicentral Direction

Figure 4.12 Velocities from Analytic Model and Substitute System at Station O06 ($0.1 < \xi_j < 1$)



(a) Along Epicentral Direction



(b) Normal to Epicentral Direction

Figure 4.13 Velocities from Analytic Model and Substitute System at Station O12 ($0.1 < \xi < 1$)

4.2.3 Stochastic Characteristics of Ground Motions

Absolute ground motions — The power spectral density of ground motion at a given station and the cross spectral density of ground motions between two stations or directions may be evaluated as follows.

Let $d^P(t)$ and $d^Q(t)$ denote the displacement time histories at any two stations P and Q or in any two directions P and Q for a given station. The base motion to the substitute system is the dislocation at the earthquake source, for which the power spectral density of the base velocity is given by Eq. (4.5). $d^P(t)$ is expressed with the Duhamel integral as

$$\begin{aligned} d^P(t) &= \sum_{m=1}^M \phi_m^P \int_0^t h_m^P(\tau_1) \left[2\xi_m^P \omega_m^P \dot{B}(t-\tau_1) + (\omega_m^P)^2 B(t-\tau_1) \right] d\tau_1 \\ &= \sum_{m=1}^M \phi_m^P \int_{-\infty}^{\infty} h_m^P(\tau_1) \left[2\xi_m^P \omega_m^P \dot{B}(t-\tau_1) + (\omega_m^P)^2 B(t-\tau_1) \right] d\tau_1, \end{aligned} \quad (4.12)$$

where:

- $\phi_m^P, \omega_m^P, \xi_m^P$ = the parameters for the m th mode at station P ,
- h_m^P = the impulse response function for the m th mode at station P ,
- \dot{B}, B = the base velocity and displacement of the substitute system, respectively,
- M = the number of modes at station P .

Eq. (4.12) implies that $h_m^P(\tau_1) = \dot{B}(\tau_1) = B(\tau_1) = 0$, for $\tau_1 < 0$. Similarly, for station Q ,

$$d^Q(t+\tau) = \sum_{n=1}^N \phi_n^Q \int_{-\infty}^{\infty} h_n^Q(\tau_2) \left[2\xi_n^Q \omega_n^Q \dot{B}(t+\tau-\tau_2) + (\omega_n^Q)^2 B(t+\tau-\tau_2) \right] d\tau_2, \quad (4.13)$$

in which N is the number of modes at station Q .

The cross-correlation function between stations P and Q is defined as

$$R_{d^P d^Q}(\tau) = E \left[d^P(t) d^Q(t+\tau) \right], \quad (4.14)$$

and the associated cross spectral density is given by

$$S_{d^P d^Q}(\omega) = \int_{-\infty}^{\infty} R_{d^P d^Q}(\tau) e^{-i\omega\tau} d\tau. \quad (4.15)$$

Eqs. (4.12) through (4.15) are combined together to give the cross spectral density between stations P and Q in terms of the stochastic excitation at the base and the modal parameters of the two substitute systems, *i.e.*,

$$S_{d^P d^Q}(\omega) = \sum_{m=1}^M \sum_{n=1}^N \frac{\phi_m^P \phi_n^Q}{\omega^2} \left[4\xi_m^P \xi_n^Q \omega_m^P \omega_n^Q \omega^2 + 2i\omega_m^P \omega_n^Q (\xi_n^Q \omega_m^P - \xi_m^P \omega_n^Q) \omega + (\omega_m^P \omega_n^Q)^2 \right] H_m^{P*}(\omega) H_n^Q(\omega) S_{\dot{B}\dot{B}}(\omega), \quad (4.16)$$

where $*$ denotes the complex conjugate, H_m^P and H_n^Q are the frequency transfer functions of the m th mode at station P and of the n th mode at station Q , respectively.

For a stationary process the cross spectral densities for velocity and acceleration are

$$S_{v^P Q}(\omega) = \omega^2 S_{a^P Q}(\omega), \quad (4.17)$$

and

$$S_{a^P Q}(\omega) = \omega^4 S_{a^P Q}(\omega), \quad (4.18)$$

respectively, where v^P and a^P denote the ground velocity and acceleration at station P , respectively.

Based on Eqs. (4.16) and (4.18), the power spectral densities of the accelerations along and normal to the epicentral direction for the seven stations from O06 to O12 were calculated. The theoretical results along with the corresponding empirical results are shown in Figs. 4.14 through 4.20.

In general, the results of the model overestimate the spectral amplitudes at the lower frequencies, but underestimate the amplitudes at the higher frequencies. The same phenomena were observed in Zerva, *et al.* (1985). These may be attributed to the inhomogeneity of the fault and the medium. The former is obvious when the overall comparison across the seven stations, especially along the epicentral direction, is viewed, whereas the latter can be realized by investigating the empirical results at different stations.

As mentioned earlier, the high-frequency content of the seismic ground motion is related to the details of faulting, and these details arise from the nonuniform distribution of various physical properties on the fault plane. Even though the spatio-temporal incoherency of the slip on the fault was simulated in the stochastic approach, it is not sufficient to fully represent the inhomogeneous faulting process because the other parameters and assumptions, including the final

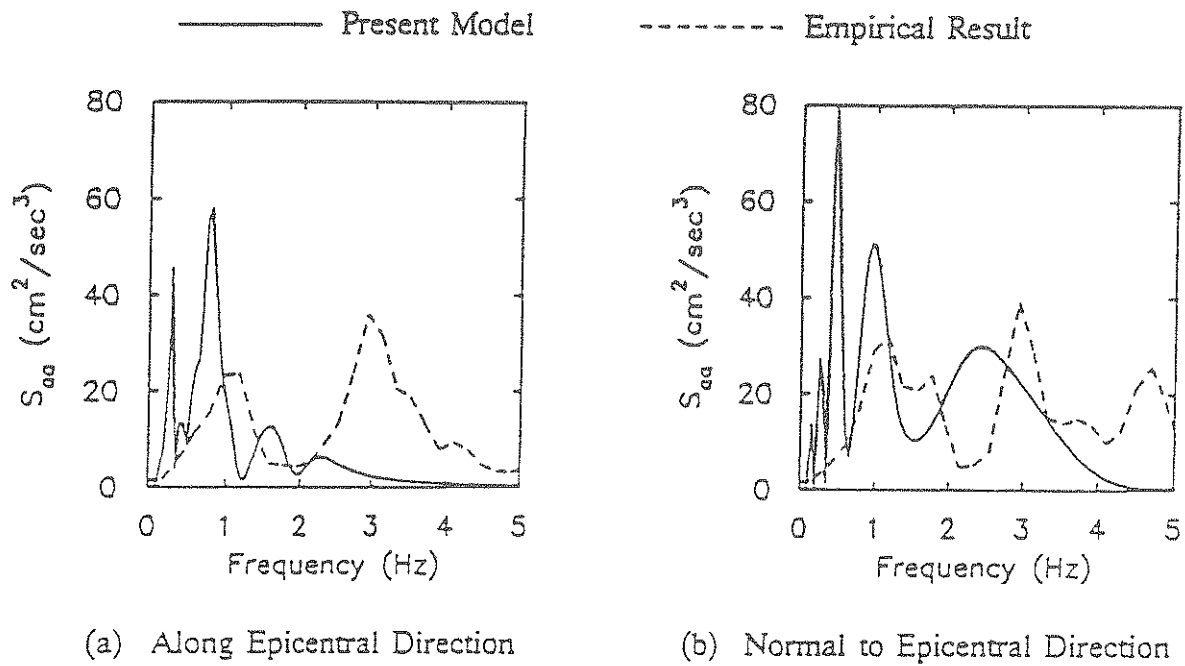


Figure 4.14 Power Spectral Densities of Acceleration at Station O06

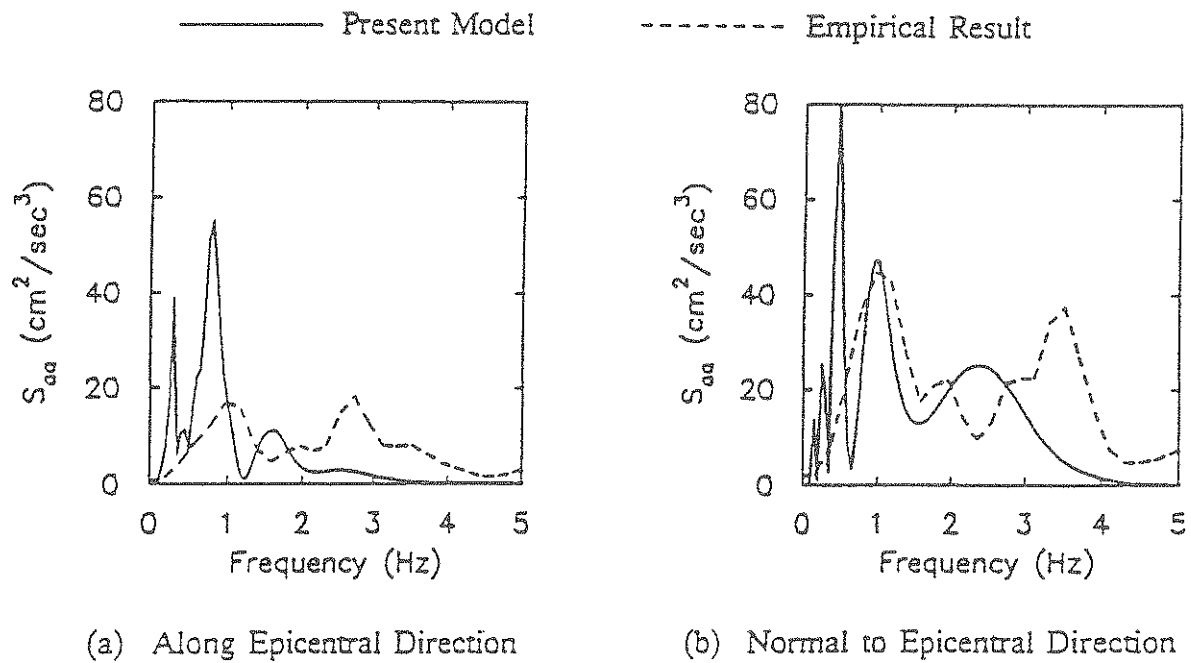


Figure 4.15 Power Spectral Densities of Acceleration at Station M06

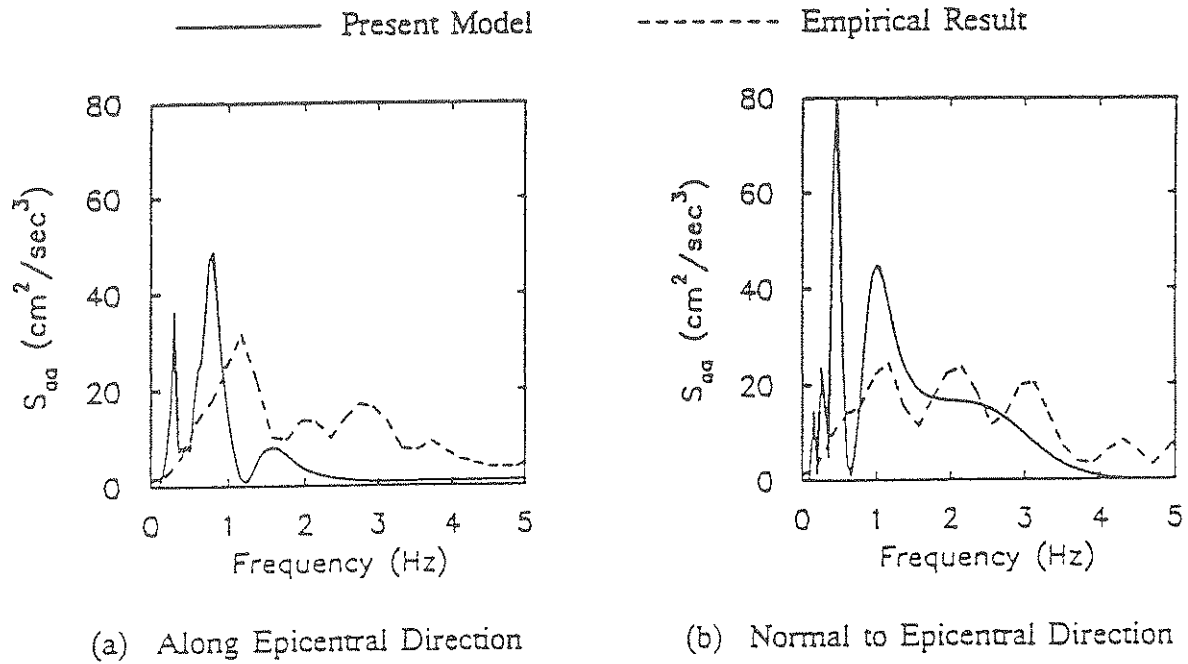


Figure 4.16 Power Spectral Densities of Acceleration at Station I06

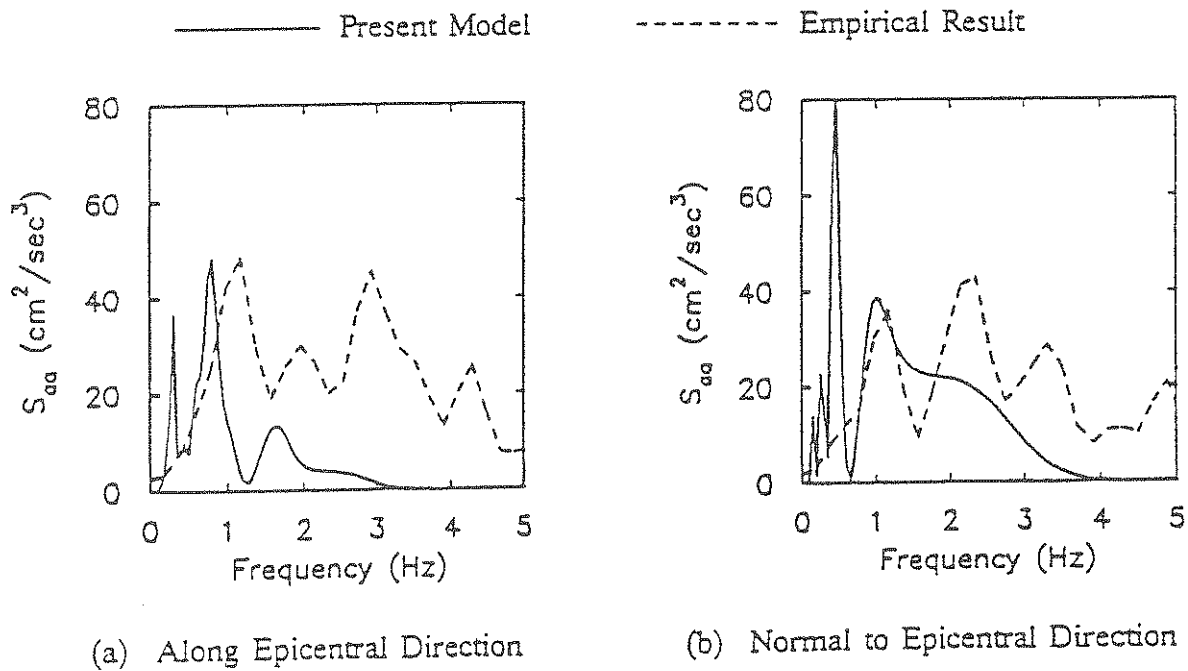


Figure 4.17 Power Spectral Densities of Acceleration at Station C00

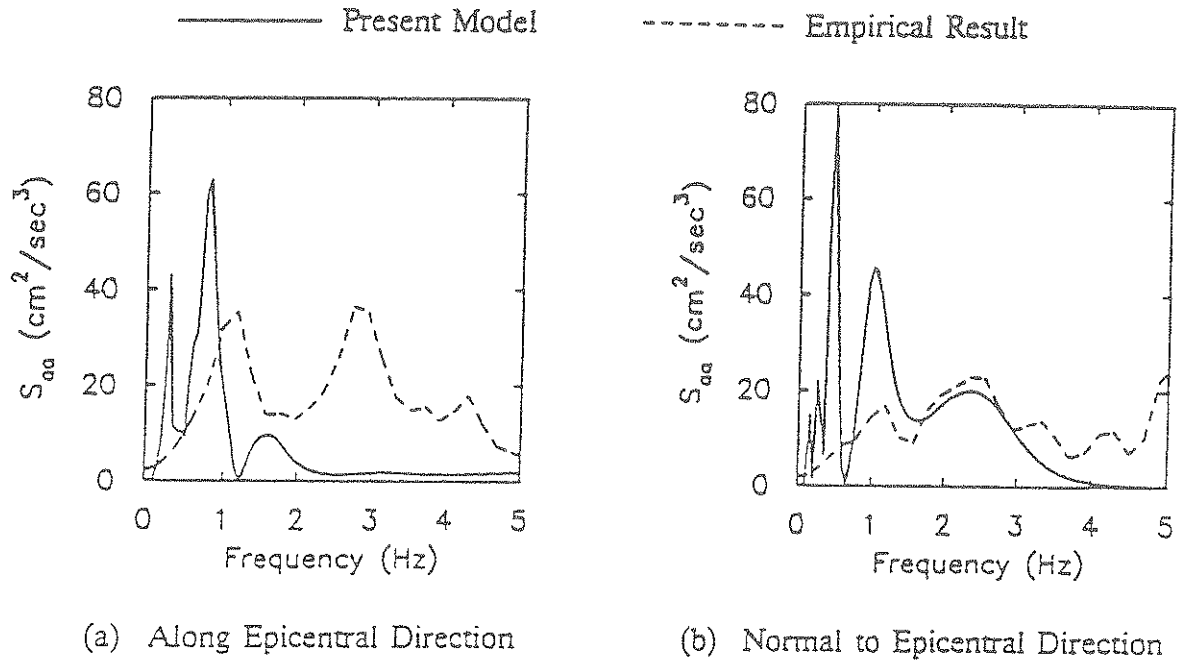


Figure 4.18 Power Spectral Densities of Acceleration at Station I12

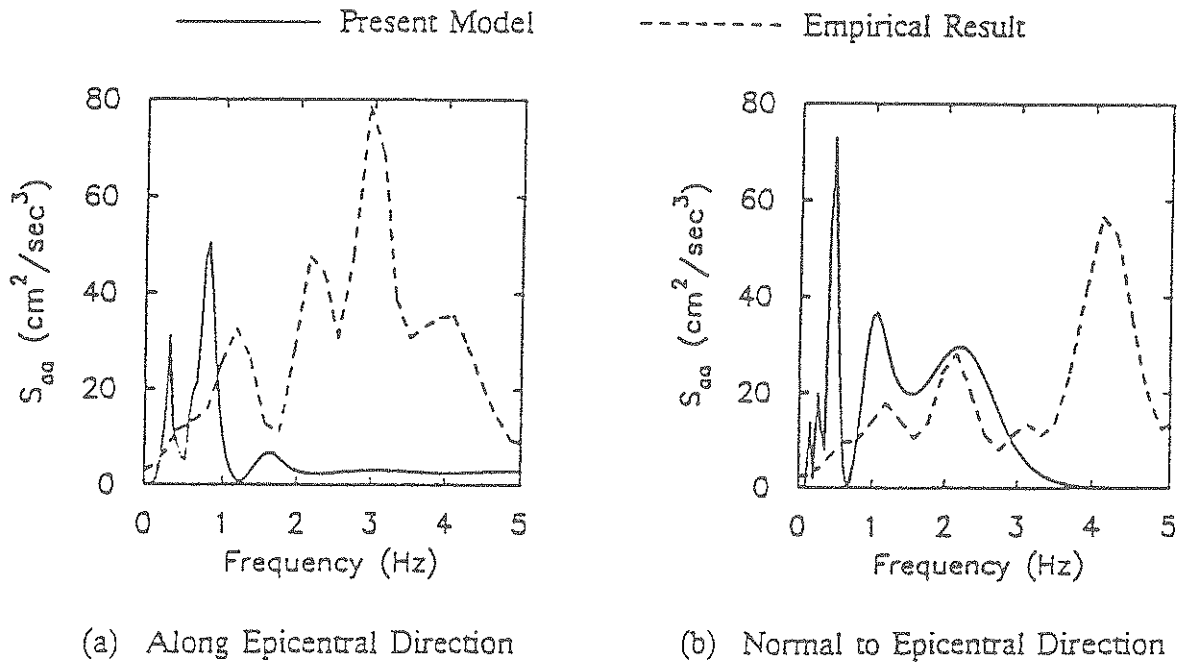


Figure 4.19 Power Spectral Densities of Acceleration at Station M12

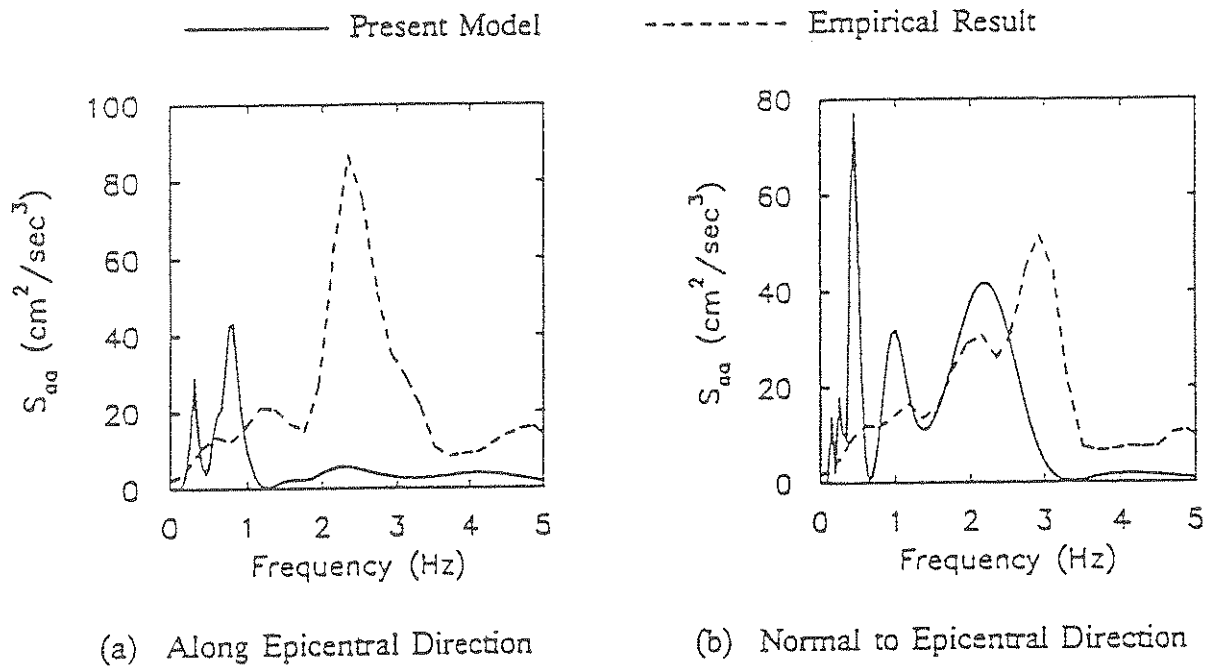


Figure 4.20 Power Spectral Densities of Acceleration at Station O12

slip, rupture direction, starting and stopping of rupture, etc., remain constant or are greatly simplified for mathematical tractability.

There might be not much need to develop more complicated model in simulating the rupture process for the analysis of pipeline response, partly because it require so many parameters that they can not be estimated practically; furthermore and more importantly, because the high-frequency region has little influence on the differential responses of pipelines. These are shown in the following section and in Section 5.

Several layers actually exist beneath the SMART-1 array (Wen and Yeh, 1984), e.g., soil, alluvium, pleistocene formation. The thickness of each layer ranges from a few meters to several hundred meters, whereas the P-wave velocity varies from 0.43 km/sec to more than 2 km/sec. The influence of these dipping layers can be seen by investigating the amplitudes of the empirical spectral at any two close stations. The peak values and the dominant frequencies of the empirical spectra vary and disperse so randomly, as shown in Figs. 4.14 through 4.20, that no general rule regarding the trend for increasing epicentral distances can be formulated. Dravinski (1984) indicated that the existence of layers results in the amplifications at some band of frequency or the reductions at other frequencies to the amplitudes of the waves propagating through the layers. The degree of amplifications or reductions as well as the affected frequencies depend on the type of wave, the number of layers, and the properties of each layer. The lower bound for the dampings in each mode of the substitute system is 0.1, which is too small to represent the effect of radiation damping in the soil, so the scattered nature of the soil may be the another reason for the overestimation of the spectra at the lower frequencies. Since the soil amplification affects the lower frequencies and

has varying effects for different stations, it should be more important than the effect of the highly irregular rupture process for the analysis of pipelines.

Differential ground motions — Two factors make the design and analysis of pipelines different from those of buildings. One is the spatial and temporal incoherent ground motions applied as the excitation to a long pipeline. Secondly, the major concern for designing a pipeline is the relative response between adjacent points. Therefore, the differential ground motion is more important than the absolute ground motion in the design and analysis of lifeline structures. Let $\Delta d(t) = d^P(t) - d^Q(t)$ be the differential ground motion between stations P and Q in a given direction. Its power spectral density is

$$S_{\Delta d \Delta d}(\omega) = S_{d^P d^P}(\omega) + S_{d^Q d^Q}(\omega) - 2 \operatorname{Re} [S_{d^P d^Q}(\omega)]. \quad (4.19)$$

In Eq. (4.19), the power and cross spectral densities of the absolute ground motions can be obtained directly from Eq. (4.16).

The power spectral densities for differential velocities and accelerations may then be evaluated as follows.

$$S_{\Delta v \Delta v}(\omega) = \omega^2 S_{\Delta d \Delta d}(\omega), \quad (4.20)$$

and

$$S_{\Delta a \Delta a}(\omega) = \omega^4 S_{\Delta d \Delta d}(\omega), \quad (4.21)$$

respectively, where Δv and Δa denote the differential ground velocity and acceleration between stations P and Q , respectively.

Figs. 4.21, 4.22 and 4.23 show the power spectral densities of the differential accelerations, velocities and displacements normal to the epicentral direction, respectively, for all the ten separation distances among the seven stations.

For the spectra of differential accelerations, the theoretical results underestimate the spectra at the lower and higher frequencies, but are almost identical at the middle range, except for distances of 0.2 km and 0.4 km. In general, the relative amplitudes of the theoretical spectra increase with the separation distance, whereas it is not the case for the empirical spectra, especially for distances of 0.4 km and 2 km. For an actual earthquake, the inhomogeneity and anisotropy of the soil medium result in a higher loss of coherence than for an idealized model, in which an elastic, homogeneous and isotropic half-space is assumed. The differences between the theoretical and empirical results may be attributed to this factor.

In the analysis of pipelines, the differential displacement response is of major concern, and it depends on the differential ground velocity and displacement. Figs. 4.22 and 4.23 show the spectra of differential ground velocities and displacements, respectively. The theoretical results show better agreement than those for differential ground accelerations. In Figs. 4.22 and 4.23, most contributions to the spectra come from the region of low frequency; that is one of the reasons why the high-frequency content is not very important for the analysis of pipelines.

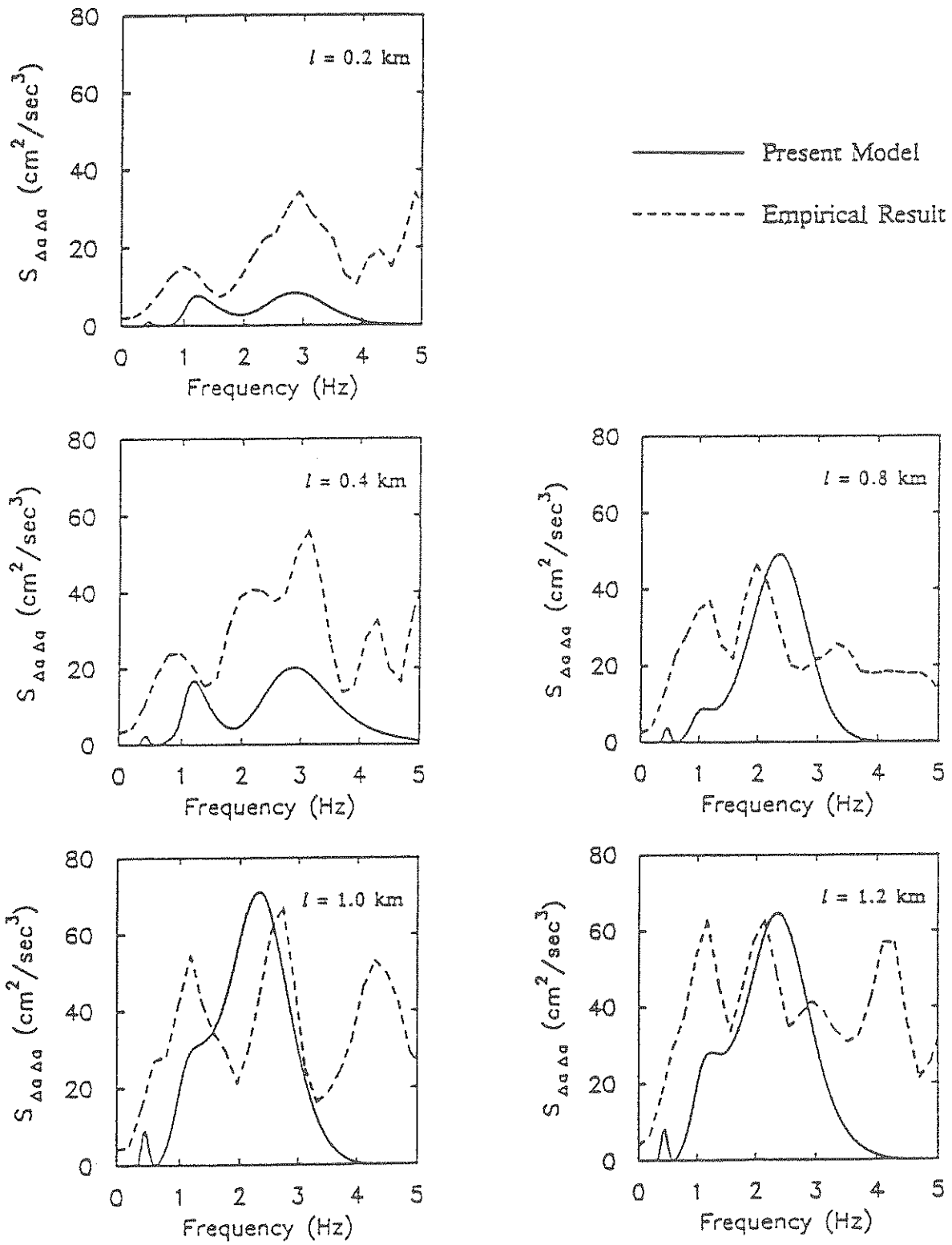


Figure 4.21 Power Spectral Densities of Differential Ground Acceleration

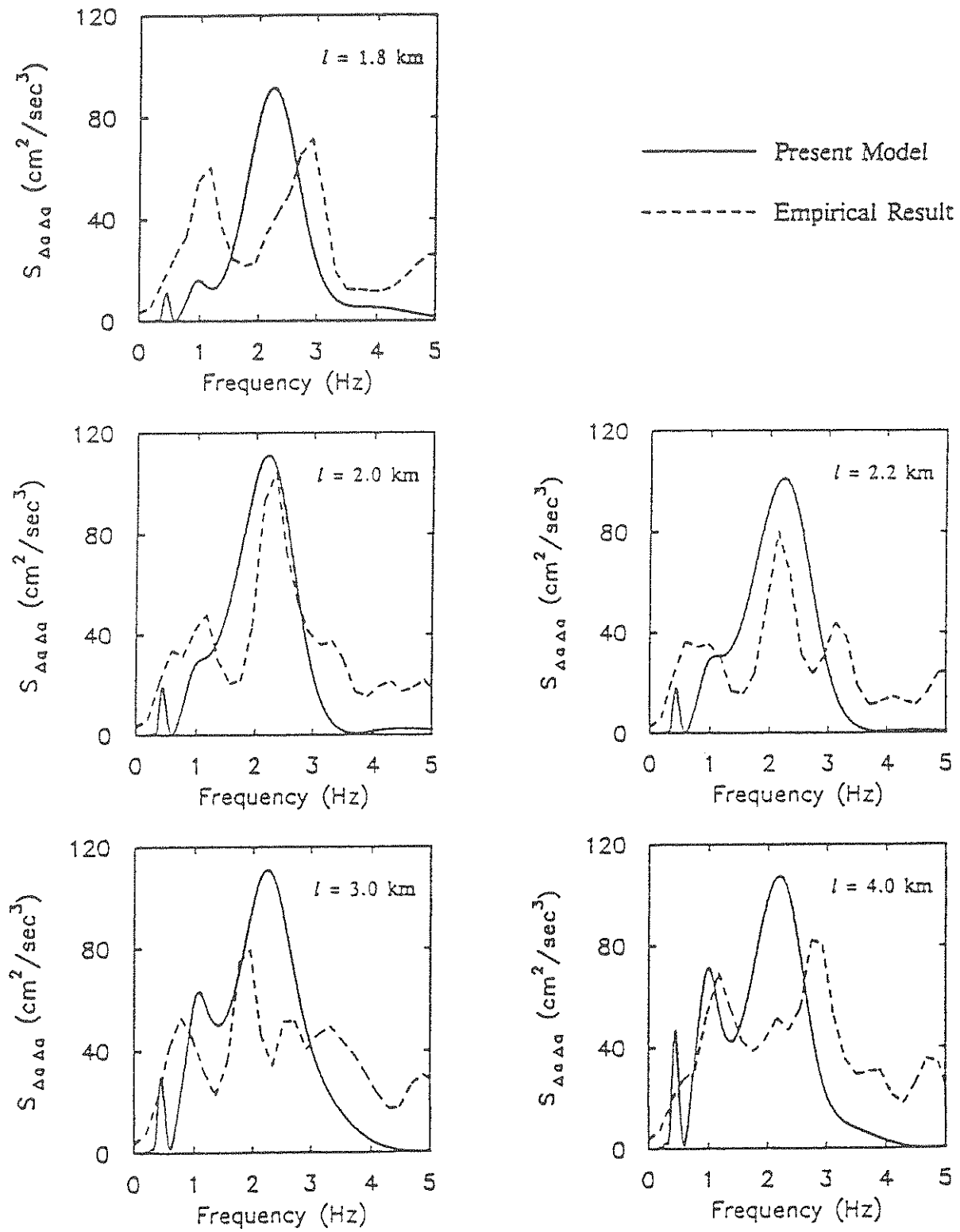


Figure 4.21 (continued)

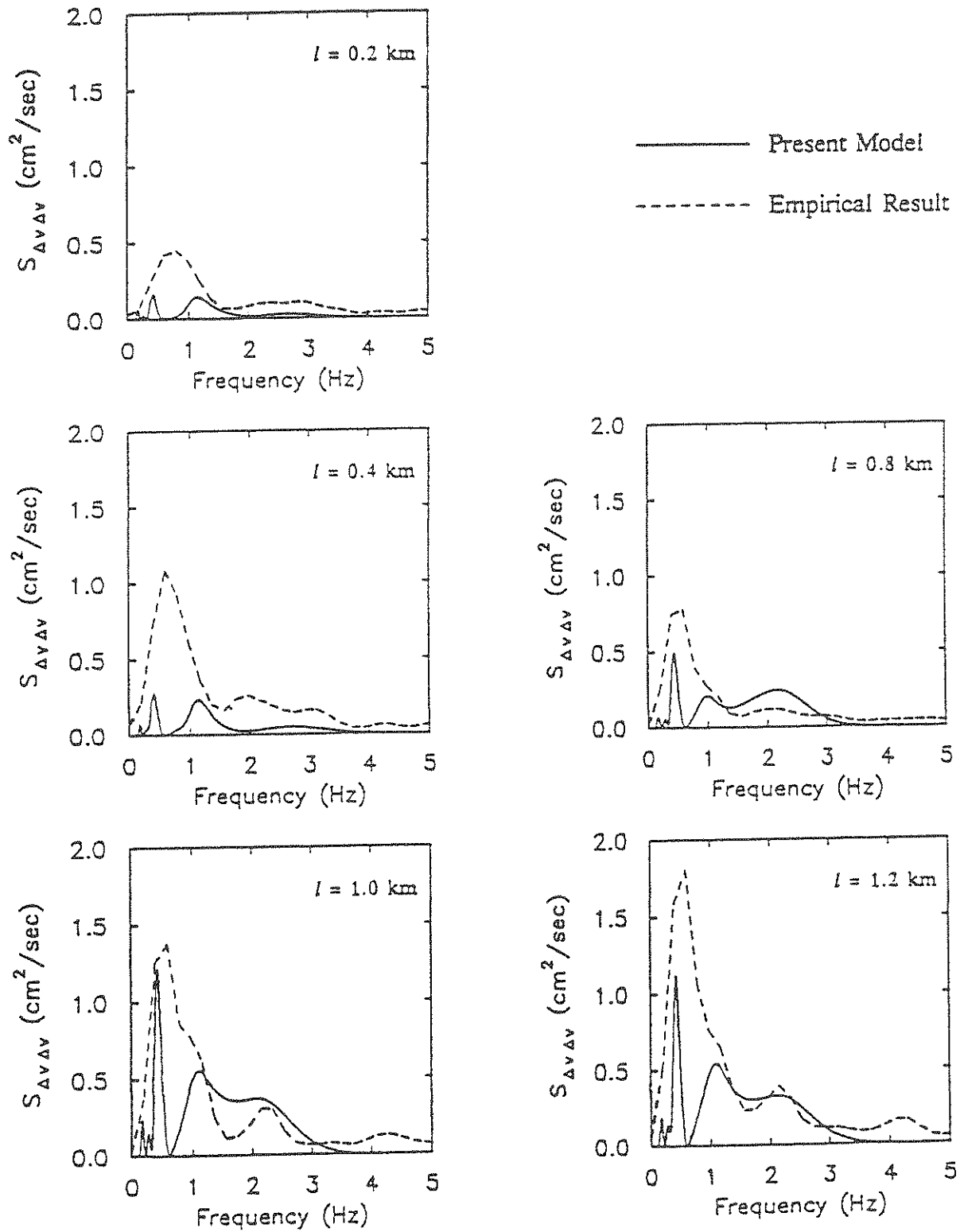


Figure 4.22 Power Spectral Densities of Differential Ground Velocity

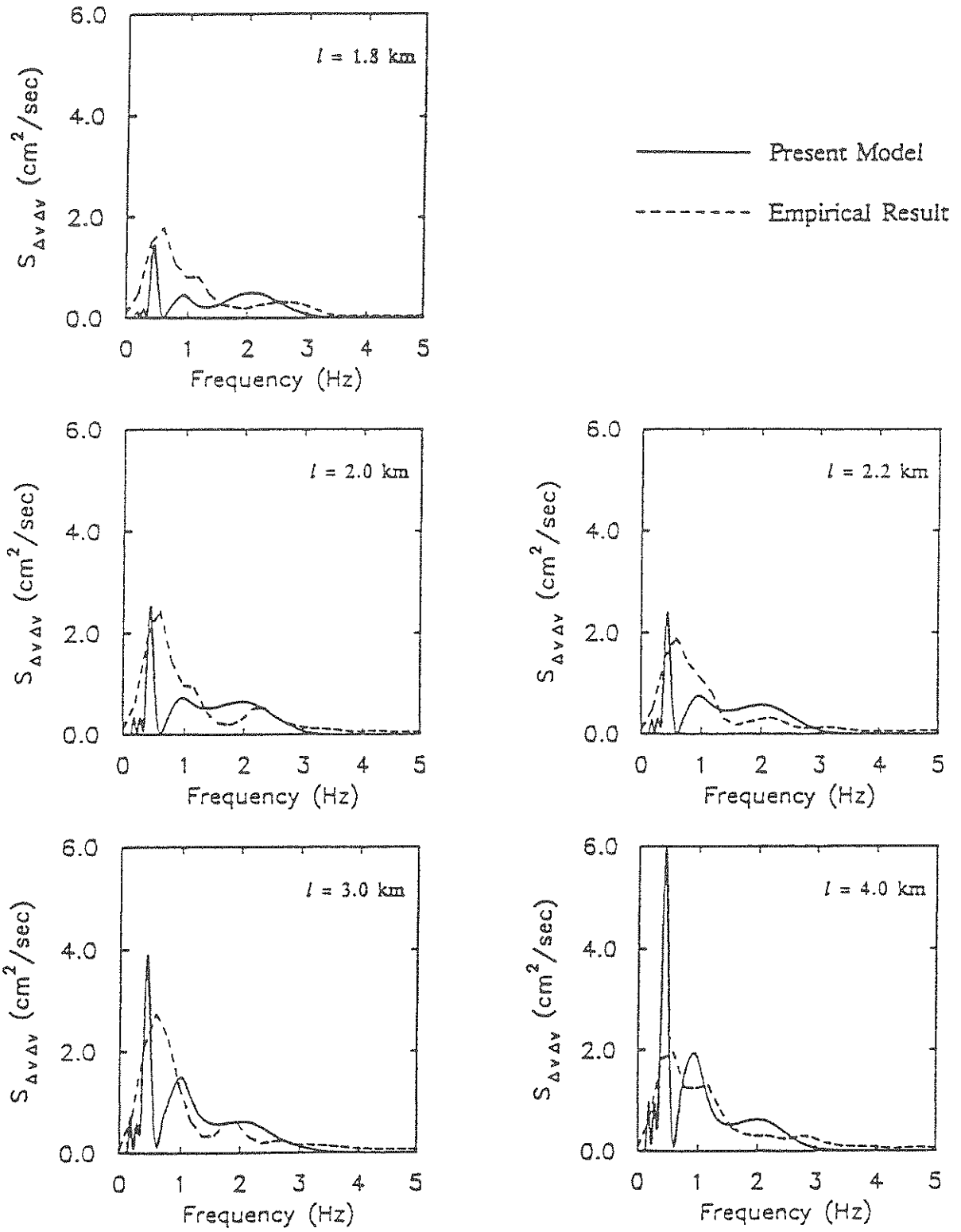


Figure 4.22 (continued)

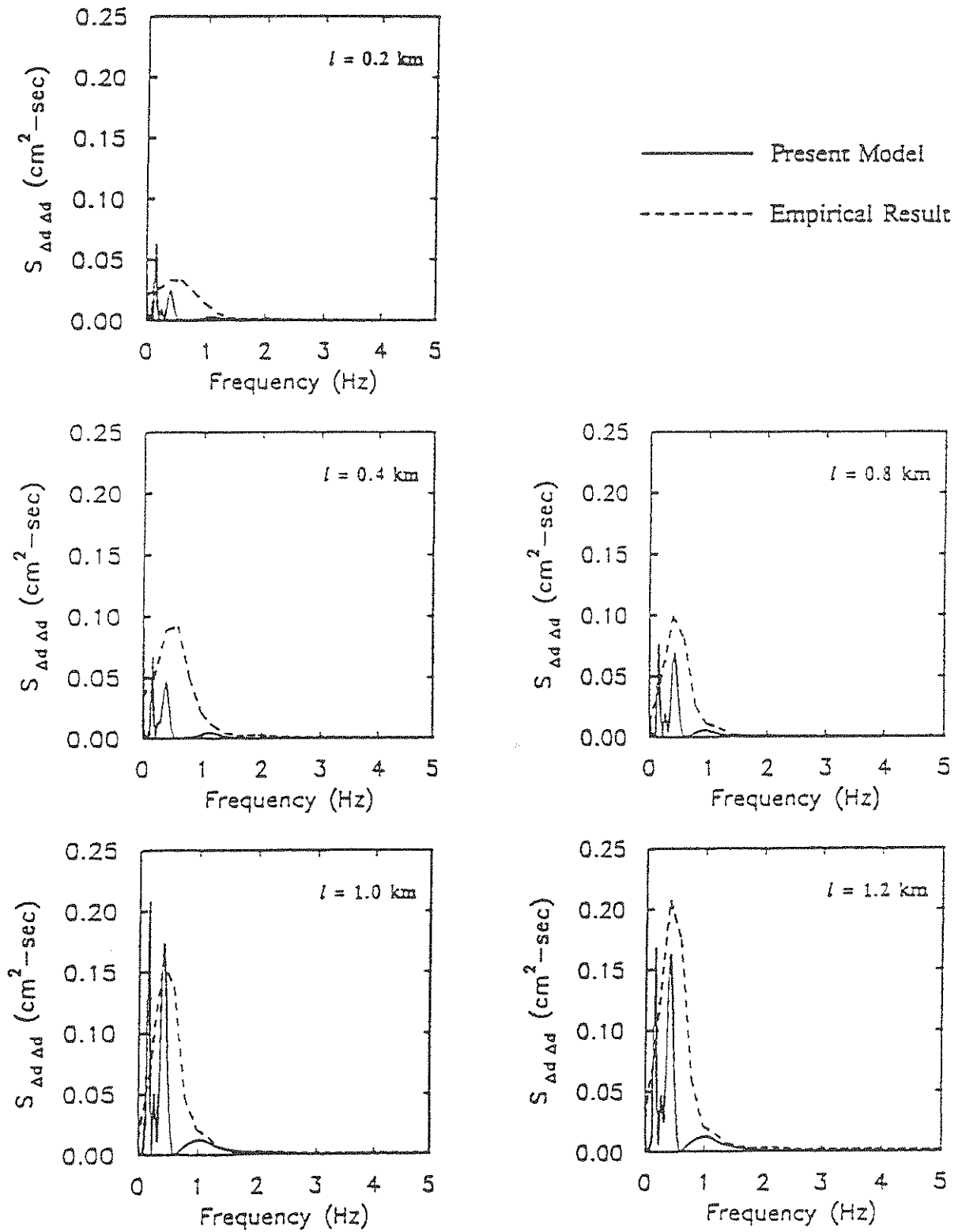


Figure 4.23 Power Spectral Densities of Differential Ground Displacement

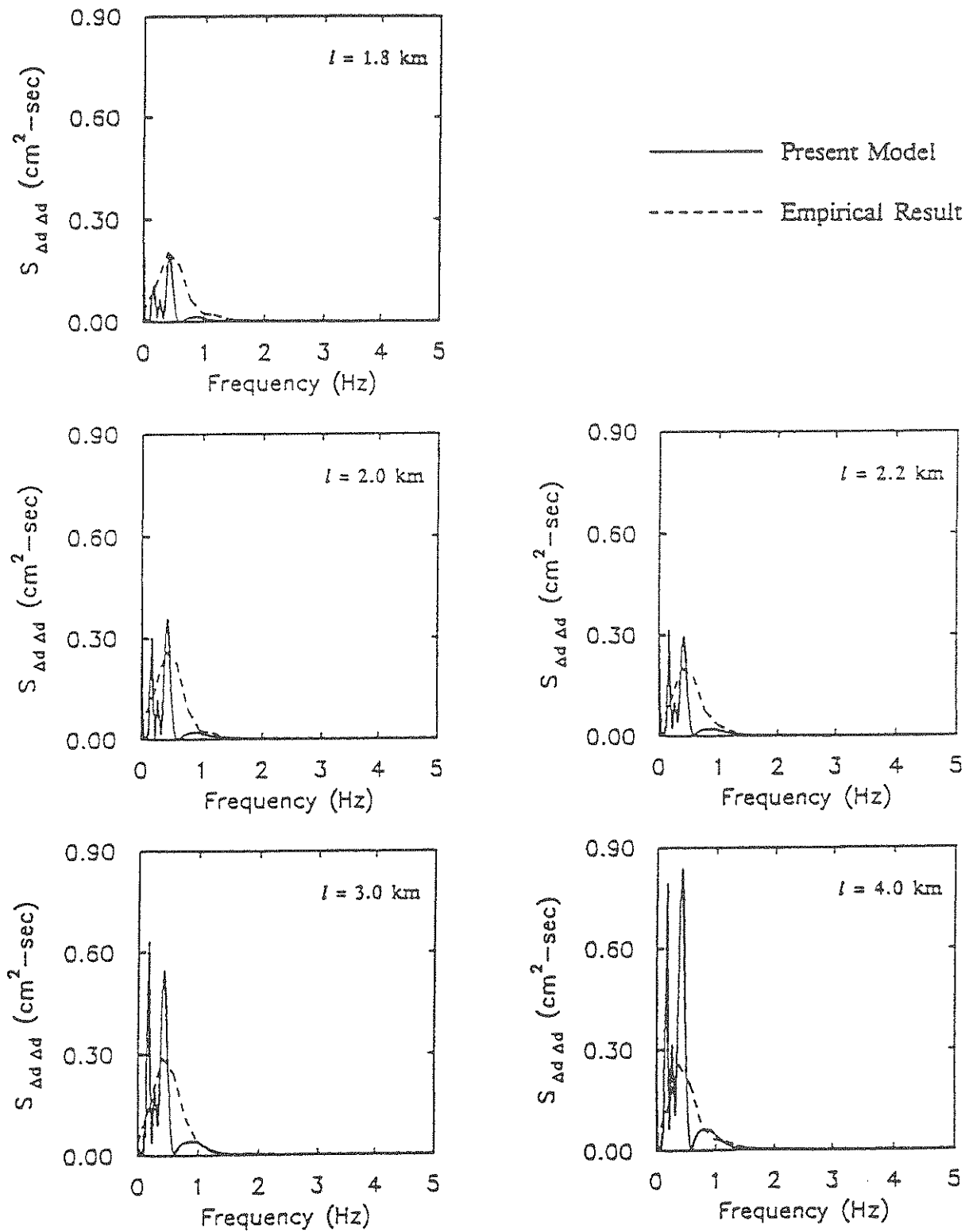


Figure 4.23 (continued)

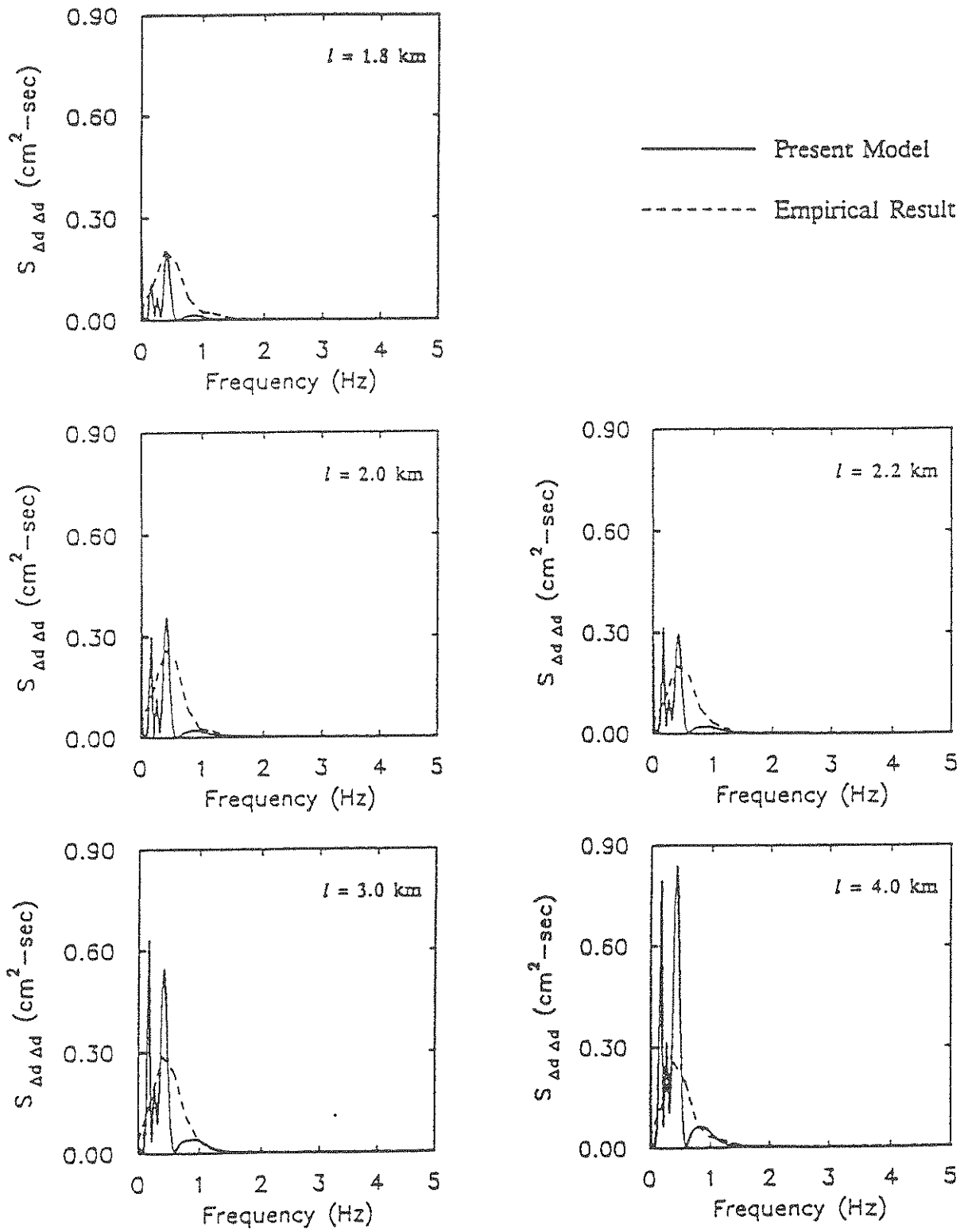


Figure 4.23 (continued)

SECTION 5

APPLICATION TO PIPELINES

5.1 Introduction

A characteristic that distinguishes a pipeline from other structures is that it extends (essentially parallel to the ground surface) over a distance which is long compared to its other dimensions. For this reason, it is inappropriate to assume that the seismic excitations at all points of ground contact are identical. When the ground motions are incoherent, the relative displacements of the points along the pipeline produce stresses, whereas coherent excitations at continuous points may result in primarily rigid body motions, with no significant strains. Therefore, the main response of engineering interest is the relative displacement of adjacent points on the pipeline, especially the differential displacements across the joints.

Nelson and Weidlinger (1977) introduced the concept of "Interference Response Spectra" in an attempt to take the incoherent seismic ground motions into account. They assumed that the interference between any two ground stations depends only on a phase shift across the separation distance, *i.e.*, the seismic wave travels with a certain constant velocity and the wave form remains unchanged. This is the simplest way to consider the traveling wave effect if only the earthquake recording at a single station is available. Although the assumption of input to pipelines is not consistent with the actual propagation of seismic waves, the discrete model of Nelson and Weidlinger (1977) representing two pipe segments connected by a joint will be used in the present study because it contains the major

elements of a pipeline and the surrounding soil, and is a basic model for analyzing the pipeline network. The incoherent ground motions developed in Section 4, however, will be applied as the ground excitations to this discrete model.

5.2 Differential Axial Motion across Joint

Fig. 5.1 shows the discrete model of pipe sections connected by a joint (Nelson and Weidlinger, 1977). The two pipe segments are assumed to behave as rigid bodies, and interconnected by a spring of stiffness k_p and a dashpot of damping c_p . Soil-structure interaction is represented by springs and dashpots of stiffness k_g and damping c_g , respectively. The constants m and l are the lumped mass and the separation of the two centroids of the segments, respectively. The axial displacements of the pipes are denoted by $x_1(t)$ and $x_2(t)$, whereas $x_{G_1}(t)$ and $x_{G_2}(t)$ are the ground excitations at the two supports. Since the axial response is of primary interest, no rotation is considered here.

5.2.1 Deterministic Analysis

The equations of motion for the discrete system in Fig. 5.1 are

$$m\ddot{x}_1 + c_p(\dot{x}_1 - \dot{x}_2) + k_p(x_1 - x_2) + c_g(\dot{x}_1 - \dot{x}_{G_1}) + k_g(x_1 - x_{G_1}) = 0, \quad (5.1)$$

$$m\ddot{x}_2 - c_p(\dot{x}_1 - \dot{x}_2) - k_p(x_1 - x_2) + c_g(\dot{x}_2 - \dot{x}_{G_2}) + k_g(x_2 - x_{G_2}) = 0. \quad (5.2)$$

Addition of the two equations, Eqs. (5.1) and (5.2), gives the equation of motion for the rigid body mode, whereas the difference of the two equations would yield the equation for differential motion, *i.e.*,

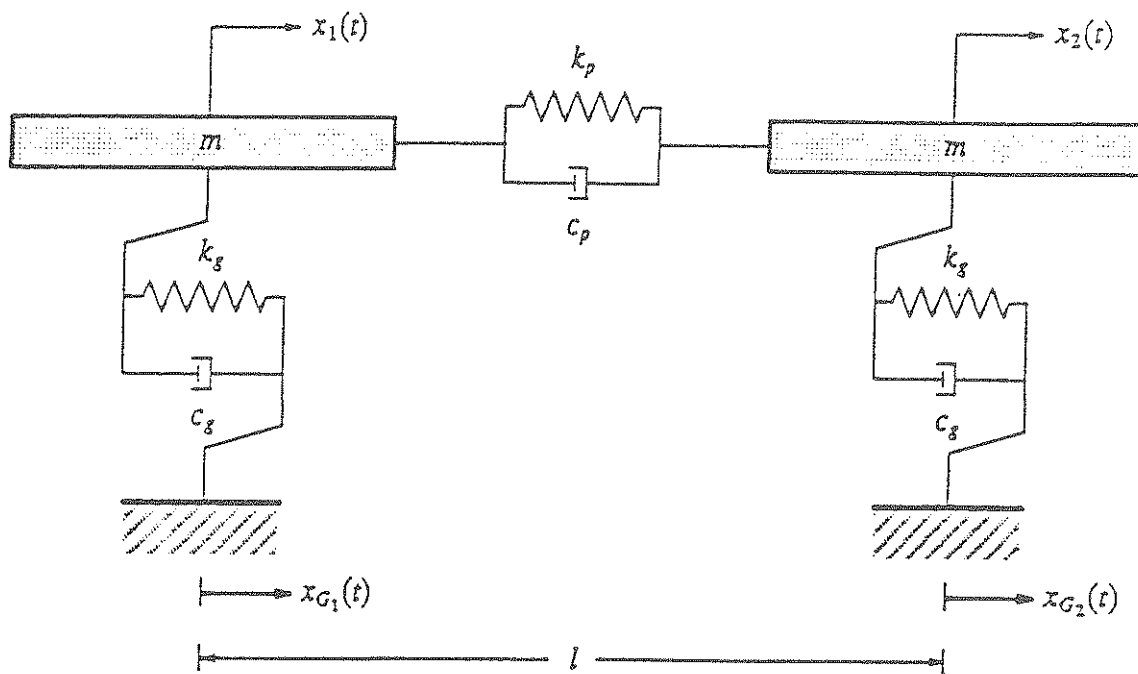


Figure 5.1 Discrete Model for Differential Axial Motion across Joint

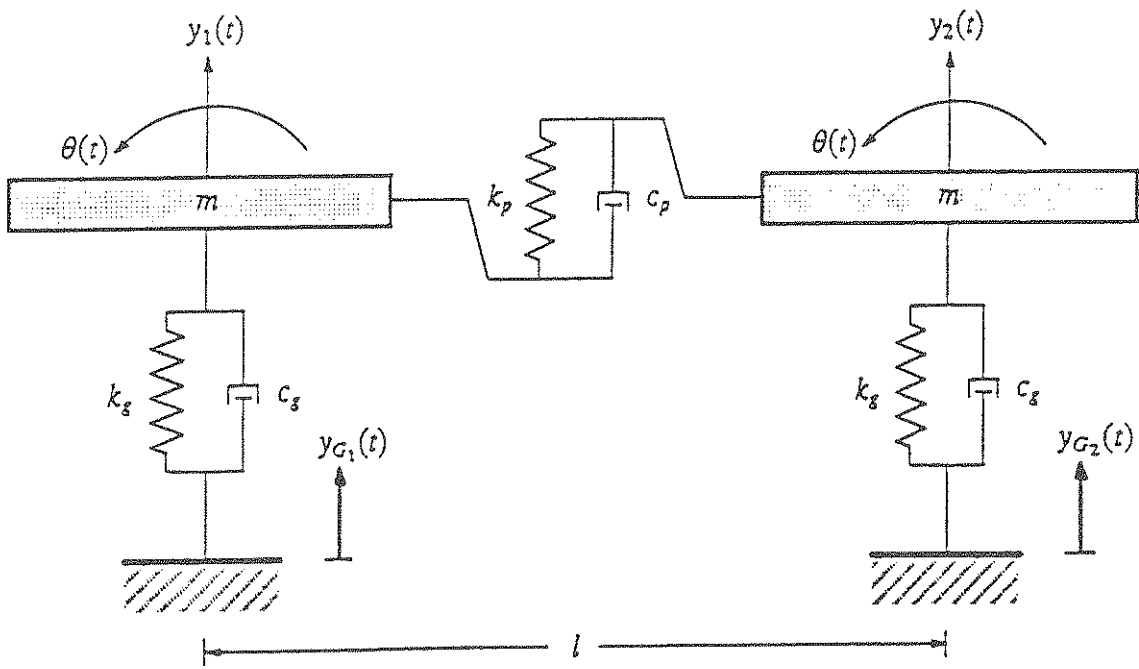


Figure 5.2 Discrete Model for Differential Transverse Motion across Joint

$$\Delta \ddot{x} + 2\xi_0 \omega_0 \Delta \dot{x} + \omega_0^2 \Delta x = \frac{1}{1+2\lambda} F_0(t), \quad (5.3)$$

where:

$$\Delta x = x_1(t) - x_2(t),$$

$$2\xi_0 \omega_0 = (c_g + 2c_p)/m,$$

$$\omega_0^2 = (k_g + 2k_p)/m,$$

$$\lambda = k_p/k_g = c_p/c_g,$$

$$F_0(t) = 2\xi_0 \omega_0 \Delta \dot{x}_G(t) + \omega_0^2 \Delta x_G(t),$$

$$\Delta x_G = x_{G1}(t) - x_{G2}(t).$$

In Eq. (5.3), Δx may be evaluated by the Duhamel integral, *i.e.*,

$$\Delta x(t) = \int_0^t h_0(t-\tau) \frac{1}{1+2\lambda} F_0(\tau) d\tau, \quad (5.4)$$

where the impulse response function is

$$h_0(t) = \frac{1}{\omega_0 \sqrt{1-\xi_0^2}} e^{-\xi_0 \omega_0 t} \sin \omega_0 \sqrt{1-\xi_0^2} t. \quad (5.5)$$

5.2.2 Stochastic Analysis

Using Eq. (5.3), the power spectral density of the differential axial displacement Δx is

$$S_{\Delta x \Delta x}(\omega) = \frac{1}{(1+2\lambda)^2} |H_0(\omega)|^2 S_{F_0 F_0}(\omega), \quad (5.6)$$

where:

$$|H_0(\omega)|^2 = \frac{1}{(\omega_0^2 - \omega^2)^2 + 4\xi_0^2\omega_0^2\omega^2},$$

$$S_{F_0\bar{F}_0}(\omega) = 4\xi_0^2\omega_0^2 S_{\Delta\ddot{x}_G\Delta\ddot{x}_G}(\omega) + \omega_0^4 S_{\Delta x_G\Delta x_G}(\omega)$$

$$= \frac{1}{\omega^4} (4\xi_0^2\omega_0^2\omega^2 + \omega_0^4) S_{\Delta\ddot{x}_G\Delta\ddot{x}_G}(\omega).$$

Therefore, Eq. (5.6) becomes

$$S_{\Delta x\Delta x}(\omega) = \frac{1}{(1+2\lambda)^2\omega^4} (4\xi_0^2\omega_0^2\omega^2 + \omega_0^4) |H_0(\omega)|^2 S_{\Delta\ddot{x}_G\Delta\ddot{x}_G}(\omega), \quad (5.7)$$

in which $S_{\Delta\ddot{x}_G\Delta\ddot{x}_G}(\omega)$ is the power spectral density of the differential ground acceleration obtained in Section 4.

5.3 Differential Transverse Motion across Joint

Zerva, *et al.* (1985) added the rotational motions to Nelson and Weidlingers' discrete model when the pipes are subjected to lateral excitations. There are two rotational motions, one for each pipe segment, in Zerva, *et al.* (1985). Since the equations of motion governing the two rotations are equal, the rotations of the two pipe segments must be identical, as shown in Fig. 5.2.

5.3.1 Deterministic Analysis

In this case, the equations of motion for the discrete system in Fig. 5.2 are

$$m\ddot{y}_1 + c_p(\dot{y}_1 - \dot{y}_2 + l\dot{\theta}) + k_p(y_1 - y_2 + l\theta) + c_s(\dot{y}_1 - \dot{y}_{G_1}) + k_s(y_1 - y_{G_1}) = 0, \quad (5.8)$$

$$m\ddot{y}_2 - c_p(\dot{y}_1 - \dot{y}_2 + l\dot{\theta}) - k_p(y_1 - y_2 + l\theta) + c_s(\dot{y}_2 - \dot{y}_{G_2}) + k_s(y_2 - y_{G_2}) = 0, \quad (5.9)$$

$$\frac{1}{12}ml^2\ddot{\theta} + c_p \frac{l}{2}(\dot{y}_1 - \dot{y}_2 + l\dot{\theta}) + k_p \frac{l}{2}(y_1 - y_2 + l\theta) = 0, \quad (5.10)$$

where:

y_1, y_2 = the transverse displacements of the pipe segments,

θ = the rotation of the pipe segments,

m = the mass of the pipe segments,

l = the distance between the centers of the two pipe segments,

k_p, c_p = the stiffness and damping between the pipe segments, respectively,

k_s, c_s = the stiffness and damping of the soil, respectively,

y_{G_1}, y_{G_2} = the transverse ground displacements at the two supports.

The differential transverse displacement between the two pipe segments is

$$\Delta y(t) = y_1(t) - y_2(t) + l\theta(t). \quad (5.11)$$

Hence, Eqs. (5.8) through (5.10) can be represented in matrix form by

$$[M]\{\ddot{Y}\} + [C]\{\dot{Y}\} + [K]\{Y\} = \{F(t)\}, \quad (5.12)$$

where:

$$[M] = \begin{bmatrix} m & 0 & 0 \\ 0 & m & 0 \\ -m/6 & m/6 & m/6 \end{bmatrix},$$

$$[C] = \begin{bmatrix} c_g & 0 & c_p \\ 0 & c_g & -c_p \\ 0 & 0 & c_p \end{bmatrix},$$

$$[K] = \begin{bmatrix} k_g & 0 & k_p \\ 0 & k_g & -k_p \\ 0 & 0 & k_p \end{bmatrix},$$

$$\{Y\} = \begin{Bmatrix} y_1(t) \\ y_2(t) \\ \Delta y(t) \end{Bmatrix},$$

$$\{F(t)\} = \begin{Bmatrix} c_g \dot{y}_{G_1}(t) + k_g y_{G_1}(t) \\ c_g \dot{y}_{G_2}(t) + k_g y_{G_2}(t) \\ 0 \end{Bmatrix}.$$

The natural frequencies of the system are

$$\omega_{1,2}^2 = \frac{(8k_p + k_g) \mp \sqrt{64k_p^2 - 8k_p k_g + k_g^2}}{2m}, \quad (5.13)$$

and

$$\omega_3^2 = \frac{k_g}{m}. \quad (5.14)$$

The corresponding modal shapes are

$$\{\Phi_{1,2}\} = \begin{Bmatrix} 1 \\ -1 \\ \phi_{1,2} \end{Bmatrix}, \quad (5.15)$$

and

$$\{\Phi_3\} = \begin{Bmatrix} 1 \\ 1 \\ 0 \end{Bmatrix}, \quad (5.16)$$

in which

$$\phi_{1,2} = \frac{\omega_{1,2}^2 m - k_g}{k_p} = \frac{(8k_p - k_g) \mp \sqrt{64k_p^2 - 8k_p k_g + k_g^2}}{2k_p}. \quad (5.17)$$

Observe that the third mode is the rigid body motion. For simplicity, it is assumed again that

$$\frac{k_p}{k_g} = \frac{c_p}{c_g} = \lambda.$$

Then, the natural frequencies of the first two modes are

$$\omega_{1,2}^2 = \left[(8\lambda + 1) \mp \sqrt{64\lambda^2 - 8\lambda + 1} \right] \frac{\omega_3^2}{2}, \quad (5.18)$$

and the associated mode shapes become

$$\phi_{1,2} = \frac{1}{2\lambda} \left[(8\lambda - 1) \mp \sqrt{64\lambda^2 - 8\lambda + 1} \right]. \quad (5.19)$$

If modal superposition is applicable, *i.e.*, stiffness proportional damping is assumed, then Eq. (5.12) yields the uncoupled equations,

$$\ddot{z}_n + 2\dot{\xi}_n \omega_n \dot{z}_n + \omega_n^2 z_n = \frac{F_n(t)}{M_n}, \quad n = 1, 2, 3; \quad (5.20)$$

where:

$$\begin{Bmatrix} y_1(t) \\ y_2(t) \\ \Delta y(t) \end{Bmatrix} = \begin{bmatrix} 1 & 1 & 1 \\ -1 & -1 & 1 \\ \phi_1 & \phi_2 & 0 \end{bmatrix} \begin{Bmatrix} z_1(t) \\ z_2(t) \\ z_3(t) \end{Bmatrix},$$

$\dot{\xi}_n$ = the modal damping,

$$M_{1,2} = m \left(2 - \frac{1}{3} \phi_{1,2} + \frac{1}{6} \phi_{1,2}^2 \right),$$

$$M_3 = 2m,$$

$$F_{1,2} = c_g (\dot{y}_{G_1} - \dot{y}_{G_2}) + k_g (y_{G_1} - y_{G_2}),$$

$$F_3 = c_g (\dot{y}_{G_1} + \dot{y}_{G_2}) + k_g (y_{G_1} + y_{G_2}),$$

$$c_g = 2\dot{\xi}_3 \omega_3 m,$$

$$k_g = \omega_3^2 m.$$

The generalized displacement for each mode, $z_n(t)$, may be evaluated through the Duhamel integral, *i.e.*,

$$z_n(t) = \frac{1}{M_n} \int_0^t h_n(t-\tau) F_n(\tau) d\tau, \quad n = 1, 2, 3; \quad (5.21)$$

in which

$$h_n(t) = \frac{1}{\omega_n \sqrt{1 - \xi_n^2}} e^{-\xi_n \omega_n t} \sin \omega_n \sqrt{1 - \xi_n^2} t, \quad n = 1, 2, 3. \quad (5.22)$$

Moreover, the differential transverse displacement between the two pipe segments is expressed in terms of the generalized displacements as

$$\Delta y(t) = \phi_1 z_1(t) + \phi_2 z_2(t). \quad (5.23)$$

5.3.2 Stochastic Analysis

Using Eq. (5.23), the power spectral density of the differential transverse displacement Δy can be obtained as

$$S_{\Delta y \Delta y}(\omega) = \phi_1^2 S_{z_1 z_1}(\omega) + \phi_1 \phi_2 [S_{z_1 z_2}(\omega) + S_{z_2 z_1}(\omega)] + \phi_2^2 S_{z_2 z_2}(\omega). \quad (5.24)$$

In Eq. (5.24), the power and cross spectral densities of the generalized displacements are obtained from Eq. (5.21), *i.e.*,

$$S_{z_m z_n}(\omega) = \frac{1}{M_m M_n} H_m^*(\omega) H_n(\omega) S_{F_m F_n}(\omega), \quad m, n = 1, 2; \quad (5.25)$$

in which $*$ denotes the complex conjugate, and H is the frequency transfer function given by

$$H_n(\omega) = \frac{1}{\omega_n^2 - \omega^2 + 2i\xi_n\omega_n\omega}, \quad n = 1, 2. \quad (5.26)$$

The corresponding cross spectral density of the generalized force is

$$\begin{aligned} S_{F_m F_n}(\omega) &= c_g^2 S_{\Delta \dot{y}_G \Delta \dot{y}_G}(\omega) + c_g k_g [S_{\Delta \dot{y}_G \Delta y_G}(\omega) + S_{\Delta y_G \Delta \dot{y}_G}(\omega)] + k_g^2 S_{\Delta y_G \Delta y_G}(\omega). \\ &= \left(\frac{c_g^2}{\omega^2} + \frac{k_g^2}{\omega^4} \right) S_{\Delta \dot{y}_G \Delta \dot{y}_G}(\omega), \quad m, n = 1, 2. \end{aligned} \quad (5.27)$$

Finally, substituting Eqs. (5.25) and (5.27) into Eq. (5.24), the power spectral density of the differential transverse displacement for the pipes excited by the incoherent ground motions is

$$\begin{aligned} S_{\Delta y \Delta y}(\omega) &= \left[\frac{\phi_1^2}{M_1^2} |H_1(\omega)|^2 + 2 \frac{\phi_1 \phi_2}{M_1 M_2} \text{Re} \{ H_1(\omega) H_2(\omega) \} + \frac{\phi_2^2}{M_2^2} |H_2(\omega)|^2 \right] \\ &\quad \cdot \left(\frac{c_g^2}{\omega^2} + \frac{k_g^2}{\omega^4} \right) S_{\Delta \dot{y}_G \Delta \dot{y}_G}(\omega). \end{aligned} \quad (5.28)$$

5.4 Comparison of Results

In order to compare the results derived from the present model with the field recordings from the SMART-1 array, the orientation and location of the pipeline studied in this section will be assumed to coincide with the epicentral direction of Event 5 (*i.e.*, N26.2°W) and close to station C00, respectively. Therefore, the ground excitations applied to the pipeline in the axial direction are the seismic ground motions along the epicentral direction, whereas the input in the transverse direction are the ground motions normal to the epicentral direction.

Loh, *et al.* (1983) used the interference response spectra to estimate the differential axial motion between two pipe segments for the earthquake of Event 5. Zerva, *et al.* (1985) then compared the results of a 2-D model with those from the interference response spectra. Since the method of interference response spectra oversimplified the propagation of waves between the two supports of the pipeline and the field data from a dense array are now available, the comparison in the study will be performed primarily between the results of the current 3-D model and the responses excited by the recordings of the SMART-1 array. The corresponding interference response spectra are also shown.

First of all, two parameters in the discrete model of a pipeline should be evaluated to represent an actual pipeline. λ stands for the ratio of c_p , the damping of the connection between the pipe segments, to c_s , the damping of the soil. The former is much less than the latter, so a value of 1/5 will be assumed for λ . Furthermore, since the damping of pipelines may be higher than that in buildings, two values of damping ratio, namely 5% and 10% of critical, will be adopted here, *i.e.*,

$$\xi_0 = \xi_1 = \xi_2 = \xi_3 = 5\% \text{ or } 10\%,$$

where ξ_0 is the damping ratio in Eq. (5.3) for the analysis of the differential axial displacement in pipelines, and ξ_n , $n = 1, 2, 3$, are the model damping in Eq. (5.20) for the analysis of the differential transverse motion. These two selected values (5% and 10%) could conceivably be the lower and upper bound damping values for a practical pipeline.

The differential displacements of the pipes subjected to the earthquake of

Event 5 were obtained through the deterministic analyses in the previous sections by using the array recordings as input. For the interference method, the recordings at the station with the shortest epicentral distance were used; the ground motion at the other station was determined by assuming the above excitation traveling with a constant velocity which was obtained by the separation distance and the difference in the arrival times of the two stations. On the other hand, the power spectral densities of differential displacements are evaluated through the stochastic analyses using the power spectral densities of the differential ground motions obtained for the substitute system. Because of its importance in the analysis and design of pipelines, the maximum differential displacement across a joint is emphasized. For the stochastic analysis, the mean maximum differential displacement and the associated standard deviation over the duration of an earthquake are evaluated using an asymptotic expression (Davenport, 1964), as follows:

$$\mu_{\Delta u_m} = \left[\sqrt{2 \ln(\nu T)} + \frac{0.5772}{\sqrt{2 \ln(\nu T)}} \right] \sigma_{\Delta u}, \quad (5.29)$$

$$\sigma_{\Delta u_m} = \frac{\pi}{\sqrt{6}} \frac{1}{\sqrt{2 \ln(\nu T)}} \sigma_{\Delta u}, \quad (5.30)$$

where:

$$\Delta u_m = \max_{0 \leq t \leq T} |\Delta u(t)|,$$

Δu = the differential displacement, *i.e.*, Δx for axial motion, Δy for transverse motion,

T = the duration of the record,

$$\nu = \frac{1}{\pi} \frac{\sigma_{\Delta \dot{u}}}{\sigma_{\Delta u}},$$

$$\sigma_{\Delta u}^2 = \int_{-\infty}^{\infty} S_{\Delta u \Delta u}(\omega) d\omega,$$

$$\sigma_{\Delta \dot{u}}^2 = \int_{-\infty}^{\infty} \omega^2 S_{\Delta u \Delta u}(\omega) d\omega.$$

The results shown in Figs. 5.3 through 5.6 include the maximum differential displacements from the deterministic analysis, the mean maximum differential displacements and the mean plus one standard deviation obtained by the stochastic analysis. Each figure, which was called the "interference response spectrum" in Nelson and Weidlinger (1977) or "differential response spectrum" in Zerva, *et al.* (1985), shows the maximum differential response plotted as a function of the natural frequency of a system. The natural frequency in Figs. 5.3 and 5.4 for the axial discrete model of pipelines is that in the equation of the differential axial motion, *i.e.*, ω_0 in Eq. (5.3), whereas the natural frequency in Figs. 5.5 and 5.6 for the transverse motion stands for the natural frequency of the rigid body mode, *i.e.*, ω_3 in Eq. (5.20). Seven separation distances, namely $l = 20$ m, 50 m, 200 m, 0.4 km, 0.8 km, 1 km, and 1.2 km, as well as two representative dampings, *i.e.*, 5% and 10%, are considered in these figures. Observe that there are no field recordings at separation distances of $l = 20$ m and 50 m.

In general, the mean maximum differential displacements of pipelines predicted with the proposed model are on the safe side for all frequencies. The existence of local layers in the SMART-1 array site produced the seismic ground motions so incoherently, even for short distances, that the spatial variation of ground motions can not be simulated well by a homogeneous theoretical model

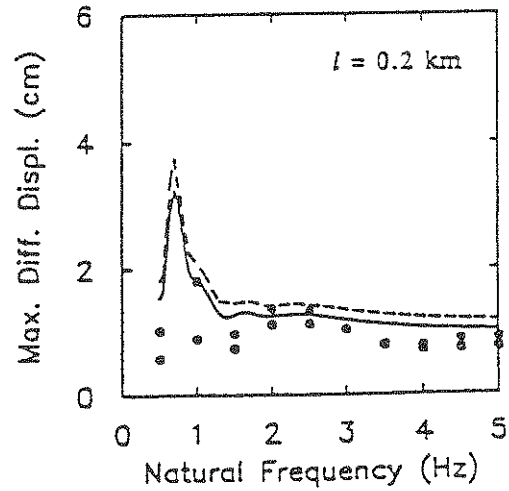
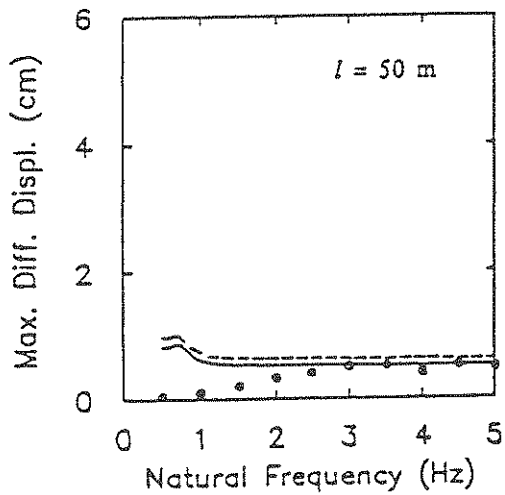
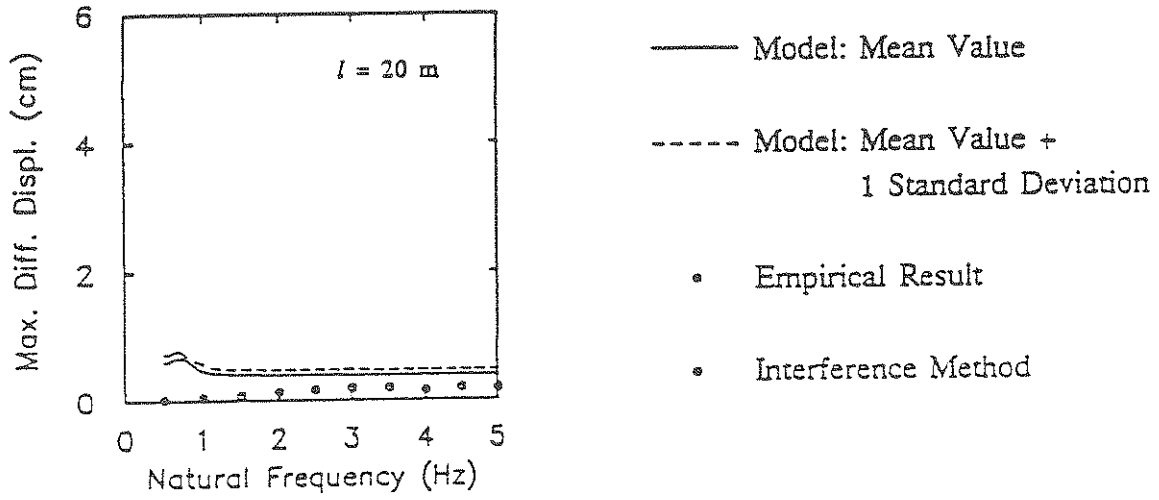


Figure 5.3 Differential Axial Displacement Response Spectra ($\xi_0 = 5\%$)

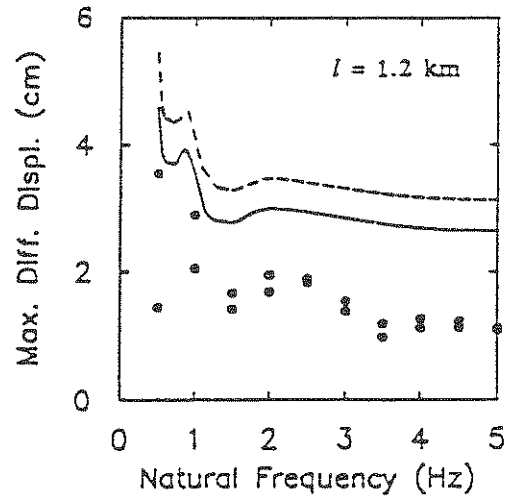
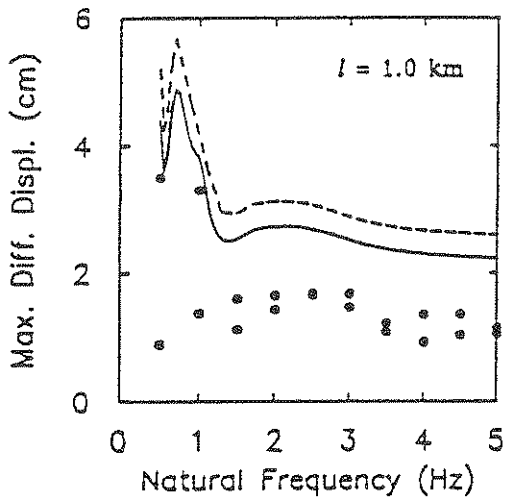
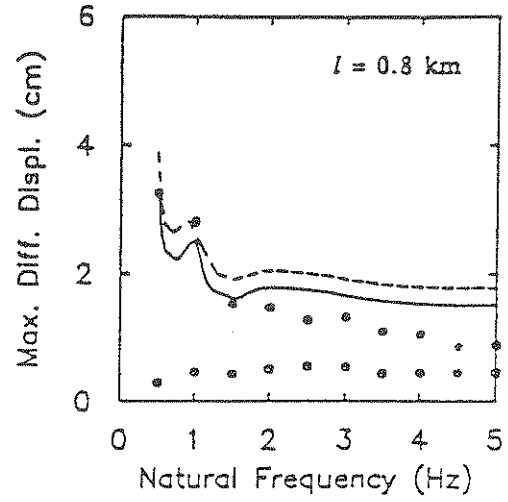
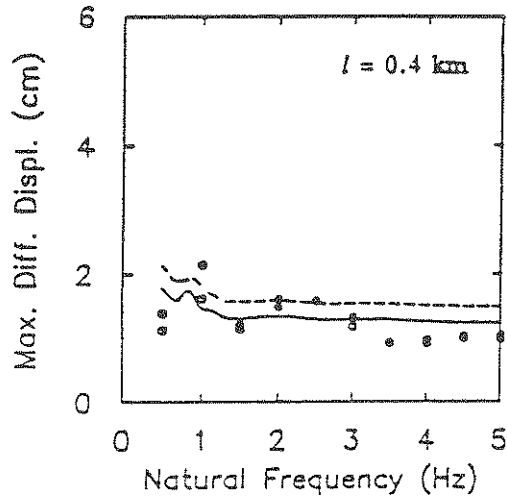


Figure 5.3 (continued)

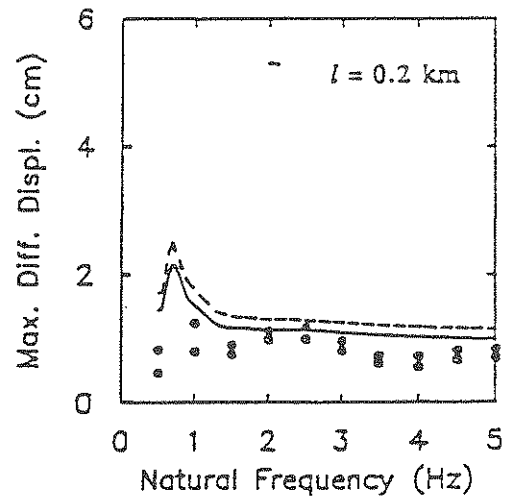
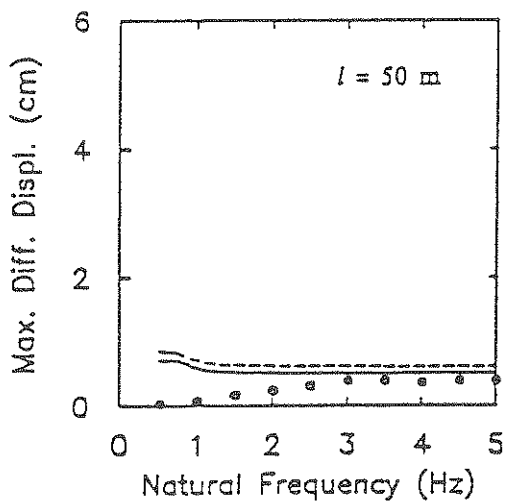
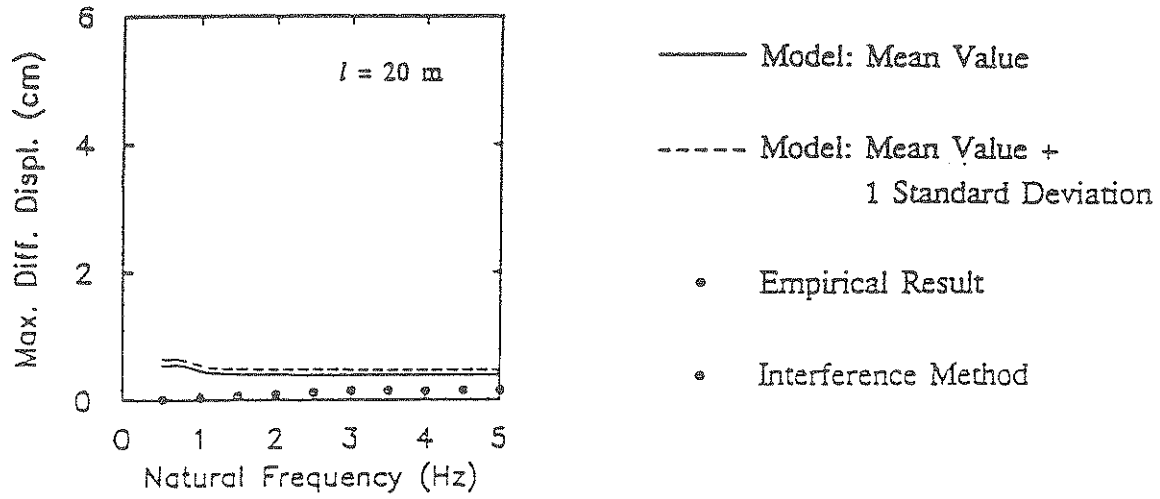


Figure 5.4 Differential Axial Displacement Response Spectra ($\xi_0=10\%$)

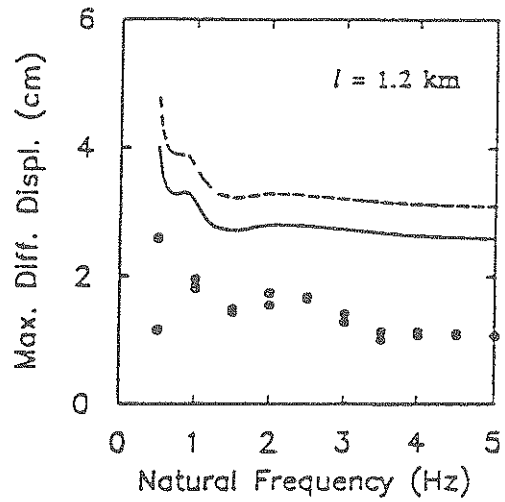
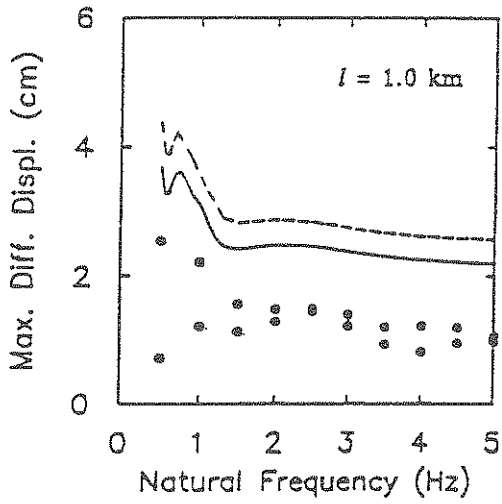
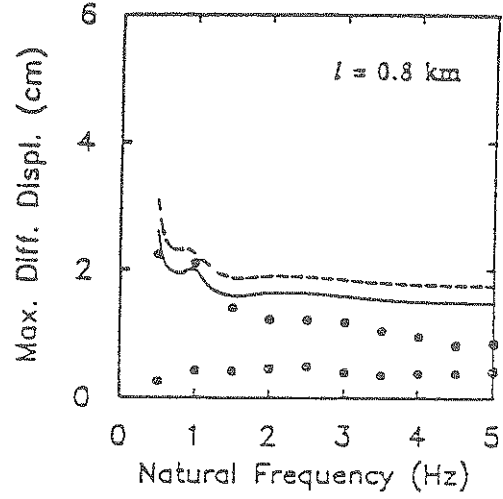
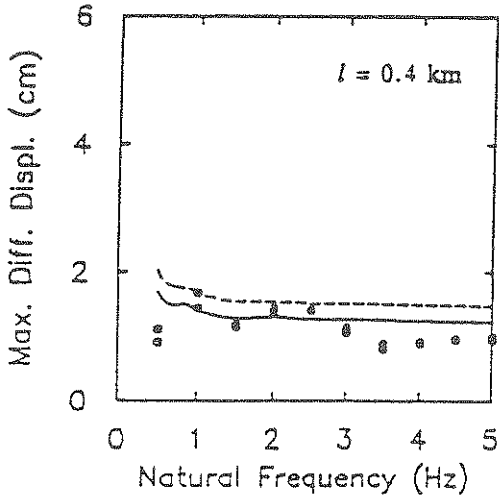


Figure 5.4 (continued)

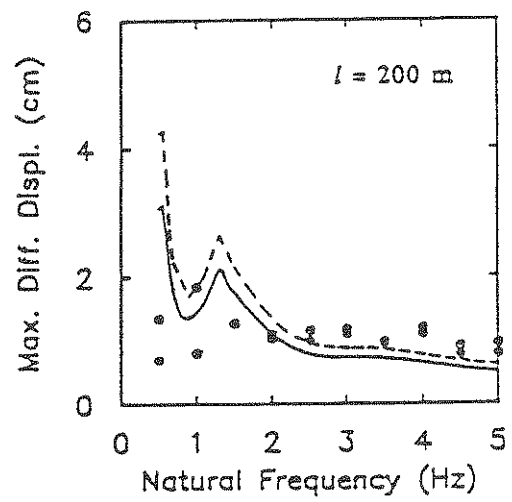
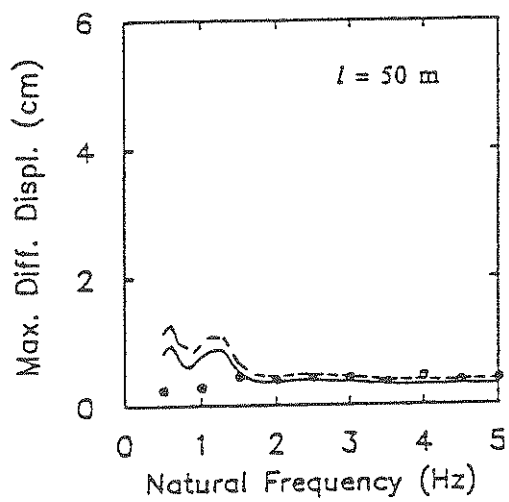
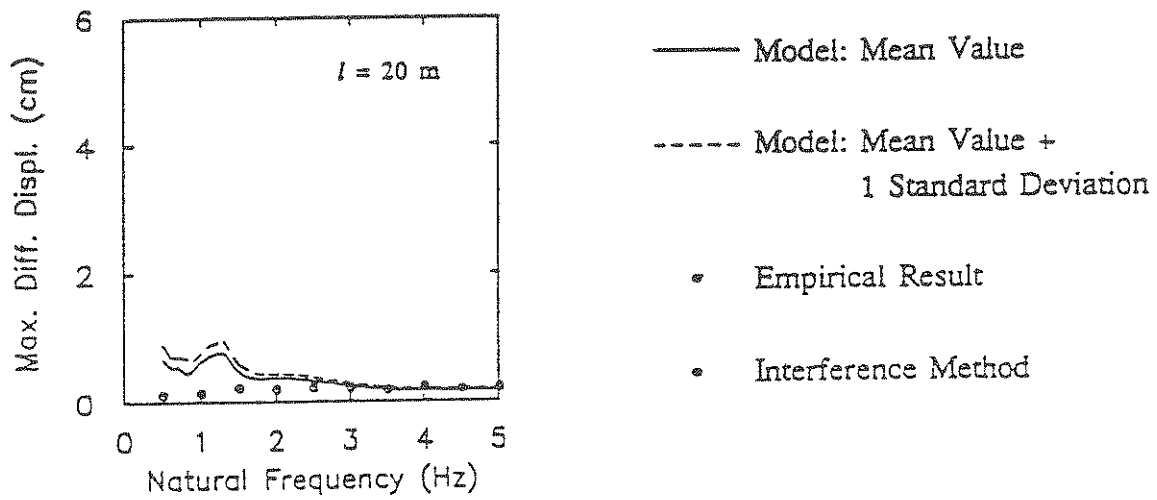


Figure 5.5 Differential Transverse Displacement Response Spectra ($\xi_{1,2,3}=5\%$)

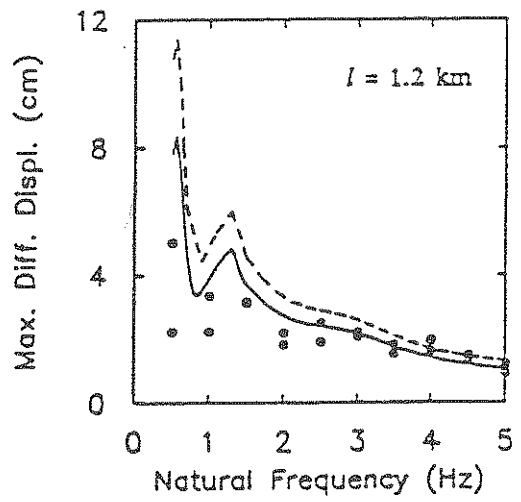
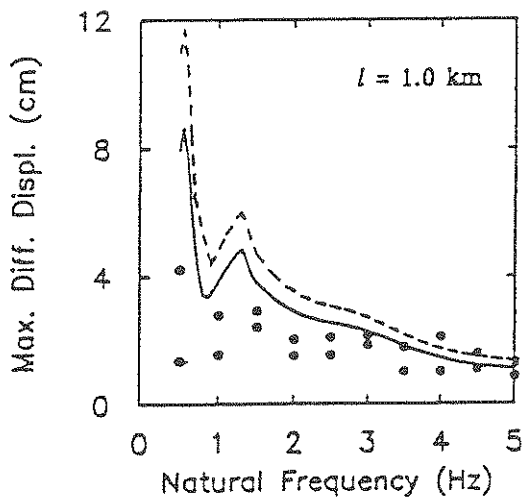
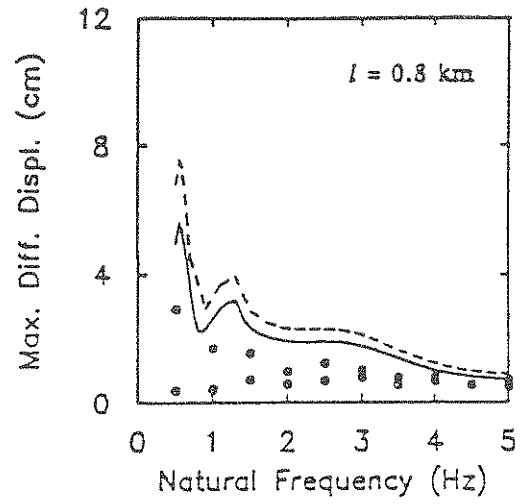
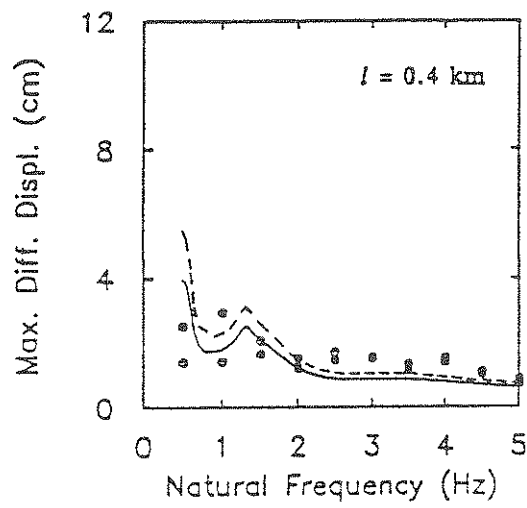
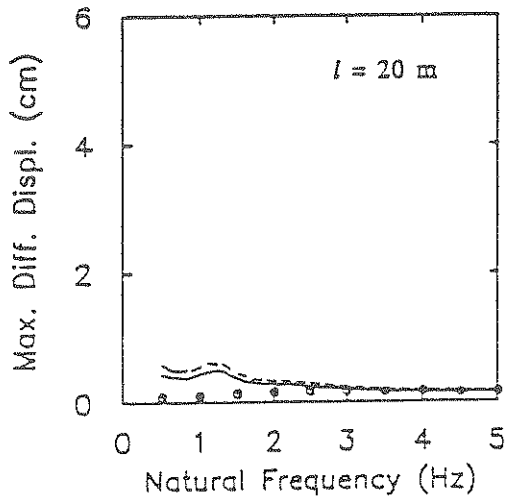


Figure 5.5 (continued)



- Model: Mean Value
- - - - Model: Mean Value + 1 Standard Deviation
- Empirical Result
- Interference Method

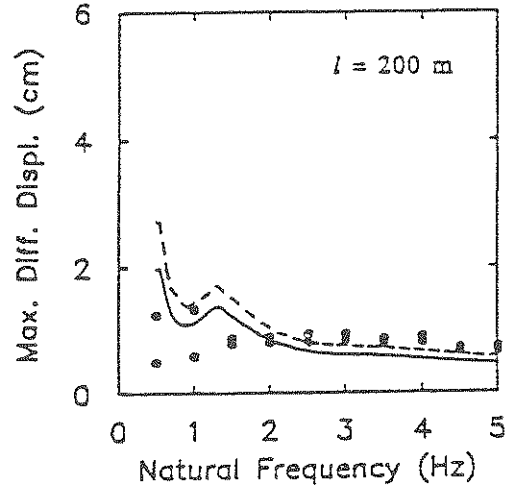
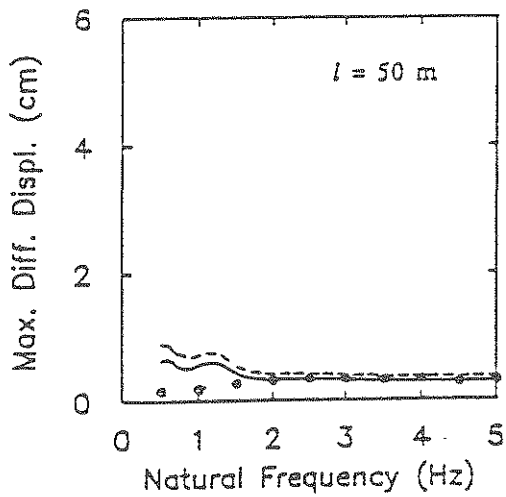


Figure 5.6 Differential Transverse Displacement Response Spectra ($\xi_{1,2,3}=10\%$)

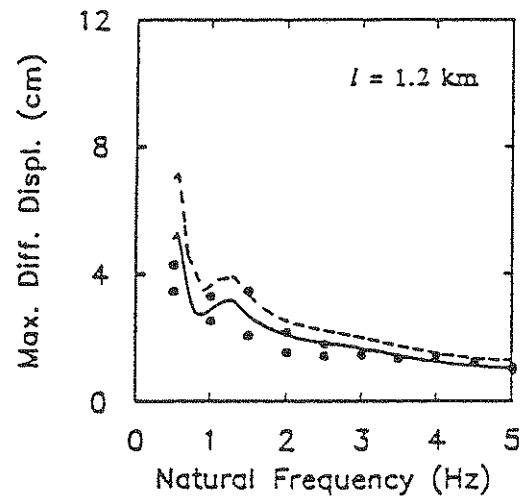
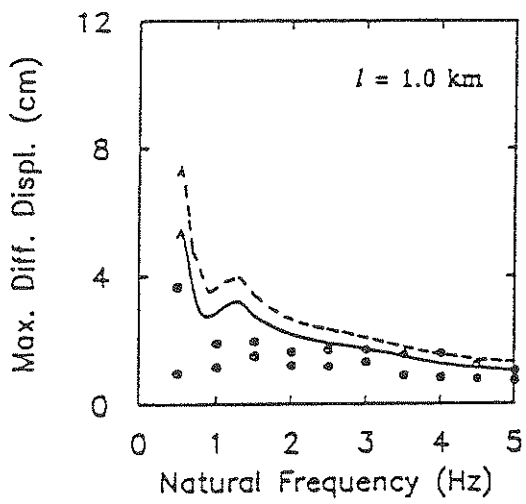
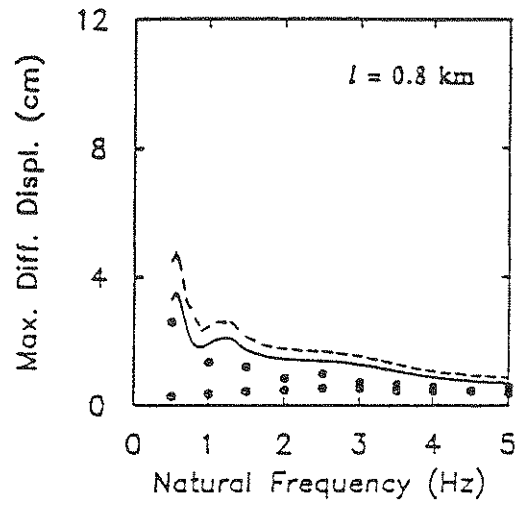
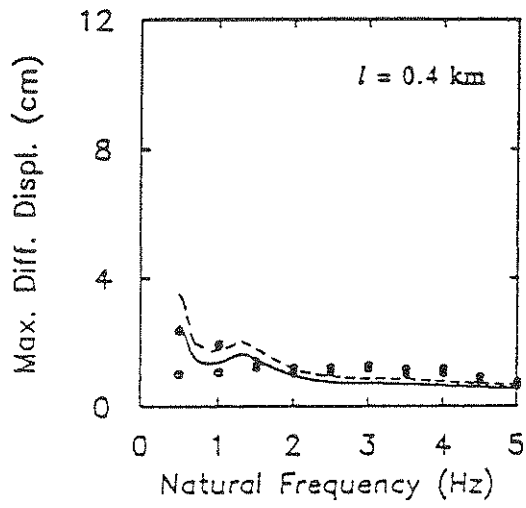


Figure 5.6 (continued)

(*i.e.*, without layers). However, as shown in Figs. 5.3 through 5.6, the relative displacement response spectra obtained with the proposed model give results that are even on the safe side over the entire range of frequencies. Observe also that, on the other hand, the method of interference response spectrum consistently underestimates the maximum differential displacement of the pipelines particularly for natural frequencies less than 2 Hz.

SECTION 6

SUMMARY AND CONCLUSIONS

6.1 Summary

A shearing fault rupture of the Haskell type was presented for modeling the earthquake source mechanism. In such a model, the rupture motion is described as a line dislocation sweeping over the entire fault plane at a constant rupture velocity, and the slip may be a strike-slip or dip-slip motion. A two-step method of solution is used to determine the ground responses in a three-dimensional homogeneous half-space. The ground motion in the Laplace transform domain was obtained by solving the transformed wave equations subject to the boundary conditions specified in the above fault plane. The generalized ray theorem was used for this purpose and might be extended systematically to solve the wave propagation problem in a layered medium. The analytic solution in the time domain was formulated through the Cagniard-de Hoop technique in which the inverse Laplace transform was taken by direct investigation. The correctness of the formulation was validated by comparing the results with those obtained by the method of Green's function.

In order to take the incoherent slip into account, the rupture motion was treated as a random process by introducing a spatio-temporal autocorrelation function of dislocation velocity, from which the power spectral density of the averaged dislocation velocity over the fault length was estimated. A multi-degree-of-freedom substitute system is introduced to represent the path effect, separately

from the source effect. The parameters of the substitute system were determined through system identification using the results of the 3-D analytical solutions. With the power spectral density available at the source and the transfer function obtained from the substitute system, the power spectral density of differential ground motions can be obtained.

An actual earthquake, Event 5 recorded at the SMART-1 array, was selected for validating the results of the model. The parameters in the model, such as the fault orientation, the fault dimension, the final dislocation, and the characteristics of the medium, *etc.*, were carefully investigated. Some of the parameters were evaluated based on the earthquake magnitude. Emphasis was directed to the stochastic properties of the differential ground motions, which are significant for the response analysis and design of lifeline systems.

The theoretical results are applicable to analyze lifeline systems. Two discrete models of pipelines were examined. The maximum differential displacements across the joint connecting two pipe segments subjected to either axial or lateral ground excitations were presented in terms of the differential response spectra.

6.2 Conclusions

In this study, a hybrid deterministic and stochastic model, which depends on the parameters at the earthquake source and the characteristics of the soil, was developed to investigate the spatial variation of ground motions necessary for the analysis of pipelines. Based on the results of the study, including the validation with the SMART-1 data, the following conclusions may be drawn:

1. In the deterministic approach, the method of solution for calculating the ground responses is effective and efficient when compared with other methods, such as the Green's function solution. For layered media, the generalized ray theory offers a systematical procedure to obtain the ground responses in the transform domain. In addition to the source functions and receiver functions for a homogeneous medium, only the reflection or refraction coefficients are needed. The Cagniard-de Hoop method has been shown to be an efficient way to take the inverse transform for obtaining solutions in the time domain for each ray.
2. The high-frequency content of the seismic waves is not important for the analysis of pipelines, because the differential ground velocity and displacement are the base excitations to a pipeline in which the differential displacement response is of major concern. The frequency transfer function of a pipeline system will tend to filter out the high-frequency excitations.
3. The effect of soil amplification is different at various stations so that the differential ground motions at some pair of stations with a short separation distance are more incoherent than those with distant separation. Any discrepancy between the analytic and empirical results for a single earthquake can be attributed to the assumptions made in the study, such as the fixed rupture direction, the continuous offsetting, the homogeneity and isotropy of the medium.
4. The proposed differential response spectrum predicts the mean maximum differential displacement between the pipe segments as a function of the

system frequency, and is generally on the safe side as compared with empirical results.

5. The interference response spectrum consistently underestimates the maximum differential displacement between the pipe segments, particularly when the natural frequency of the pipe system is less than 2 Hz.

6.3 Suggestions for Further Study

On the basis of this study, suggestions for further work would include the following:

1. The multi-degree-of-freedom system may be a good theoretical model for structures, but it is probably not suitable for soils. A modified substitute system, *e.g.*, including the epicentral distance or containing two subsystems (one for rock, one for soil), may be more effective to simulate the transmission effect.
2. A 3-D analytic model for layered media can be readily extended from the current model; however, this would involve much more calculations because multiple rays will be necessary. Simplification is necessary for developing a suitable model to account for the inhomogeneity of the soil.
3. Basically, the ground motions are determined by solving the wave equations subject to the boundary conditions specified at the source. A standard procedure is to take the Fourier transform over the time variable and the two horizontal space variables, and then obtain the responses in the transform domain through algebraic manipulation. In the Fourier

transform solution (*i.e.*, a function of the frequency and the two wave-numbers), the source factor, the effects of wave propagation, reflection and refraction, along with the characteristics of the response at the receiver (*i.e.*, displacement or stress) are all collected together through multiplication. Therefore, another possible approach is to represent the spatial variation of ground motions in a random field of frequency and wave numbers when the randomness is introduced at the source and/or to the medium.

4. Since the layer beneath the SMART-1 array is oblique (dipping toward north with an angle of about 6 degrees), a semi-analytic method may be applicable to study the local soil effect. In June 1983, an extension station E02 was installed at the outcrop which is located 4.8 km south of station C00. Most events triggered the SMART-1 array with epicenters located south of station E02. Therefore, the ground motions at station E02 can be obtained analytically in a 3-D model with waves propagating through the homogeneous medium for these events, and the soil amplification can be characterized by the transfer function with the recordings at station E02 as the input and the recordings at other stations as the output, if, in each station, the transfer functions are similar for different events. Obviously, it is an approximate approach because the waves transmitted through the interface are all forced to pass through station E02. However, this may be a practical method for examining soil amplification.

SECTION 7

REFERENCES

1. Abrahamson, N. A., "Estimation of Seismic Wave Coherency and Rupture Velocity Using the SMART 1 Strong-Motion Array Recording," *Earthquake Engineering Research Center Report*, No. UCB/EERC-85/02, University of California, Berkeley, California, March 1985.
2. Achenbach, J. D. and Harris, J. G., "Asymptotic Modeling of Strong Ground Motion Excited by Subsurface Sliding Events," Chapter 1 in *Seismic Strong Motion Synthetics*, Ed. by Bolt, B. A., Computational Techniques Series, Academic Press Inc., Orlando, 1987.
3. Aki, K., "Scaling Law of Seismic Spectrum," *Journal of Geophysical Research*, Vol. 72, No. 4, pp. 1217-1231, February 1967.
4. Aki, K., "Seismic Displacements near a Fault," *Journal of Geophysical Research*, Vol. 73, No. 16, pp. 5359-5376, August 1968.
5. Aki, K., "Strong Motion Prediction Using Mathematical Modeling Techniques," *Bulletin of the Seismological Society of America*, Vol. 72, No. 6, pp. S29-S41, December 1982.
6. Anderson, J. G., "Motions Near a Shallow Rupturing Fault: Evaluation of Effects Due to the Free Surface," *Geophysical Journal of the Royal Astronomical Society*, Vol. 46, No. pp. 575-593, September 1976.
7. Andrews, D. J., "A Stochastic Fault Model 1. Static Case," *Journal of Geophysical Research*, Vol. 85, No. B7, pp. 3867-3877, July 1980.
8. Andrews, D. J., "A Stochastic Fault Model 2. Time-Dependent Case," *Journal of Geophysical Research*, Vol. 86, No. B11, pp. 10821-10834, November 1981.
9. Beck, J. L., "Determining Models of Structures from Earthquake Records," *Earthquake Engineering Research Laboratory Report*, No. EERL 78-01, California Institute of Technology, Pasadena, California, June 1978.

10. Bendat, J. S. and Piersol A. G., *Random Data: Analysis and Measurement Procedures*, John Wiley & Sons Inc., New York, 1971.
11. Boatwright, J., "A Dynamic Model for Far-Field Acceleration," *Bulletin of the Seismological Society of America*, Vol. 72, No. 4, pp. 1049-1068, August 1982.
12. Bonilla, M. G., "Surface Faulting and Related Effects," in *Earthquake Engineering*, Ed. by Wiegel R. L., Prentice-Hall, Inc., Englewood Cliffs, New Jersey, 1970.
13. Boore, D. M. and Joyner, W. B., "The Influence of Rupture Incoherence on Seismic Directivity," *Bulletin of the Seismological Society of America*, Vol. 68, No. 2, pp. 283-300, April 1978.
14. Boore, D. M. and Zoback, M. D., "Near-Field Motions from Kinematic Models of Propagating Faults," *Bulletin of the Seismological Society of America*, Vol. 64, No. 2, pp. 321-342, April 1974.
15. Bouchon, M., "Discrete Wave Number Representation of Elastic Wave Fields in Three-Space Dimensions," *Journal of Geophysical Research*, Vol. 84, No. B7, pp. 3609-3614, July 1979.
16. Burridge, R. and Knopoff, L., "Body Force Equivalents for Seismic Dislocations," *Bulletin of the Seismological Society of America*, Vol. 54, No. 6, pp. 1875-1888, December 1964.
17. Cagniard, L., *Reflection and Refraction of Progressive Seismic Waves*, translated by Flinn, E. A., and Dix, C. H., McGraw-Hill, New York, 1962.
18. Chen, P. L., "Ground Response Due to Fault Motion," Ph.D. Dissertation, National Taiwan University, Taipei, Taiwan, R. O. C., July 1981 (In Chinese).
19. Das, S., "A Numerical Method for Determination of Source Time Functions for General Three-Dimensional Rupture Propagation," *Geophysical Journal of the Royal Astronomical Society*, Vol. 62, No. 3, pp. 591-604, September 1980.

20. Davenport, A. G., "Note on the Distribution of the Largest Value of a Random Function with Application to Gust Loading," *Proceedings, Institution of Civil Engineers*, Vol. 28, Paper No. 6739, pp. 187-196, June 1964.
21. de Hoop, A. T., "A Modification of Cagniard's Method for Solving Seismic Pulse Problems," *Applied Scientific Research, Section B*, Vol. 8, No. 4, pp. 349-356, 1960.
22. Dravinski, M., "Evaluation of Strong Ground Motion Using Boundary Integral Equation Approach," in *Earthquake Source Modeling, Ground Motion and Structural Response*, Ed. by Datta, S. K., ASME, PVP-Vol. 80, AMD-Vol 60, pp. 61-80, 1984.
23. Geller, R. J., "Representation Theorems for an Infinite Shear Fault," *Geophysical Journal of the Royal Astronomical Society*, Vol. 39, No. 1, pp. 123-131, October 1974.
24. Geller, R. J., "Scaling Relations for Earthquake Source Parameters and Magnitudes," *Bulletin of the Seismological Society of America*, Vol. 66, No. 5, pp. 1501-1523, October 1976.
25. Harada, T., "Probabilistic Modeling of Spatial Variation of Strong Earthquake Ground Displacements," *Proceedings of the Eighth World Conference on Earthquake Engineering*, San Francisco, Vol. II, pp. 605-612, July 1984.
26. Hartzell, S. H.; Frazier, G. A.; and Brune, J. N., "Earthquake Modeling in a Homogeneous Half-Space," *Bulletin of the Seismological Society of America*, Vol. 68, No. 2, pp. 301-316, April 1978.
27. Haskell, N. A., "Total Energy and Energy Spectral Density of Elastic Wave Radiation from Propagating Faults," *Bulletin of the Seismological Society of America*, Vol. 54, No. 6, pp. 1811-1841, December 1964.
28. Haskell, N. A., "Total Energy and Energy Spectral Density of Elastic Wave Radiation from Propagating Faults. Part II. A Statistical Source Model," *Bulletin of the Seismological Society of America*, Vol. 56, No. 1, pp. 125-140, February 1966.

29. Haskell, N. A., "Elastic Displacements in the Near-Field of a Propagating Fault," *Bulletin of the Seismological Society of America*, Vol. 59, No. 2, pp. 865-908, April 1969.
30. Iida, K., "Earthquake Magnitude, Earthquake Fault, and Source Dimensions," *Journal of Earth Sciences, Nagoya University*, Vol. 13, No. 2, pp. 115-132, December 1965.
31. Israel, M. and Kovach, R. L., "Near-Field Motions from a Propagating Strike-Slip Fault in an Elastic Half-Space," *Bulletin of the Seismological Society of America*, Vol. 67, No. 4, pp. 977-994, August 1977.
32. Johnson, L. R., "Green's Function for Lamb's Problem," *Geophysical Journal of the Royal Astronomical Society*, Vol. 37, No. 1, pp. 99-131, April 1974.
33. Kawasaki, I., "On the Dynamical Process of the Parkfield Earthquake of June 28, 1966," *Journal of Physics of Earth*, Vol. 23, No. 2, pp. 127-144, June 1975.
34. King, C. Y. and Knopoff, L., "Stress Drop in Earthquakes," *Bulletin of the Seismological Society of America*, Vol. 58, No. 1, pp. 249-257, February 1968.
35. Levy, N. A. and Mal, A. K., "Calculation of Ground Motion in a Three-Dimensional Model of the 1966 Parkfield Earthquake," *Bulletin of the Seismological Society of America*, Vol. 66, No. 2, pp. 405-423, April 1976.
36. Loh, C. H.; Ang, A. H-S.; and Wen, Y. K., "Spatial Correlation Study of Strong Motion Array Data with Application to Lifeline Earthquake Engineering," *Civil Engineering Studies, Structural Research Series*, No. 503, University of Illinois at Urbana-Champaign, Urbana, Illinois, March 1983.
37. Loh, C. H., "Analysis of the Spatial Variation of Seismic Waves and Ground Movements from SMART-1 Array Data," *Earthquake Engineering & Structural Dynamics*, Vol. 13, No. 5, pp. 561-581, October 1985.
38. Luco, J. E. and Anderson, J. G., "Steady-State Response of an Elastic Half-Space to a Moving Dislocation of Finite Width," *Bulletin of the Seismological Society of America*, Vol. 73, No. 1, pp. 1-22, February 1983.

39. Luco, J. E., "Dislocation Models of Near-Source Earthquake Ground Motion: A Review," Department of Applied Mechanics and Engineering Sciences, University of California, San Diego, La Jolla, California, July 1986.
40. Madariaga, R., "The Dynamic Field of Haskell's Rectangular Dislocation Fault Model," *Bulletin of the Seismological Society of America*, Vol. 68, No. 4, pp. 869-887, August 1978.
41. Matsuda, T., "Magnitude and Recurrence Interval of Earthquakes from a Fault," *J. Seismol. Soc. Japan*, Vol. 28, pp. 269-283, 1975.
42. Mohammadi, J. and Ang, A. H-S., "A Method for the Analysis of Seismic Reliability of Lifeline Systems," *Civil Engineering Studies, Structural Research Series*, No. 474, University of Illinois at Urbana-Champaign, Urbana, Illinois, February 1980.
43. Nelson, I. and Weidlinger, P., "Development of Interference Response Spectra for Lifelines Seismic Analysis," Weidlinger Associate, New York, Report No. NEF/RA-770313, prepared for National Science Foundation, July 1977.
44. Pao, Y. H. and Gajewski, R. R., "The Generalized Ray Theory and Transient Response of Layered Elastic Solids," *Physical Acoustics*, Vol. 13, pp. 183-265, 1977.
45. Papageorgiou, A. S. and Aki, K., "A Specific Barrier Model for the Quantitative Description of Inhomogeneous Faulting and the Prediction of Strong Ground Motion. I. Description of the Model," *Bulletin of the Seismological Society of America*, Vol. 73, No. 3, pp. 693-722, June 1983a.
46. Papageorgiou, A. S. and Aki, K., "A Specific Barrier Model for the Quantitative Description of Inhomogeneous Faulting and the Prediction of Strong Ground Motion. Part II. Applications of the Model," *Bulletin of the Seismological Society of America*, Vol. 73, No. 4, pp. 953-978, August 1983b.
47. Roecker, S. W.; Yeh, Y. H.; and Tsai, Y. B., "Three-Dimensional P and S Wave Velocity Structures beneath Taiwan: Deep Structure beneath an Arc-Continent Collision," *Journal of Geophysical Research*, Vol. 92, No. B10, pp. 10547-10570, September 1987.

48. Seyyedien-Choobi, M. and Robinson, A. R., "Motion on the Surface of a Layered Elastic Half-Space Produced by a Buried Dislocation Pulse," *Civil Engineering Studies, Structural Research Series*, No. 421, University of Illinois at Urbana-Champaign, Urbana, Illinois, November 1975.
49. Suzuki, S. and Kiremidjian, A. S., "A Stochastic Ground Motion Forecast Model with Geophysical Considerations," *John A. Blume Earthquake Engineering Center Report*, No. 88, Stanford University, Stanford, California, September 1988.
50. Tanimoto, T., "Cagniard de-Hoop Method for a Haskell Type Vertical Fault," *Geophysical Journal of the Royal Astronomical Society*, Vol. 70, No. 3, pp. 639-646, September 1982.
51. Virieux, J. and Madariaga, R., "Dynamic Faulting Studied by a Finite Difference Method," *Bulletin of the Seismological Society of America*, Vol. 72, No. 2, pp. 345-369, April 1982.
52. Wang, T. K., "A Study of Dipping Rectangular Fault in an Elastic Half-Space," M.S. Dissertation, National Taiwan University, Taipei, Taiwan, R. O. C., July 1988 (In Chinese).
53. Wen, K. L. and Yeh, Y. T., "Seismic Velocity Structure beneath the SMART 1 Array," *Bulletin of the Institute of Earth Sciences, Academia Sinica*, R. O. C., Vol. 4, pp. 51-72, December 1984.
54. Yeh, C. S.; Chen P. L.; Kuo, M. K.; and Wang T. K., "Ground Motions Generated by a Finite Fault," *IUTAM Symposium on Elastic Wave Propagation*, Galway, Ireland, March 1988.
55. Zerva, A.; Ang, A. H-S.; and Wen, Y. K., "A Study of Seismic Ground Motion for Lifeline Response Analysis," *Civil Engineering Studies, Structural Research Series*, No. 521, University of Illinois at Urbana-Champaign, Urbana, Illinois, October 1985.

APPENDIX A

LAPLACE TRANSFORM ELEMENTS FOR OBLIQUE FAULT

(1) Strike-slip Fault:

$$\{F_p\} = \left\{ \begin{array}{c} -8i\xi^2\eta\zeta_s \\ -8i\xi\eta^2\zeta_s \\ -4\xi\eta(\zeta_s^2 + \xi^2 + \eta^2) \end{array} \right\} \sin \delta + \left\{ \begin{array}{c} 8\xi^2\zeta_p\zeta_s \\ 8\xi\eta\zeta_p\zeta_s \\ -4i\xi\zeta_p(\zeta_s^2 + \xi^2 + \eta^2) \end{array} \right\} \cos \delta, \quad (\text{A.1})$$

and

$$\{F_s\} = \left\{ \begin{array}{c} 2i\eta \left[\frac{(\zeta_s^2 - \xi^2 + \eta^2)(\zeta_s^2 + \xi^2 + \eta^2)}{\zeta_s} + 4\zeta_p(\xi^2 - \eta^2) \right] \\ 2i\xi \left[\frac{(\zeta_s^2 + \xi^2 - \eta^2)(\zeta_s^2 + \xi^2 + \eta^2)}{\zeta_s} - 4\zeta_p(\xi^2 - \eta^2) \right] \\ 8\xi\eta\zeta_p\zeta_s \end{array} \right\} \sin \delta$$

$$+ \left\{ \begin{array}{c} 8\eta^2\zeta_p\zeta_s - 2(\zeta_s^2 + \xi^2 + \eta^2)^2 \\ -8\xi\eta\zeta_p\zeta_s \\ 4i\xi\zeta_p(\zeta_s^2 + \xi^2 + \eta^2) \end{array} \right\} \cos \delta. \quad (\text{A.2})$$

(2) Dip-slip Fault:

$$\{F_p\} = \left\{ \begin{array}{c} -4i\xi\zeta_s(\zeta_p^2 + \eta^2) \\ -4i\eta\zeta_s(\zeta_p^2 + \eta^2) \\ -2(\zeta_p^2 + \eta^2)(\zeta_s^2 + \xi^2 + \eta^2) \end{array} \right\} \sin 2\delta + \left\{ \begin{array}{c} 8\xi\eta\zeta_p\zeta_s \\ 8\eta^2\zeta_p\zeta_s \\ -4i\eta\zeta_p(\zeta_s^2 + \xi^2 + \eta^2) \end{array} \right\} \cos 2\delta, \quad (\text{A.3})$$

and

$$\{F_s\} = \left\{ \begin{array}{c} 2i\xi \left[\frac{(\zeta_s^2 - \eta^2)(\zeta_s^2 + \xi^2 + \eta^2)}{\zeta_s} + 4\eta^2\zeta_p \right] \\ 2i\eta \left[\frac{(2\zeta_s^2 + \xi^2)(\zeta_s^2 + \xi^2 + \eta^2)}{\zeta_s} - 4\xi^2\zeta_p \right] \\ 4\zeta_p\zeta_s(\xi^2 + 2\eta^2) \end{array} \right\} \sin 2\delta$$

$$+ \left\{ \begin{array}{c} -8\xi\eta\zeta_p\zeta_s \\ 8\xi^2\zeta_p\zeta_s - 2(\zeta_s^2 + \xi^2 + \eta^2)^2 \\ 4i\eta\zeta_p(\zeta_s^2 + \xi^2 + \eta^2) \end{array} \right\} \cos 2\delta. \quad (\text{A.4})$$

APPENDIX B

ANALYTICAL SOLUTION OF HASKELL MODEL

$$(1) U_1(x, y, 0, t) = \frac{D_0}{4\pi^2} \sum_{j=p, s} H(t-t_{1j}) \int_{-q_j}^{q_j} \operatorname{Re} \left\{ \frac{(-i) F_j \frac{d\sigma_j}{dt}}{(i\xi + b)(i\eta \cos \delta + \zeta_j \sin \delta)R} \right\} dq, \quad (\text{B.1})$$

where:

$$t_{1j} = R_0 b_j, \quad R_0 = \sqrt{x^2 + y^2 + z_0^2},$$

$$q_j = \sqrt{t^2 - t_{1j}^2} / R_0,$$

$$\begin{cases} \xi = i\sigma_j \cos \theta - q \sin \theta, \\ \eta = i\sigma_j \sin \theta + q \cos \theta, \end{cases}$$

$$\zeta_j = \sqrt{b_j^2 + \xi^2 + \eta^2},$$

$$\sigma_j = \frac{rt}{R_0^2} + i \frac{z_0 \sqrt{t^2 - t_{1j}^2}}{R_0^2},$$

$$\frac{d\sigma_j}{dt} = \frac{r}{R_0^2} + i \frac{z_0 t}{R_0^2 \sqrt{t^2 - t_{1j}^2}},$$

$$t_{qj} = R_0 \sqrt{b_j^2 + q^2}.$$

$$\begin{aligned}
(2) \ U_{1h}(x, y, 0, t) = & \frac{D_0}{4\pi^2} H\left(\frac{r}{R_0} - \frac{b_p}{b_s}\right) \left[H(t - t_{1h})H(t_{1s} - t) \int_{-q_h}^{q_h} \operatorname{Re}\left\{\frac{H_A}{H_B}\right\} dq \right. \\
& \left. + H(t - t_{1s})H(t_{hm} - t) \left(\int_{-q_h}^{-q_s} \operatorname{Re}\left\{\frac{H_A}{H_B}\right\} dq + \int_{q_s}^{q_h} \operatorname{Re}\left\{\frac{H_A}{H_B}\right\} dq \right) \right], \quad (B.2)
\end{aligned}$$

where:

$$t_{1h} = z_0 \sqrt{b_s^2 - b_p^2} + r b_p,$$

$$t_{hm} = \frac{R_0^2}{z_0} \sqrt{b_s^2 - b_p^2},$$

$$q_h = \sqrt{\left(\frac{t - z_0 \sqrt{b_s^2 - b_p^2}}{r}\right)^2 - b_p^2},$$

$$\left\{ \frac{H_A}{H_B} \right\} = \left\{ \frac{(-i) F_s \frac{d\sigma_h}{dt}}{(i\xi + b)(i\eta \cos \delta + \zeta_s \sin \delta)R} \right\},$$

$$\begin{cases} \xi = i\sigma_h \cos \theta - q \sin \theta, \\ \eta = i\sigma_h \sin \theta + q \cos \theta, \end{cases}$$

$$\sigma_h = \frac{rt}{R_0^2} - \frac{z_0 \sqrt{t_{qs}^2 - t^2}}{R_0^2},$$

$$\frac{d\sigma_h}{dt} = \frac{r}{R_0^2} + \frac{z_0 t}{R_0^2 \sqrt{t_{qs}^2 - t^2}}.$$

$$(3) U_2(x, y, 0, t) = \frac{D_0}{2\pi \cos \theta} H(x) \sum_{j=p,s} \left[H\left(\frac{x}{R_0} - \frac{b}{b_j}\right) H(t - t_{2j}) + H\left(\frac{b}{b_j} - \frac{x}{R_0}\right) H(t - t_2) \right] \operatorname{Re} \left\{ \frac{(-i) F_j \frac{da_j}{dt}}{(i\eta \cos \delta + \zeta_j \sin \delta) R} \right\}, \quad (\text{B.3})$$

where:

$$t_{2j} = xb + \sqrt{y^2 + z_0^2} \sqrt{b_j^2 - b^2},$$

$$t_2 = \frac{R_0^2}{x} b,$$

$$\begin{cases} \xi = ib, \\ \eta = i \frac{(a_j + b \sin \theta)}{\cos \theta}, \end{cases}$$

$$a_j = -b \sin \theta + \frac{\cos \theta}{y^2 + z_0^2} \left[yt' + iz_0 \sqrt{t'^2 + (y^2 + z_0^2)(b^2 - b_j^2)} \right],$$

$$\frac{da_j}{dt} = \frac{\cos \theta}{y^2 + z_0^2} \left[y + i \frac{z_0 t'}{\sqrt{t'^2 + (y^2 + z_0^2)(b^2 - b_j^2)}} \right],$$

$$t' = t - xb.$$

$$\begin{aligned}
(4) \quad U_{2h}(x, y, 0, t) &= \frac{D_0}{2\pi \cos \theta} H(x) H\left(\frac{x}{R_0} - \frac{b}{b_s}\right) \left\{ H\left(\frac{x}{r} - \frac{b}{b_p}\right) H(H_C) H(t - t_{2h}) \right. \\
&\quad \left. + \left[H\left(\frac{b}{b_p} - 1\right) + H\left(1 - \frac{b}{b_p}\right) H\left(\frac{b}{b_p} - \cos \theta\right) H(H_C) \right] H(t - t_{2h}^*) \right\} \\
&\quad \cdot H(t_{2r} - t) \operatorname{Re} \left\{ \frac{(-i) F_s \frac{d\alpha_h}{dt}}{(i\eta \cos \delta + \xi_s \sin \delta) R} \right\}, \tag{B.4}
\end{aligned}$$

where:

$$H_C = \frac{|y|}{\sqrt{y^2 + z_0^2}} - \frac{\sqrt{b_p^2 - b^2}}{\sqrt{b_s^2 - b^2}},$$

$$t_{2h} = xb + z_0 \sqrt{b_s^2 - b_p^2} + |y| \sqrt{b_p^2 - b^2},$$

$$t_{2h}^* = \frac{1}{\cos \theta} (rb + z_0 \sqrt{b_s^2 \cos^2 \theta - b^2}),$$

$$\begin{cases} \xi = ib, \\ \eta = i \frac{(a_h + b \sin \theta)}{\cos \theta}, \end{cases}$$

$$\beta_h = \begin{cases} -b \sin \theta + \frac{\cos \theta}{y^2 + z_0^2} \left[yt' - z_0 \sqrt{(y^2 + z_0^2)(b_s^2 - b^2) - t'^2} \right], & \text{for } y > 0, \\ -b \sin \theta + \frac{\cos \theta}{y^2 + z_0^2} \left[yt' + z_0 \sqrt{(y^2 + z_0^2)(b_s^2 - b^2) - t'^2} \right], & \text{for } y < 0, \end{cases}$$

$$\frac{d\beta_h}{dt} = \begin{cases} \frac{\cos \theta}{y^2 + z_0^2} \left[y + \frac{z_0 t'}{\sqrt{(y^2 + z_0^2)(b_s^2 - b^2) - t'^2}} \right], & \text{for } y > 0, \\ \frac{\cos \theta}{y^2 + z_0^2} \left[y - \frac{z_0 t'}{\sqrt{(y^2 + z_0^2)(b_s^2 - b^2) - t'^2}} \right], & \text{for } y < 0. \end{cases}$$

$$(5) U_3(x, y, 0, t) = \frac{D_0}{2\pi} H(y) H(y') \sum_{j=p, s} H(t - t_{3j}) \operatorname{Re} \left\{ \frac{(-i) F_j \frac{d\beta_j}{dt}}{(i\xi + b) G_j R} \right\}, \quad (\text{B.5})$$

where:

$$t_{3j} = \sqrt{x^2 + z'^2} b_j,$$

$$\begin{cases} \xi = i\sigma_2 \cos \theta + i\beta_j \sin \theta, \\ \eta = i\sigma_2 \sin \theta - i\beta_j \cos \theta, \end{cases}$$

$$\sigma_2 = \frac{\beta_j \sin \theta \cos \theta \cos^2 \delta + \sin \delta \sqrt{b_j^2 (1 - \cos^2 \theta \cos^2 \delta) - \beta_j^2}}{1 - \cos^2 \theta \cos^2 \delta},$$

$$\beta_j = \frac{1}{x^2 + z'^2} \left[y' t \cos \theta \cos \delta + i(r \sin \delta + z_0 \sin \theta \cos \delta) \sqrt{t^2 - t_{3j}^2} \right],$$

$$\frac{d\beta_j}{dt} = \frac{1}{x^2 + z'^2} \left[y' \cos \theta \cos \delta + i \frac{(r \sin \delta + z_0 \sin \theta \cos \delta) t}{\sqrt{t^2 - t_{3j}^2}} \right],$$

$$\begin{cases} y' = y \cos \delta - z_0 \sin \delta, \\ z' = -y \sin \delta - z_0 \cos \delta, \end{cases}$$

$$G_j = \frac{\sigma_2 \sin \delta + \xi_j \sin \theta \cos \delta}{\xi_j}.$$

$$(6) U_{3h}(x, y, 0, t) = \frac{D_0}{2\pi} H(y) H(y') \left[H\left(\frac{b_p}{b_s} - \frac{\sin \delta}{\sqrt{1 - \cos^2 \theta \cos^2 \delta}}\right) H(H_D) H(t - t_{3h}) \right. \\ \left. + H\left(\frac{\sin \delta}{\sqrt{1 - \cos^2 \theta \cos^2 \delta}} - \frac{b_p}{b_s}\right) H(t - t_{3h}^*) \right] H(t_{3s} - t) \operatorname{Re} \left\{ \frac{(-i) F_s \frac{d\beta_h}{dt}}{(i\xi + b) G_s R} \right\}, \quad (\text{B.6})$$

where:

$$H_D = \left(\frac{b_s y' \cos \theta \cos^2 \delta}{\sqrt{x^2 + z'^2}} + \cos \theta \sin \delta \sqrt{b_s^2 - b_p^2} \right)^2 - \sin^2 \theta (b_p^2 - b_s^2 \sin^2 \delta),$$

$$t_{3h} = \frac{1}{\cos \delta} \left[|x| \sqrt{b_p^2 - b_s^2 \sin^2 \delta} - z' \sqrt{b_s^2 - b_p^2} \right],$$

$$t_{3h}^* = \frac{b_s}{\sqrt{1 - \cos^2 \theta \cos^2 \delta}} (r \sin \delta + z_0 \sin \theta \cos \delta),$$

$$\begin{cases} \xi = i\sigma_2 \cos \theta + i\beta_h \sin \theta, \\ \eta = i\sigma_2 \sin \theta - i\beta_h \cos \theta, \end{cases}$$

$$\sigma_2 = \frac{\beta_h \sin \theta \cos \theta \cos^2 \delta + \sin \delta \sqrt{b_s^2 (1 - \cos^2 \theta \cos^2 \delta) - \beta_h^2}}{1 - \cos^2 \theta \cos^2 \delta},$$

$$\beta_h = \begin{cases} \frac{1}{x^2 + z'^2} \left[y' t \cos \theta \cos \delta - (r \sin \delta + z_0 \sin \theta \cos \delta) \sqrt{t_{3s}^2 - t^2} \right], & \text{for } x > 0, \\ \frac{1}{x^2 + z'^2} \left[y' t \cos \theta \cos \delta + (r \sin \delta + z_0 \sin \theta \cos \delta) \sqrt{t_{3s}^2 - t^2} \right], & \text{for } x < 0, \end{cases}$$

$$\frac{d\beta_h}{dt} = \begin{cases} \frac{1}{x^2 + z'^2} \left[y' \cos \theta \cos \delta + \frac{(r \sin \delta + z_0 \sin \theta \cos \delta) t}{\sqrt{t_{3s}^2 - t^2}} \right], & \text{for } x > 0, \\ \frac{1}{x^2 + z'^2} \left[y' \cos \theta \cos \delta - \frac{(r \sin \delta + z_0 \sin \theta \cos \delta) t}{\sqrt{t_{3s}^2 - t^2}} \right], & \text{for } x < 0. \end{cases}$$

APPENDIX C

POWER SPECTRAL DENSITY OF BASE VELOCITY

The spatio-temporal autocorrelation function for the dislocation velocity in the fault plane is defined as

$$\psi(\epsilon, \tau) = \int_{-\infty}^{\infty} \int_{-\infty}^{\infty} \dot{D}(x, t) \dot{D}(x + \epsilon, t + \tau) dx dt, \quad (\text{C.1})$$

where:

$\dot{D}(x, t)$ = the dislocation velocity at a point x and time t ,

ϵ = the spatial separation,

τ = the temporal separation.

The double Fourier transform over the spatial and temporal coordinates is performed for $\dot{D}(x, t)$ and $\psi(\epsilon, \tau)$, *i.e.*, the transform pair of $\dot{D}(x, t)$ is

$$\dot{D}^{FF}(k, \omega) = \int_{-\infty}^{\infty} \int_{-\infty}^{\infty} \dot{D}(x, t) e^{-i(\omega t - kx)} dx dt, \quad (\text{C.2})$$

$$\dot{D}(x, t) = \frac{1}{4\pi^2} \int_{-\infty}^{\infty} \int_{-\infty}^{\infty} \dot{D}^{FF}(k, \omega) e^{i(\omega t - kx)} dk d\omega. \quad (\text{C.3})$$

and that of $\psi(\epsilon, \tau)$ is

$$\psi^{FF}(k, \omega) = \int_{-\infty}^{\infty} \int_{-\infty}^{\infty} \psi(\epsilon, \tau) e^{-i(\omega\tau - k\epsilon)} d\epsilon d\tau, \quad (C.4)$$

$$\psi(\epsilon, \tau) = \frac{1}{4\pi^2} \int_{-\infty}^{\infty} \int_{-\infty}^{\infty} \psi^{FF}(k, \omega) e^{i(\omega\tau - k\epsilon)} dk d\omega, \quad (C.5)$$

where k and ω are the wave number and the frequency, respectively.

Substituting Eq. (C.3) into Eq. (C.1), *i.e.*,

$$\begin{aligned} \psi(\epsilon, \tau) &= \int_{-\infty}^{\infty} \int_{-\infty}^{\infty} \dot{D}(x, t) \left[\frac{1}{4\pi^2} \int_{-\infty}^{\infty} \int_{-\infty}^{\infty} \dot{D}^{FF}(k, \omega) e^{i\omega(t+\tau) - ik(x+\epsilon)} dk d\omega \right] dx dt \\ &= \frac{1}{4\pi^2} \int_{-\infty}^{\infty} \int_{-\infty}^{\infty} \left[\int_{-\infty}^{\infty} \int_{-\infty}^{\infty} \dot{D}(x, t) e^{i(\omega t - kx)} dx dt \right] \dot{D}^{FF}(k, \omega) e^{i(\omega\tau - k\epsilon)} dk d\omega, \end{aligned}$$

and then using Eq. (C.2), *i.e.*,

$$\psi(\epsilon, \tau) = \frac{1}{4\pi^2} \int_{-\infty}^{\infty} \int_{-\infty}^{\infty} \dot{D}^{FF}(-k, -\omega) \dot{D}^{FF}(k, \omega) e^{i(\omega\tau - k\epsilon)} dk d\omega,$$

the spatio-temporal autocorrelation function of the dislocation velocity is expressed by the double Fourier transform of the dislocation velocity as

$$\psi(\epsilon, \tau) = \frac{1}{4\pi^2} \int_{-\infty}^{\infty} \int_{-\infty}^{\infty} |\dot{D}^{FF}(k, \omega)|^2 e^{i(\omega\tau - k\epsilon)} dk d\omega. \quad (C.6)$$

Comparing Eq. (C.5) with Eq. (C.6), a useful relation is obtained,

$$\psi^{FF}(k, \omega) = |\dot{D}^{FF}(k, \omega)|^2. \quad (C.7)$$

The Fourier transform of the base velocity of the substitute system is

$$\dot{B}^F(\omega) = \int_{-\infty}^{\infty} \dot{B}(t) e^{-i\omega t} dt = \int_{-\infty}^{\infty} \frac{1}{L} \left[\int_0^L \dot{D}(x, t) dx \right] e^{-i\omega t} dt = \frac{1}{L} \dot{D}^{FF}(0, \omega). \quad (C.8)$$

Comparing Eq. (C.7) with Eq. (C.8), the equivalent point base velocity is, in frequency domain, related to the spatio-temporal autocorrelation function of the dislocation velocity by

$$|\dot{B}^F(\omega)|^2 = \frac{1}{L^2} \psi^{FF}(0, \omega). \quad (C.9)$$

Following Aki (1967), the spatio-temporal autocorrelation function of the dislocation velocity was defined in Eq. (4.3), and the corresponding double Fourier transform is

$$\psi^{FF}(k, \omega) = \frac{4\psi_0 k_T k_L}{(k_T^2 + \omega^2) [k_L^2 + (k - \frac{\omega}{v})^2]}. \quad (C.10)$$

where:

ψ_0 = a constant,

k_T^{-1} = the correlation time,

k_L^{-1} = the correlation length.

Therefore, from Eq. (C.9),

$$|\dot{B}^F(\omega)|^2 = \frac{1}{L^2} \frac{4\psi_0 k_T k_L}{(k_T^2 + \omega^2)(k_L^2 + \frac{\omega^2}{v^2})}. \quad (C.11)$$

Notice that

$$|\dot{B}^F(0)|^2 = \frac{4\psi_0}{L^2 k_T k_L} = D_0^2, \quad (C.12)$$

in which D_0 is the final dislocation, so the square of the Fourier amplitude of the base velocity is in terms of the final dislocation, the correlation time, and the correlation length as

$$|\dot{B}^F(\omega)|^2 = \frac{D_0^2}{(1 + \frac{\omega^2}{k_T^2})(1 + \frac{\omega^2}{k_L^2 v^2})}. \quad (C.13)$$

For a transient random process $X(t)$ with nonzero values only in the range of $0 \leq t \leq T$, Bendat and Piersol (1971) suggested that

$$S_{XX}(\omega) = \frac{2\pi}{T} |X^F(\omega)|^2. \quad (C.14)$$

Therefore, the power spectral density of the base velocity of the substitute system is estimated by

$$S_{\dot{B}\dot{B}}(\omega) = \frac{2\pi}{T_0} |\dot{B}^F(\omega)|^2 = \frac{2\pi}{T_0} \frac{D_0^2}{(1 + \frac{\omega^2}{k_T^2})(1 + \frac{\omega^2}{k_L^2 v^2})}, \quad (C.15)$$

in which $T_0 = L/v$ is the duration of rupture.

APPENDIX D
LISTING OF COMPUTER PROGRAM

```

PROGRAM    MAIN
C
C THIS PROGRAM EVALUATES SEISMIC GROUND MOTIONS
C EXCITED BY A HASKELL FAULT
C EMBEDDED IN A THREE-DIMENSIONAL HALF-SPACE
C
PARAMETER ( N = 4096 )
INPLICIT  COMPLEX (C)
CHARACTER DIR(3)*1, TITLE(8)*10
DIMENSION DX(4), DY(4), DZ(4), TR(4), SGN(4), TIM(N), RSP(N)
C
COMMON      T
COMMON /LUNT/ LIN, LOU
COMMON /IDEX/ IWAVE, IDISP, ISLIP
COMMON /SLOW/ BP, BS, BR, BP2, BS2, BSP, B2
COMMON /RAYL/ BRL, RPB
COMMON /GEMF/ YP, ZP, FS, FC, FS2, FC2
COMMON /GEMG/ X, Y, Z, QS, QC, R0, R, R2
COMMON /TIME/ T1P, T1S, T1H, THM, T2, T3P, T3S, T3H
COMMON /FACT/ SGR, SGI, AFR, AFI, AFP, AFS, BTR, BTI,
+           S2R, S2I, S2P, S2S
COMMON /SUMS/ NJ, PT(1000), WT
COMMON /SUM0/ NH0, PH0(1000), WHO(1000)
COMMON /SUM1/ NH1, PH1(1000), WH1(1000)
C
DATA DIR / 'X', 'Y', 'Z' /
DATA SGN / 1., -1., -1., 1. /
DATA CI / ( 0., 1. ) /
C
C --- LOGICAL UNITS AND DATA FILES
C
LIN = 1
LOU = 2
OPEN ( LIN, FILE='INPUT' )
OPEN ( LOU, FILE='OUTPUT' )
C
C --- DATA INPUT IN 6 LINES
C
C 1 [8A10]
READ ( LIN, 1001 ) ( TITLE(I), I = 1, 8 )
C
C 2 [5F10.0]
READ ( LIN, 1002 ) XC, YC, ZC, XL, YW
C

```

```

C      XC
C      YC      = COORDINATES OF SHALLOWEST CORNER OF FAULT
C      ZC
C      XL      = LENGTH OF FAULT
C      YW      = WIDTH OF FAULT
C
C 3    [I10, 3F10.0]
      READ ( LIN, 1003 ) ISLIP, VR, D, PHI
C
C      ISLIP = 1 FOR STRIKE-SLIP FAULT
C            = 2 FOR DIP-SLIP FAULT
C      VR    = RUPTURE VELOCITY
C      D     = DISLOCATION AMPLITUDE
C      PHI   = DIPPING ANGLE IN DEGREE
C
C 4    [2F10.0]
      READ ( LIN, 1002 ) VP, VS
C
C      VP    = P-WAVE VELOCITY
C      VS    = S-WAVE VELOCITY
C
C 5    [3F10.0]
      READ ( LIN, 1002 ) XS, YS, ZS
C
C      XS
C      YS      = COORDINATES OF STATION
C      ZS
C
C 6    [I10, 2F10.0, I10]
      READ ( LIN, 1004 ) IDISP, T0, DT, NT
C
C            1                X-
C      IDISP = 2 FOR RESPONSES IN Y-DIRECTION
C            3                Z-
C      T0    = INITIAL TIME OF RESPONSE
C      DT    = TIME INCREMENT
C      NT    = TOTAL NUMBER OF RESPONSES
C
C      CLOSE ( LIN )
C
C --- GAUSSIAN POINTS AND WEIGHTS
C
C      NJ = 100
C      NH0 = 100
C      NH1 = 100
C      CALL GAUSCHB ( NJ, PT, WT )
C      CALL GAUSJCB ( NH0, 0., 0., PH0, WHO )
C      CALL GAUSJCB ( NH1, 0., -0.5, PH1, WH1 )
C
C      PI = 4. * ATAN(1.)
C      D1 = D / ( 4. * PI * PI )
C      D3 = D / ( 2. * PI )

```

```

C
BP = 1. / VP
BS = 1. / VS
BR = 1. / VR
BP2 = BP * BP
BS2 = BS * BS
BSP = SQRT ( BS2 - BP2 )
CALL RAYLEIGH ( BP2, BS2, BRL, RPB )

```

```

C
PHI = PHI * PI / 180.
FS = SIN ( PHI )
FC = COS ( PHI )
FS2 = 2. * FS * FC
FC2 = 1. - 2. * FS * FS

```

```

C
X0 = XS - XC
Y0 = YS - YC
Z0 = ZS - ZC

```

```

C
DX(1) = 0.
DX(2) = 0.
DX(3) = XL
DX(4) = XL
DY(1) = 0.
DY(2) = YW * FC
DY(3) = 0.
DY(4) = YW * FC
DZ(1) = 0.
DZ(2) = YW * FS
DZ(3) = 0.
DZ(4) = YW * FS
TR(1) = 0.
TR(2) = 0.
TR(3) = XL / VR
TR(4) = XL / VR

```

```

C
DO 100 I = 1, NT
    TIM(I) = TO + ( I - 1 ) * DT
    RSP(I) = 0.
100 CONTINUE

```

```

C
DO 300 J = 1, 4
    X = X0 - DX(J)
    Y = Y0 - DY(J)
    Z = ABS ( Z0 - DZ(J) )
    CALL GEMTIM
    D2 = D3 / QC

```

```

C
DO 200 I = 1, NT
    T = TIM(I) - TR(J)
    IF ( T .LE. 0. ) GO TO 200

```

```

        U1T      = D1 * ( U1 (T) + U1H (T) )
        U2T      = D2 * ( U2 (T) + U2H (T) )
        U3T      = D3 * ( U3 (T) + U3H (T) )
        U        = U1T + U2T + U3T
        RSP(I)   = RSP(I) + SGN(J) * U
200    CONTINUE
C
300 CONTINUE
C
WRITE ( LOU, 1001 ) ( TITLE(I), I = 1, 8 )
WRITE ( LOU, 2001 ) DIR (IDISP)
WRITE ( LOU, 2002 ) ( TIM(I), RSP(I), I = 1, NT )
CLOSE ( LOU )
C
1001 FORMAT ( 8A10 )
1002 FORMAT ( 5F10.0 )
1003 FORMAT ( I10, 3F10.0 )
1004 FORMAT ( I10, 2F10.0, I10 )
C
2001 FORMAT ( // ' TOTAL RESPONSE',
+           // 6X, 'TIME', 6X, A1, '-DIR RESPONSE' / )
2002 FORMAT ( F10.2, 5X, E15.5 )
C
STOP
END
C
C
C-----
C
C
SUBROUTINE GAUSCHB ( N, PT, WT )
C
POINTS AND WEIGHT IN GAUSS-CHEBYSHEV QUADRATURE
C
Int from (-1) to (1) [ f(X) / ( 1 - X*X ) ** 0.5 ] dX
C
= WT * Sum from (i=1) to (i=N) [ f( PT(i) ) ]
C
DIMENSION PT(N)
C
PI = 4. * ATAN (1.)
C
WT = PI / N
C
FT = WT / 2.
DO 100 I = 1, N
    PT(I) = COS ( ( 2 * I - 1 ) * FT )
100 CONTINUE
C
RETURN
END
C

```



```

C
C -----
C
C
C SUBROUTINE GAUSJCB ( NN, ALF, BTA, X, A )
C
C POINTS AND WEIGHTS IN GAUSS-JACOBI QUADRATURE
C
C Int from (-1) to (1) [ (1-X)**ALF * (1+X)**BTA * f(X) ] dX
C
C = Sum from (i=1) to (i=NN) [ A(i) * f( X(i) ) ]
C
C REAL LNGAMA
C DIMENSION X(1000), A(1000), B(1000), C(1000)
C
C FN = NN
C CSX = 0.
C CSA = 0.
C EPS = 1.E-13
C BETA = EXP ( LNGAMA (ALF+1.) + LNGAMA (BTA+1.)
+         - LNGAMA (ALF+BTA+2.) )
C CC = 2.***(ALF+BTA+1.) * BETA
C TSX = FN * (BTA-ALF) / (ALF+BTA+2.*FN)
C TSA = CC
C B(2) = (ALF+BTA) * (BTA-ALF) / ( (ALF+BTA+4.) * (ALF+BTA+2.) )
C C(2) = 4. * (ALF+1.) * (BTA+1.)
+       / ( (ALF+BTA+3.) * (ALF+BTA+2.)**2 )
C CC = CC * C(2)
C DO 100 J = 3, NN
C B(J) = (ALF+BTA) * (BTA-ALF)
+       / ( (ALF+BTA+2.*J) * (ALF+BTA+2.*J-2.) )
C C(J) = 4. * (J-1.) * (ALF+J-1.) * (BTA+J-1.)
1       * (ALF+BTA+J-1.) / ( (ALF+BTA+2.*J-1.)
2       * (ALF+BTA+2.*J-2.)**2 * (ALF+BTA+2.*J-3.) )
C CC = CC * C(J)
100 CONTINUE
C
C DO 200 I = 1, NN
C IF ( I .EQ. 1 ) THEN
C AN = ALF / FN
C BN = BTA / FN
C R1 = (1.+ALF) * ( 2.78/(4.+FN*FN) + 0.768*AN/FN )
C R2 = 1. + 1.48*AN + 0.96*BN + 0.452*AN*AN
+     + 0.83*AN*BN
C XT = 1. - R1 / R2
C ELSE IF ( I .EQ. 2 ) THEN
C R1 = (4.1+ALF) / ( (1.+ALF) * (1.+0.156*ALF) )
C R2 = 1. + 0.06 * (FN-8.) * (1.+0.12*ALF) / FN
C R3 = 1. + 0.012 * BTA * (1.+0.25*ABS(ALF)) / FN
C RATIO = R1 * R2 * R3
C XT = XT - RATIO * ( 1. - XT )
C ELSE IF ( I .EQ. 3 ) THEN

```

```

R1 = ( 1.67 + 0.28*ALF ) / ( 1. + 0.37*ALF )
R2 = 1. + 0.22 * (FN-8.) / FN
R3 = 1. + 8. * BTA / ( (6.28+BTA)*FN*FN )
RATIO = R1 * R2 * R3
XT = XT - RATIO * ( X(1) - XT )
ELSE IF ( I .LE. NN-2 ) THEN
  XT = 3. * X(I-1) - 3. * X(I-2) + X(I-3)
ELSE IF ( I .EQ. NN-1 ) THEN
  R1 = ( 1. + 0.235*BTA ) / ( 0.766 + 0.119*BTA )
  R2 = 1. / (1.+0.639*(FN-4.)/(1.+0.71*(FN-4.)))
  R3 = 1. / ( 1. + 20. * ALF / ( (7.5+ALF)*FN*FN ) )
  RATIO = R1 * R2 * R3
  XT = XT + RATIO * ( XT - X(I-2) )
ELSE
  R1 = ( 1. + 0.37*BTA ) / ( 1.67 + 0.28*BTA )
  R2 = 1. / ( 1. + 0.22*(FN-8.)/FN )
  R3 = 1. / ( 1. + 8. * ALF / ( (6.28+ALF)*FN*FN ) )
  RATIO = R1 * R2 * R3
  XT = XT + RATIO * ( XT - X(I-2) )
END IF

```

C

```

CALL ROOT ( NN, ALF, BTA, B, C, EPS, XT, DPN, PN1 )
X(I) = XT
A(I) = CC / ( DPN * PN1 )
CSX = CSX + XT
CSA = CSA + A(I)

```

200 CONTINUE

C

```

IF ( ABS(CSX-TSX) .GE. 1.E-9 .OR. ABS(CSA-TSA) .GE. 1.E-9 ) THEN
  WRITE (*,999) TSX, CSX, TSA, CSA
999  FORMAT(' TSX, CSX = ',2E20.10 / ' TSA, CSA = ',2E20.10)
ENDIF

```

C

```

RETURN
END

```

C

C

C

C

C

```

REAL FUNCTION  LNGAMA (X)

```

C

```

PI = 4. * ATAN (1.)

```

C

```

IF ( X .LT. 0.5 ) THEN
  P = PI / SIN(X*PI)
  IF ( P .LE. 0. ) THEN
    WRITE (*,99) X
99  FORMAT ( ' GAMMA( ',E12.5, ' ) IS NOT POSITIVE.' )
    STOP 1
  END IF
Y = 1. - X

```

```

ELSE
  Y = X
END IF
C
IF ( Y .LE. 6. ) THEN
  IK = 7 - Y
  FK = 1.
  DO 100 I = 0, IK-1
    FK = FK * ( Y + I )
100 CONTINUE
  Z = Y + IK
ELSE
  Z = Y
END IF
ZZ = Z * Z
LNGAMA = 0.5 * LOG(2.*PI) + (Z-0.5) * LOG(Z) - Z
1 + (((((-4146./ZZ + 1820.)/ZZ - 1287.)/ZZ + 1716.)
2 /ZZ - 6006.)/ZZ + 180180.) / (Z*2162160.)
C
IF ( Y .LE. 6. ) THEN
  LNGAMA = LNGAMA - LOG(FK)
END IF
C
IF ( X .LT. 0.5 ) THEN
  LNGAMA = LOG(P) - LNGAMA
END IF
C
RETURN
END
C
C
C -----
C
C SUBROUTINE ROOT ( NN, ALF, BTA, B, C, EPS, X, DPN, PN1 )
C DIMENSION B(NN), C(NN)
C DO 100 ITER = 1, 10
  CALL RECUR ( NN, ALF, BTA, B, C, X, P, DPN, PN1 )
  D = P / DPN
  X = X - D
  IF ( ABS(D) .LE. EPS ) RETURN
100 CONTINUE
C RETURN
  END
C
C
C -----
C
C

```

```

SUBROUTINE RECUR ( NN, ALF, BTA, B, C, X, P, DP, P0 )
C
C DIMENSION B(NN), C(NN)
C
P0 = 1.
P1 = X + (ALF-BTA) / (ALF+BTA+2.)
DP0 = 0.
DP1 = 1.
C
DO 100 J = 2, NN
P = ( X-B(J) ) * P1 - C(J) * P0
DP = ( X-B(J) ) * DP1 + P1 - C(J) * DP0
P0 = P1
P1 = P
DP0 = DP1
DP1 = DP
100 CONTINUE
C
RETURN
END
C
C -----
C
SUBROUTINE RAYLEIGH ( BP2, BS2, BRL, RPB )
C
C SLOWNESS OF RAYLEIGH WAVE
C
R (B) = 4. * B * B * SQRT ( ( B * B - BP2 ) * ( B * B - BS2 ) )
+ ( 2. * B * B - BS2 ) ** 2
RPRIME (B) = 4. * B**3 * ( SQRT ( (B*B-BS2)/(B*B-BP2) )
+ SQRT ( (B*B-BP2)/(B*B-BS2) ) )
+ -8.*B*( 2.*B*B - BS2 - SQRT ( (B*B-BP2)*(B*B-BS2) ) )
C
EPS = 1.0E-13
XNU = 0.5 * ( BS2 - 2. * BP2 ) / ( BS2 - BP2 )
C
C INITIAL TRY VALUE
C
B = SQRT (BS2) * ( 1. + XNU ) / ( 0.87 + 1.12 * XNU )
C
100 BRL = B - R (B) / RPRIME (B)
ERR = ABS ( ( BRL - B ) / B )
IF ( ERR .GT. EPS ) THEN
B = BRL
GO TO 100
ELSE
RPB = RPRIME (BRL) / BRL
RETURN
END IF
C

```

END

C
C
C
C
C

SUBROUTINE GEMTIM

C

COMMON /SLOW/ BP, BS, BR, BP2, BS2, BSP
COMMON /GEMF/ YP, ZP, FS, FC
COMMON /GEMG/ X, Y, Z, QS, QC, R0, R, R2
COMMON /TIME/ T1P, T1S, T1H, THM, T2, T3P, T3S, T3H
COMMON /FACT/ SGR, SGI, AFR, AFI, AFP, AFS, BTR, BTI,
+ S2R, S2I, S2P, S2S

C
C
C

GEOMETRICAL PROPERTIES

YP = Y * FC - Z * FS
ZP = -Y * FS - Z * FC
R0 = SQRT (X * X + Y * Y)
R2 = X * X + Y * Y + Z * Z
R = SQRT (R2)
QS = Y / R0
QC = X / R0

C
C
C

CONSTANTS USED IN THIS SUBROUTINE

QFC = 1. - QC * QC * FC * FC
YZ = Y * Y + Z * Z
XZP = X * X + ZP * ZP
BFS = BP2 - BS2 * FS * FS
R0Z = R0 * FS + Z * QS * FC

C
C
C

CONDITIONS TO ENSURE HEAD WAVE CONTRIBUTIONS

H1 = R0 / R - BP / BS
H3A = BP / BS - FS / SQRT (QFC)
H3B = (BS*YP*QC*FC*FC / SQRT (XZP) + QC*FS*BSP) ** 2 - QS*QS*BFS

C
C
C

ARRIVAL TIMES

C
C
C
C
C
C

TP = P WAVE ARRIVAL TIME
TS = S WAVE ARRIVAL TIME
TH = HEAD WAVE ARRIVAL TIME
THM = CONICAL HEAD WAVE COMPLETION TIME

C

T1P = R * BP
T1S = R * BS
IF (H1 .GT. 0.) THEN
T1H = Z * BSP + R0 * BP
ELSE
T1H = 1.0E10

```

END IF
THM = R2 * BSP / Z
C
T2 = R2 * BR / X
C
T3P = SQRT (XZP) * BP
T3S = SQRT (XZP) * BS
IF ( H3A .GT. 0. ) THEN
  IF ( H3B .GT. 0. ) THEN
    T3H = ( ABS (X) * SQRT (BFS) - ZP * BSP ) / FC
  ELSE
    T3H = 1.0E10
  END IF
ELSE
  T3H = BS * R0Z / SQRT (QFC)
END IF

```

C
C
C
USEFUL FACTORS IN OTHER SUBROUTINES

```

SGR = R0 / R2
SGI = Z / R2
AFR = Y * QC / YZ
AFI = Z * QC / YZ
AFP = YZ * ( BR * BR - BP2 )
AFS = YZ * ( BR * BR - BS2 )
BTR = YP * QC * FC / XZP
BTI = R0Z / XZP
S2R = QS * QC * FC * FC / QFC
S2I = FS / QFC
S2P = BP2 * QFC
S2S = BS2 * QFC

```

C
RETURN
END

C
C
C
C
C
C
FUNCTION U1 (T)

```

IMPLICIT COMPLEX (C)
COMMON /IDEX/ IWAVE
COMMON /SLOW/ BP, BS, BR, BP2, BS2, BSP, B2
COMMON /GEMG/ X, Y, Z, QS, QC, R0, R
COMMON /TIME/ T1P, T1S

```

C
U1 = 0.
IF (T .LE. T1P) RETURN

C
C
C
SPHERICAL P WAVE CONTRIBUTION

```

IWAVE = 1
B2     = BP2
QJ     = SQRT ( T * T - T1P * T1P ) / R
U1     = SUMPS (QJ)
IF ( T .LE. T1S ) RETURN

```

```

C
C
C
SPHERICAL S WAVE CONTRIBUTION

```

```

IWAVE = 2
B2     = BS2
QJ     = SQRT ( T * T - T1S * T1S ) / R
U1     = U1 + SUMPS (QJ)
RETURN

```

```

C
END

```

```

C
C
C
-----
C
C
C
FUNCTION    U1H (T)

```

```

C
IMPLICIT COMPLEX (C)
COMMON /IDEX/ IWAVE
COMMON /SLOW/ BP, BS, BR, BP2, BS2, BSP
COMMON /GEMG/ X, Y, Z, QS, QC, R0, R
COMMON /TIME/ T1P, T1S, T1H, THM

```

```

C
U1H = 0.
IF ( ( T .LE. T1H ) .OR. ( T .GE. THM ) ) RETURN

```

```

C
C
C
CONICAL HEAD WAVE CONTRIBUTION

```

```

IWAVE = 2
QQ     = ( T - Z * BSP ) / R0
QH     = SQRT ( QQ * QQ - BP2 )

```

```

C
IF ( T .LE. T1S ) THEN
    U1H = SUMH0 (QH)
ELSE
    QJ = SQRT ( T * T - T1S * T1S ) / R
    U1H = SUMH1 ( QJ, QH )
END IF
RETURN

```

```

C
END

```

```

C
C
C
-----
C
C
C
FUNCTION    U2 (T)

```

```

C
IMPLICIT COMPLEX (C)
COMMON /IDEX/ IWAVE
COMMON /SLOW/ BP, BS, BR, BP2, BS2
COMMON /GEMF/ YP, ZP, FS, FC
COMMON /GEMG/ X, Y, Z, QS, QC
COMMON /TIME/ TDUM(4), T2
COMMON /FACT/ FDUM(2), AFR, AFI, AFP, AFS

C
DATA CI / ( 0., 1. ) /

C
U2 = 0.
IF ( ( X .LE. 0. ) .OR. ( T .LE. T2 ) ) RETURN

C
C
C
CONICAL P WAVE CONTRIBUTION

IWAVE = 1
TP = T - X * BR
TEM = SQRT ( TP * TP + AFP )
CAF = AFR * TP + CI * AFI * TEM
CAFT = AFR + CI * AFI * TP / TEM
CX = CI * BR
CY = CI * CAF / QC
CXY = CX * CX + CY * CY
CZP = SQRT ( BP2 + CXY )
CZS = SQRT ( BS2 + CXY )
CALL SOURCV ( CX, CY, CXY, CZP, CZS, CR, CF )
CG = ( CI * CY * FC + CZP * FS ) * CR
U2 = REAL ( -CI * CF * CAFT / CG )

C
C
C
CONICAL S WAVE CONTRIBUTION

IWAVE = 2
TEM = SQRT ( TP * TP + AFS )
CAF = AFR * TP + CI * AFI * TEM
CAFT = AFR + CI * AFI * TP / TEM
CX = CI * BR
CY = CI * CAF / QC
CXY = CX * CX + CY * CY
CZP = SQRT ( BP2 + CXY )
CZS = SQRT ( BS2 + CXY )
CALL SOURCV ( CX, CY, CXY, CZP, CZS, CR, CF )
CF = CF / CZS
CG = ( CI * CY * FC + CZS * FS ) * CR
U2 = U2 + REAL ( -CI * CF * CAFT / CG )
RETURN

C
END

C
C
C
C
-----
C

```



```

C
FUNCTION    U2H (T)
C
IMPLICIT   COMPLEX (C)
COMMON    /IDEX/ IWAVE
COMMON    /SLOW/ BP, BS, BR, BP2, BS2
COMMON    /GEMF/ YP, ZP, FS, FC
COMMON    /GEMG/ X, Y, Z, QS, QC
COMMON    /TIME/ TDUM(5), T2S, T2H
COMMON    /FACT/ FDUM(2), AFR, AFI, AFP, AFS
C
DATA      CI / ( 0., 1. ) /
C
U2H = 0.
IF ( ( T .LE. T2H ) .OR. ( T .GE. T2S ) ) RETURN
C
C
PLANE HEAD WAVE CONTRIBUTION
C
IWAVE = 2
TP     = T - X * BR
TEM    = SQRT ( AFS - TP * TP )
C
IF ( Y .GE. 0. ) THEN
    AFH = AFR * TP - AFI * TEM
    AFHT = AFR + AFI * TP / TEM
    SGNP = -1.
ELSE
    AFH = AFR * TP + AFI * TEM
    AFHT = AFR - AFI * TP / TEM
    SGNP = 1.
END IF
C
CX     = CI * BR
CY     = CI * AFH / QC
CXY    = CX * CX + CY * CY
CZP    = SGNP * CI * SQRT ( ABS ( REAL ( BP2 + CXY ) ) )
CZS    = SQRT ( ABS ( REAL ( BS2 + CXY ) ) )
CALL   SOURCV ( CX, CY, CXY, CZP, CZS, CR, CF )
CF     = CF / CZS
CG     = ( CI * CY * FC + CZS * FS ) * CR
U2H    = REAL ( -CI * CF * AFHT / CG )
RETURN
C
END
C
C
-----
C
FUNCTION    U3 (T)
C
IMPLICIT   COMPLEX (C)

```

```

COMMON /IDEX/ IWAVE
COMMON /SLOW/ BP, BS, BR, BP2, BS2
COMMON /GEMF/ YP, ZP, FS, FC
COMMON /GEMG/ X, Y, Z, QS, QC
COMMON /TIME/ TDUM(5), T3P, T3S
COMMON /FACT/ FDUM(6), BTR, BTI, S2R, S2I, S2P, S2S

```

```

C
C
DATA CI / ( 0., 1. ) /

```

```

C
C
U3 = 0.
IF ( ( Y .LE. 0. ) .OR. ( YP .LE. 0. ) .OR. ( T .LE. T3P ) )
+ RETURN

```

```

C
C
C
CYLINDRICAL P WAVE CONTRIBUTION

```

```

IWAVE = 1
TEM = SQRT ( T * T - T3P * T3P )
CBT = BTR * T + CI * BTI * TEM
CBTT = BTR + CI * BTI * T / TEM
CSG = S2R * CBT + S2I * SQRT ( S2P - CBT * CBT )
CX = CI * CSG * QC + CI * CBT * QS
CY = CI * CSG * QS - CI * CBT * QC
CXY = CX * CX + CY * CY
CZP = SQRT ( BP2 + CXY )
CZS = SQRT ( BS2 + CXY )
CALL SOURCV ( CX, CY, CXY, CZP, CZS, CR, CF )
CG = ( CI * CX + BR ) * ( CSG * FS / CZP + QS * FC ) * CR
U3 = REAL ( -CI * CF * CBTT / CG )

```

```

IF ( T .LE. T3S ) RETURN

```

```

C
C
C
CYLINDRICAL S WAVE CONTRIBUTION

```

```

IWAVE = 2
TEM = SQRT ( T * T - T3S * T3S )
CBT = BTR * T + CI * BTI * TEM
CBTT = BTR + CI * BTI * T / TEM
CSG = S2R * CBT + S2I * SQRT ( S2S - CBT * CBT )
CX = CI * CSG * QC + CI * CBT * QS
CY = CI * CSG * QS - CI * CBT * QC
CXY = CX * CX + CY * CY
CZP = SQRT ( BP2 + CXY )
CZS = SQRT ( BS2 + CXY )
CALL SOURCV ( CX, CY, CXY, CZP, CZS, CR, CF )
CF = CF / CZS
CG = ( CI * CX + BR ) * ( CSG * FS / CZS + QS * FC ) * CR
U3 = U3 + REAL ( -CI * CF * CBTT / CG )
RETURN

```

```

C
C
C
END

```

```

C -----
C
C
C   FUNCTION      U3H (T)
C
C   IMPLICIT      COMPLEX (C)
COMMON  /IDEX/   IWAVE
COMMON  /SLOW/   BP, BS, BR, BP2, BS2
COMMON  /GEMF/   YP, ZP, FS, FC
COMMON  /GEMG/   X, Y, Z, QS, QC
COMMON  /TIME/   TDUM(6), T3S, T3H
COMMON  /FACT/   FDUM(6), BTR, BTI, S2R, S2I, S2P, S2S
C
C   DATA      CI / ( 0., 1. ) /
C
C   U3H = 0.
IF ( ( Y .LE. 0. ) .OR. ( YP .LE. 0. ) ) RETURN
IF ( ( T .LE. T3H ) .OR. ( T .GE. T3S ) ) RETURN
C
C   PLANE HEAD WAVE CONTRIBUTION
C
C   IWAVE = 2
TEM      = SQRT ( T3S * T3S - T * T )
C
C   IF ( X .GE. 0. ) THEN
      BTH = BTR * T - BTI * TEM
      BTHT = BTR + BTI * T / TEM
      SGNP = -1.
C   ELSE
      BTH = BTR * T + BTI * TEM
      BTHT = BTR - BTI * T / TEM
      SGNP = 1.
C   END IF
C
C   CSG      = S2R * BTH + S2I * SQRT ( S2S - BTH * BTH )
CX         = CI * CSG * QC + CI * BTH * QS
CY         = CI * CSG * QS - CI * BTH * QC
CXY        = CX * CX + CY * CY
CZP        = SGNP * CI * SQRT ( ABS ( REAL ( BP2 + CXY ) ) )
CZS        = SQRT ( ABS ( REAL ( BS2 + CXY ) ) )
CALL      SOURCV ( CX, CY, CXY, CZP, CZS, CR, CF )
CF         = CF / CZS
CG         = ( CI * CX + BR ) * ( CSG * FS / CZS + QS * FC ) * CR
U3H        = REAL ( -CI * CF * BTHT / CG )
RETURN
C
C   END
C
C -----
C

```

```

C      FUNCTION  SUMPS (QJ)
C
C      COMMON  /SUMS/  NJ, PT(1000), WT
C
C      SUM = 0.
C      DO 100  I = 1, NJ
C          SUM = SUM + FCTN ( PT(I) * QJ )
100 CONTINUE
C      SUMPS = WT * SUM
C
C      RETURN
C      END

```

```

C
C
C -----
C
C      FUNCTION  FCTN (Q)
C
C      IMPLICIT  COMPLEX (C)
C      COMMON    T
C      COMMON  /IDEX/  IWAVE
C      COMMON  /SLOW/  BP, BS, BR, BP2, BS2, BSP, B2
C      COMMON  /GEMF/  YP, ZP, FS, FC
C      COMMON  /GEMG/  X, Y, Z, QS, QC, R0, R, R2
C      COMMON  /FACT/  SGR, SGI
C
C      DATA    CI / ( 0., 1. ) /
C
C      TQ2 = R2 * ( B2 + Q * Q )
C
C      TEM = SQRT ( T * T - TQ2 )
C      CSG = SGR * T + CI * SGI * TEM
C      CX  = CI * CSG * QC - Q * QS
C      CY  = CI * CSG * QS + Q * QC
C      CXY = CX * CX + CY * CY
C      CZP = SQRT ( BP2 + CXY )
C      CZS = SQRT ( BS2 + CXY )
C      CALL  SOURCV ( CX, CY, CXY, CZP, CZS, CR, CF )
C
C      IF ( IWAVE .EQ. 1 ) THEN
C          CG  = ( CI * CX + BR ) * ( CI * CY * FC + CZP * FS ) * CR
C          FCTN = REAL ( CF * CZP / CG )
C      ELSE
C          CG  = ( CI * CX + BR ) * ( CI * CY * FC + CZS * FS ) * CR
C          FCTN = REAL ( CF / CG )
C      END IF
C
C      RETURN
C      END

```

```

C -----
C
C
C   FUNCTION    SUMHO (QH)
C
C   COMMON  /SUM0/ NH, PH(1000), WH(1000)
C
C   SUM = 0.
C   DO 100    I = 1, NH
C       SUM = SUM + WH(I) * FCTNH ( PH(I) * QH )
100 CONTINUE
C   SUMHO = QH * SUM
C
C   RETURN
C   END
C
C -----
C
C
C   FUNCTION    SUMH1 ( QJ, QH )
C
C   COMMON  /SUM1/ NH, PH(1000), WH(1000)
C
C   QC = ( QH + QJ ) / 2.
C   QL = ( QH - QJ ) / 2.
C
C   SUM = 0.
C   DO 100    I = 1, NH
C       Q   = QC + PH(I) * QL
C       QQJ = SQRT ( Q - QJ )
C       SUM = SUM + WH(I) * ( FCTNH ( Q ) + FCTNH (-Q) ) * QQJ
100 CONTINUE
C   SUMH1 = SQRT (QL) * SUM
C
C   RETURN
C   END
C
C -----
C
C
C   FUNCTION    FCTNH (Q)
C
C   IMPLICIT  COMPLEX (C)
C   COMMON    T
C   COMMON  /SLOW/ BP, BS, BR, BP2, BS2
C   COMMON  /GEMF/ YP, ZP, FS, FC
C   COMMON  /GEMG/ X, Y, Z, QS, QC, R0, R, R2
C   COMMON  /FACT/ SGR, SGI
C
C   DATA  CI / ( 0., 1. ) /

```

```

C
C   TQ2 = R2 * ( BS2 + Q * Q )
C
C   TEM  = SQRT ( TQ2 - T * T )
C   SGH  = SGR * T - SGI * TEM
C   SGHT = SGR + SGI * T / TEM
C   CX   = CI * SGH * QC - Q * QS
C   CY   = CI * SGH * QS + Q * QC
C   CXY  = CX * CX + CY * CY
C   CZP  = -CI * SQRT ( ABS ( REAL ( BP2 + CXY ) ) )
C   CZS  = SQRT ( ABS ( REAL ( BS2 + CXY ) ) )
C   CALL SOURCV ( CX, CY, CXY, CZP, CZS, CR, CF )
C   CF   = CF / CZS
C   CG   = ( CI * CX + BR ) * ( CI * CY * FC + CZS * FS ) * CR
C   FCTNH = REAL ( -CI * CF * SGHT / CG )

```

```

C
C   RETURN
C   END

```

```

C
C
C
C
C
C

```

```

-----
SUBROUTINE SOURCV ( CX, CY, CXY, CZP, CZS, CR, CF )

```

```

C

```

```

  IMPLICIT COMPLEX (C)
  COMMON /IDEX/ IWAVE, IDISP, ISLIP
  COMMON /GEMF/ DUM(2), FS, FC, FS2, FC2

```

```

C

```

```

  DATA CI / ( 0., 1. ) /

```

```

C

```

```

  CS = CZS * CZS + CXY
  CR = 4. * CZP * CZS * CXY - CS * CS

```

```

C

```

```

  GO TO ( 100, 200 ) ISLIP

```

```

C

```

```

100 CONTINUE

```

```

C

```

```

C STRIKE-SLIP

```

```

C

```

```

C P-WAVE

```

```

  IF ( IWAVE .EQ. 1 ) THEN
    IF ( IDISP .EQ. 1 ) THEN
      CF = -8. * CI * CX * CX * CY * CZS * FS
+         + 8. * CX * CX * CZP * CZS * FC
    ELSE IF ( IDISP .EQ. 2 ) THEN
      CF = -8. * CI * CX * CY * CY * CZS * FS
+         + 8. * CX * CY * CZP * CZS * FC
    ELSE IF ( IDISP .EQ. 3 ) THEN
      CF = -4. * CX * CY * CS * FS
+         - 4. * CI * CX * CZP * CS * FC
    END IF

```

```

C S-WAVE
  ELSE
    IF ( IDISP .EQ. 1 ) THEN
      CF = 2. * CI * CY * ( ( CZS * CZS - CX * CX + CY * CY ) * CS
+
      + 4. * CZP * ( CX * CX - CY * CY ) * CZS ) * FS
+
      + ( 8. * CY * CY * CZP * CZS - 2. * CS * CS ) * CZS * FC
    ELSE IF ( IDISP .EQ. 2 ) THEN
      CF = 2. * CI * CX * ( ( CZS * CZS + CX * CX - CY * CY ) * CS
+
      - 4. * CZP * ( CX * CX - CY * CY ) * CZS ) * FS
+
      - 8. * CX * CY * CZP * CZS * CZS * FC
    ELSE IF ( IDISP .EQ. 3 ) THEN
      CF = 8. * CX * CY * CZP * CZS * CZS * FS
+
      + 4. * CI * CX * CZP * CS * CZS * FC
    END IF
  END IF
C
  RETURN
C
200 CONTINUE
C
C DIP-SLIP
C
C P-WAVE
  IF ( IWAVE .EQ. 1 ) THEN
    IF ( IDISP .EQ. 1 ) THEN
      CF = -4. * CI * CX * CZS * ( CZP * CZP + CY * CY ) * FS2
+
      + 8. * CX * CY * CZP * CZS * FC2
    ELSE IF ( IDISP .EQ. 2 ) THEN
      CF = -4. * CI * CY * CZS * ( CZP * CZP + CY * CY ) * FS2
+
      + 8. * CY * CY * CZP * CZS * FC2
    ELSE IF ( IDISP .EQ. 3 ) THEN
      CF = -2. * ( CZP * CZP + CY * CY ) * CS * FS2
+
      - 4. * CI * CY * CZP * CS * FC2
    END IF
C S-WAVE
  ELSE
    IF ( IDISP .EQ. 1 ) THEN
      CF = 2. * CI * CX * ( ( CZS * CZS - CY * CY ) * CS
+
      + 4. * CY * CY * CZP * CZS ) * FS2
+
      - 8. * CX * CY * CZP * CZS * CZS * FC2
    ELSE IF ( IDISP .EQ. 2 ) THEN
      CF = 2. * CI * CY * ( ( 2. * CZS * CZS + CX * CX ) * CS
+
      - 4. * CX * CX * CZP * CZS ) * FS2
+
      + ( 8. * CX * CX * CZP * CZS - 2. * CS * CS ) * CZS * FC2
    ELSE IF ( IDISP .EQ. 3 ) THEN
      CF = 4. * CZP * CZS * ( CXY + CY * CY ) * CZS * FS2
+
      + 4. * CI * CY * CZP * CS * CZS * FC2
    END IF
  END IF
C
  RETURN
C

```


**NATIONAL CENTER FOR EARTHQUAKE ENGINEERING RESEARCH
LIST OF TECHNICAL REPORTS**

The National Center for Earthquake Engineering Research (NCEER) publishes technical reports on a variety of subjects related to earthquake engineering written by authors funded through NCEER. These reports are available from both NCEER's Publications Department and the National Technical Information Service (NTIS). Requests for reports should be directed to the Publications Department, National Center for Earthquake Engineering Research, State University of New York at Buffalo, Red Jacket Quadrangle, Buffalo, New York 14261. Reports can also be requested through NTIS, 5285 Port Royal Road, Springfield, Virginia 22161. NTIS accession numbers are shown in parenthesis, if available.

- NCEER-87-0001 "First-Year Program in Research, Education and Technology Transfer," 3/5/87, (PB88-134275/AS).
- NCEER-87-0002 "Experimental Evaluation of Instantaneous Optimal Algorithms for Structural Control," by R.C. Lin, T.T. Soong and A.M. Reinhorn, 4/20/87, (PB88-134341/AS).
- NCEER-87-0003 "Experimentation Using the Earthquake Simulation Facilities at University at Buffalo," by A.M. Reinhorn and R.L. Ketter, to be published.
- NCEER-87-0004 "The System Characteristics and Performance of a Shaking Table," by J.S. Hwang, K.C. Chang and G.C. Lee, 6/1/87, (PB88-134259/AS). This report is available only through NTIS (see address given above).
- NCEER-87-0005 "A Finite Element Formulation for Nonlinear Viscoplastic Material Using a Q Model," by O. Gyebi and G. Dasgupta, 11/2/87, (PB88-213764/AS).
- NCEER-87-0006 "Symbolic Manipulation Program (SMP) - Algebraic Codes for Two and Three Dimensional Finite Element Formulations," by X. Lee and G. Dasgupta, 11/9/87, (PB88-219522/AS).
- NCEER-87-0007 "Instantaneous Optimal Control Laws for Tall Buildings Under Seismic Excitations," by J.N. Yang, A. Akbarpour and P. Ghaemmaghami, 6/10/87, (PB88-134333/AS).
- NCEER-87-0008 "IDARC: Inelastic Damage Analysis of Reinforced Concrete Frame - Shear-Wall Structures," by Y.J. Park, A.M. Reinhorn and S.K. Kunnath, 7/20/87, (PB88-134325/AS).
- NCEER-87-0009 "Liquefaction Potential for New York State: A Preliminary Report on Sites in Manhattan and Buffalo," by M. Budhu, V. Vijayakumar, R.F. Giese and L. Baumgras, 8/31/87, (PB88-163704/AS). This report is available only through NTIS (see address given above).
- NCEER-87-0010 "Vertical and Torsional Vibration of Foundations in Inhomogeneous Media," by A.S. Veletsos and K.W. Dotson, 6/1/87, (PB88-134291/AS).
- NCEER-87-0011 "Seismic Probabilistic Risk Assessment and Seismic Margins Studies for Nuclear Power Plants," by Howard H.M. Hwang, 6/15/87, (PB88-134267/AS).
- NCEER-87-0012 "Parametric Studies of Frequency Response of Secondary Systems Under Ground-Acceleration Excitations," by Y. Yong and Y.K. Lin, 6/10/87, (PB88-134309/AS).
- NCEER-87-0013 "Frequency Response of Secondary Systems Under Seismic Excitation," by J.A. HoLung, J. Cai and Y.K. Lin, 7/31/87, (PB88-134317/AS).
- NCEER-87-0014 "Modelling Earthquake Ground Motions in Seismically Active Regions Using Parametric Time Series Methods," by G.W. Ellis and A.S. Cakmak, 8/25/87, (PB88-134283/AS).
- NCEER-87-0015 "Detection and Assessment of Seismic Structural Damage," by E. DiPasquale and A.S. Cakmak, 8/25/87, (PB88-163712/AS).
- NCEER-87-0016 "Pipeline Experiment at Parkfield, California," by J. Isenberg and E. Richardson, 9/15/87, (PB88-163720/AS). This report is available only through NTIS (see address given above).

- NCEER-87-0017 "Digital Simulation of Seismic Ground Motion," by M. Shinozuka, G. Deodatis and T. Harada, 8/31/87, (PB88-155197/AS). This report is available only through NTIS (see address given above).
- NCEER-87-0018 "Practical Considerations for Structural Control: System Uncertainty, System Time Delay and Truncation of Small Control Forces," J.N. Yang and A. Akbarpour, 8/10/87, (PB88-163738/AS).
- NCEER-87-0019 "Modal Analysis of Nonclassically Damped Structural Systems Using Canonical Transformation," by J.N. Yang, S. Sarkani and F.X. Long, 9/27/87, (PB88-187851/AS).
- NCEER-87-0020 "A Nonstationary Solution in Random Vibration Theory," by J.R. Red-Horse and P.D. Spanos, 11/3/87, (PB88-163746/AS).
- NCEER-87-0021 "Horizontal Impedances for Radially Inhomogeneous Viscoelastic Soil Layers," by A.S. Veletsos and K.W. Dotson, 10/15/87, (PB88-150859/AS).
- NCEER-87-0022 "Seismic Damage Assessment of Reinforced Concrete Members," by Y.S. Chung, C. Meyer and M. Shinozuka, 10/9/87, (PB88-150867/AS). This report is available only through NTIS (see address given above).
- NCEER-87-0023 "Active Structural Control in Civil Engineering," by T.T. Soong, 11/11/87, (PB88-187778/AS).
- NCEER-87-0024 Vertical and Torsional Impedances for Radially Inhomogeneous Viscoelastic Soil Layers," by K.W. Dotson and A.S. Veletsos, 12/87, (PB88-187786/AS).
- NCEER-87-0025 "Proceedings from the Symposium on Seismic Hazards, Ground Motions, Soil-Liquefaction and Engineering Practice in Eastern North America," October 20-22, 1987, edited by K.H. Jacob, 12/87, (PB88-188115/AS).
- NCEER-87-0026 "Report on the Whittier-Narrows, California, Earthquake of October 1, 1987," by J. Pantelic and A. Reinhorn, 11/87, (PB88-187752/AS). This report is available only through NTIS (see address given above).
- NCEER-87-0027 "Design of a Modular Program for Transient Nonlinear Analysis of Large 3-D Building Structures," by S. Srivastav and J.F. Abel, 12/30/87, (PB88-187950/AS).
- NCEER-87-0028 "Second-Year Program in Research, Education and Technology Transfer," 3/8/88, (PB88-219480/AS).
- NCEER-88-0001 "Workshop on Seismic Computer Analysis and Design of Buildings With Interactive Graphics," by W. McGuire, J.F. Abel and C.H. Conley, 1/18/88, (PB88-187760/AS).
- NCEER-88-0002 "Optimal Control of Nonlinear Flexible Structures," by J.N. Yang, F.X. Long and D. Wong, 1/22/88, (PB88-213772/AS).
- NCEER-88-0003 "Substructuring Techniques in the Time Domain for Primary-Secondary Structural Systems," by G.D. Manolis and G. Juhn, 2/10/88, (PB88-213780/AS).
- NCEER-88-0004 "Iterative Seismic Analysis of Primary-Secondary Systems," by A. Singhal, L.D. Lutes and P.D. Spanos, 2/23/88, (PB88-213798/AS).
- NCEER-88-0005 "Stochastic Finite Element Expansion for Random Media," by P.D. Spanos and R. Ghanem, 3/14/88, (PB88-213806/AS).
- NCEER-88-0006 "Combining Structural Optimization and Structural Control," by F.Y. Cheng and C.P. Pantelides, 1/10/88, (PB88-213814/AS).
- NCEER-88-0007 "Seismic Performance Assessment of Code-Designed Structures," by H.H.-M. Hwang, J.-W. Jaw and H.-J. Shau, 3/20/88, (PB88-219423/AS).

- NCEER-88-0008 "Reliability Analysis of Code-Designed Structures Under Natural Hazards," by H.H-M. Hwang, H. Ushiba and M. Shinozuka, 2/29/88, (PB88-229471/AS).
- NCEER-88-0009 "Seismic Fragility Analysis of Shear Wall Structures," by J-W Jaw and H.H-M. Hwang, 4/30/88, (PB89-102867/AS).
- NCEER-88-0010 "Base Isolation of a Multi-Story Building Under a Harmonic Ground Motion - A Comparison of Performances of Various Systems," by F-G Fan, G. Ahmadi and I.G. Tadjbakhsh, 5/18/88, (PB89-122238/AS).
- NCEER-88-0011 "Seismic Floor Response Spectra for a Combined System by Green's Functions," by F.M. Lavelle, L.A. Bergman and P.D. Spanos, 5/1/88, (PB89-102875/AS).
- NCEER-88-0012 "A New Solution Technique for Randomly Excited Hysteretic Structures," by G.Q. Cai and Y.K. Lin, 5/16/88, (PB89-102883/AS).
- NCEER-88-0013 "A Study of Radiation Damping and Soil-Structure Interaction Effects in the Centrifuge," by K. Weissman, supervised by J.H. Prevost, 5/24/88, (PB89-144703/AS).
- NCEER-88-0014 "Parameter Identification and Implementation of a Kinematic Plasticity Model for Frictional Soils," by J.H. Prevost and D.V. Griffiths, to be published.
- NCEER-88-0015 "Two- and Three- Dimensional Dynamic Finite Element Analyses of the Long Valley Dam," by D.V. Griffiths and J.H. Prevost, 6/17/88, (PB89-144711/AS).
- NCEER-88-0016 "Damage Assessment of Reinforced Concrete Structures in Eastern United States," by A.M. Reinhorn, M.J. Seidel, S.K. Kunnath and Y.J. Park, 6/15/88, (PB89-122220/AS).
- NCEER-88-0017 "Dynamic Compliance of Vertically Loaded Strip Foundations in Multilayered Viscoelastic Soils," by S. Ahmad and A.S.M. Israil, 6/17/88, (PB89-102891/AS).
- NCEER-88-0018 "An Experimental Study of Seismic Structural Response With Added Viscoelastic Dampers," by R.C. Lin, Z. Liang, T.T. Soong and R.H. Zhang, 6/30/88, (PB89-122212/AS).
- NCEER-88-0019 "Experimental Investigation of Primary - Secondary System Interaction," by G.D. Manolis, G. Juhn and A.M. Reinhorn, 5/27/88, (PB89-122204/AS).
- NCEER-88-0020 "A Response Spectrum Approach For Analysis of Nonclassically Damped Structures," by J.N. Yang, S. Sarkani and F.X. Long, 4/22/88, (PB89-102909/AS).
- NCEER-88-0021 "Seismic Interaction of Structures and Soils: Stochastic Approach," by A.S. Veletsos and A.M. Prasad, 7/21/88, (PB89-122196/AS).
- NCEER-88-0022 "Identification of the Serviceability Limit State and Detection of Seismic Structural Damage," by E. DiPasquale and A.S. Cakmak, 6/15/88, (PB89-122188/AS).
- NCEER-88-0023 "Multi-Hazard Risk Analysis: Case of a Simple Offshore Structure," by B.K. Bhartia and E.H. Vanmarcke, 7/21/88, (PB89-145213/AS).
- NCEER-88-0024 "Automated Seismic Design of Reinforced Concrete Buildings," by Y.S. Chung, C. Meyer and M. Shinozuka, 7/5/88, (PB89-122170/AS).
- NCEER-88-0025 "Experimental Study of Active Control of MDOF Structures Under Seismic Excitations," by L.L. Chung, R.C. Lin, T.T. Soong and A.M. Reinhorn, 7/10/88, (PB89-122600/AS).
- NCEER-88-0026 "Earthquake Simulation Tests of a Low-Rise Metal Structure," by J.S. Hwang, K.C. Chang, G.C. Lee and R.L. Ketter, 8/1/88, (PB89-102917/AS).
- NCEER-88-0027 "Systems Study of Urban Response and Reconstruction Due to Catastrophic Earthquakes," by F. Kozin and H.K. Zhou, 9/22/88, (PB90-162348/AS).

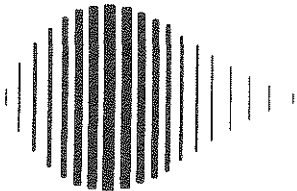
- NCEER-88-0028 "Seismic Fragility Analysis of Plane Frame Structures," by H.H-M. Hwang and Y.K. Low, 7/31/88, (PB89-131445/AS).
- NCEER-88-0029 "Response Analysis of Stochastic Structures," by A. Kardara, C. Bucher and M. Shinozuka, 9/22/88, (PB89-174429/AS).
- NCEER-88-0030 "Nonnormal Accelerations Due to Yielding in a Primary Structure," by D.C.K. Chen and L.D. Lutes, 9/19/88, (PB89-131437/AS).
- NCEER-88-0031 "Design Approaches for Soil-Structure Interaction," by A.S. Veletsos, A.M. Prasad and Y. Tang, 12/30/88, (PB89-174437/AS).
- NCEER-88-0032 "A Re-evaluation of Design Spectra for Seismic Damage Control," by C.J. Turkstra and A.G. Tallin, 11/7/88, (PB89-145221/AS).
- NCEER-88-0033 "The Behavior and Design of Noncontact Lap Splices Subjected to Repeated Inelastic Tensile Loading," by V.E. Sagan, P. Gergely and R.N. White, 12/8/88, (PB89-163737/AS).
- NCEER-88-0034 "Seismic Response of Pile Foundations," by S.M. Mamoon, P.K. Banerjee and S. Ahmad, 11/1/88, (PB89-145239/AS).
- NCEER-88-0035 "Modeling of R/C Building Structures With Flexible Floor Diaphragms (IDARC2)," by A.M. Reinhorn, S.K. Kunnath and N. Panahshahi, 9/7/88, (PB89-207153/AS).
- NCEER-88-0036 "Solution of the Dam-Reservoir Interaction Problem Using a Combination of FEM, BEM with Particular Integrals, Modal Analysis, and Substructuring," by C-S. Tsai, G.C. Lee and R.L. Ketter, 12/31/88, (PB89-207146/AS).
- NCEER-88-0037 "Optimal Placement of Actuators for Structural Control," by F.Y. Cheng and C.P. Pantelides, 8/15/88, (PB89-162846/AS).
- NCEER-88-0038 "Teflon Bearings in Aseismic Base Isolation: Experimental Studies and Mathematical Modeling," by A. Mokha, M.C. Constantinou and A.M. Reinhorn, 12/5/88, (PB89-218457/AS).
- NCEER-88-0039 "Seismic Behavior of Flat Slab High-Rise Buildings in the New York City Area," by P. Weidlinger and M. Ettouney, 10/15/88, (PB90-145681/AS).
- NCEER-88-0040 "Evaluation of the Earthquake Resistance of Existing Buildings in New York City," by P. Weidlinger and M. Ettouney, 10/15/88, to be published.
- NCEER-88-0041 "Small-Scale Modeling Techniques for Reinforced Concrete Structures Subjected to Seismic Loads," by W. Kim, A. El-Attar and R.N. White, 11/22/88, (PB89-189625/AS).
- NCEER-88-0042 "Modeling Strong Ground Motion from Multiple Event Earthquakes," by G.W. Ellis and A.S. Cakmak, 10/15/88, (PB89-174445/AS).
- NCEER-88-0043 "Nonstationary Models of Seismic Ground Acceleration," by M. Grigoriu, S.E. Ruiz and E. Rosenblueth, 7/15/88, (PB89-189617/AS).
- NCEER-88-0044 "SARCF User's Guide: Seismic Analysis of Reinforced Concrete Frames," by Y.S. Chung, C. Meyer and M. Shinozuka, 11/9/88, (PB89-174452/AS).
- NCEER-88-0045 "First Expert Panel Meeting on Disaster Research and Planning," edited by J. Pantelic and J. Stoyale, 9/15/88, (PB89-174460/AS).
- NCEER-88-0046 "Preliminary Studies of the Effect of Degrading Infill Walls on the Nonlinear Seismic Response of Steel Frames," by C.Z. Chrysostomou, P. Gergely and J.F. Abel, 12/19/88, (PB89-208383/AS).

- NCEER-88-0047 "Reinforced Concrete Frame Component Testing Facility - Design, Construction, Instrumentation and Operation," by S.P. Pessiki, C. Conley, T. Bond, P. Gergely and R.N. White, 12/16/88, (PB89-174478/AS).
- NCEER-89-0001 "Effects of Protective Cushion and Soil Compliancy on the Response of Equipment Within a Seismically Excited Building," by J.A. HoLung, 2/16/89, (PB89-207179/AS).
- NCEER-89-0002 "Statistical Evaluation of Response Modification Factors for Reinforced Concrete Structures," by H.H-M. Hwang and J-W. Jaw, 2/17/89, (PB89-207187/AS).
- NCEER-89-0003 "Hysteretic Columns Under Random Excitation," by G-Q. Cai and Y.K. Lin, 1/9/89, (PB89-196513/AS).
- NCEER-89-0004 "Experimental Study of 'Elephant Foot Bulge' Instability of Thin-Walled Metal Tanks," by Z-H. Jia and R.L. Ketter, 2/22/89, (PB89-207195/AS).
- NCEER-89-0005 "Experiment on Performance of Buried Pipelines Across San Andreas Fault," by J. Isenberg, E. Richardson and T.D. O'Rourke, 3/10/89, (PB89-218440/AS).
- NCEER-89-0006 "A Knowledge-Based Approach to Structural Design of Earthquake-Resistant Buildings," by M. Subramani, P. Gergely, C.H. Conley, J.F. Abel and A.H. Zaghaw, 1/15/89, (PB89-218465/AS).
- NCEER-89-0007 "Liquefaction Hazards and Their Effects on Buried Pipelines," by T.D. O'Rourke and P.A. Lane, 2/1/89, (PB89-218481).
- NCEER-89-0008 "Fundamentals of System Identification in Structural Dynamics," by H. Imai, C-B. Yun, O. Maruyama and M. Shinozuka, 1/26/89, (PB89-207211/AS).
- NCEER-89-0009 "Effects of the 1985 Michoacan Earthquake on Water Systems and Other Buried Lifelines in Mexico," by A.G. Ayala and M.J. O'Rourke, 3/8/89, (PB89-207229/AS).
- NCEER-89-R010 "NCEER Bibliography of Earthquake Education Materials," by K.E.K. Ross, Second Revision, 9/1/89, (PB90-125352/AS).
- NCEER-89-0011 "Inelastic Three-Dimensional Response Analysis of Reinforced Concrete Building Structures (IDARC-3D), Part I - Modeling," by S.K. Kunnath and A.M. Reinhorn, 4/17/89, (PB90-114612/AS).
- NCEER-89-0012 "Recommended Modifications to ATC-14," by C.D. Poland and J.O. Malley, 4/12/89, (PB90-108648/AS).
- NCEER-89-0013 "Repair and Strengthening of Beam-to-Column Connections Subjected to Earthquake Loading," by M. Corazao and A.J. Durrani, 2/28/89, (PB90-109885/AS).
- NCEER-89-0014 "Program EXKAL2 for Identification of Structural Dynamic Systems," by O. Maruyama, C-B. Yun, M. Hoshiya and M. Shinozuka, 5/19/89, (PB90-109877/AS).
- NCEER-89-0015 "Response of Frames With Bolted Semi-Rigid Connections, Part I - Experimental Study and Analytical Predictions," by P.J. DiCorso, A.M. Reinhorn, J.R. Dickerson, J.B. Radzinski and W.L. Harper, 6/1/89, to be published.
- NCEER-89-0016 "ARMA Monte Carlo Simulation in Probabilistic Structural Analysis," by P.D. Spanos and M.P. Mignolet, 7/10/89, (PB90-109893/AS).
- NCEER-89-P017 "Preliminary Proceedings from the Conference on Disaster Preparedness - The Place of Earthquake Education in Our Schools," Edited by K.E.K. Ross, 6/23/89.
- NCEER-89-0017 "Proceedings from the Conference on Disaster Preparedness - The Place of Earthquake Education in Our Schools," Edited by K.E.K. Ross, 12/31/89, (PB90-207895).

- NCEER-89-0018 "Multidimensional Models of Hysteretic Material Behavior for Vibration Analysis of Shape Memory Energy Absorbing Devices, by E.J. Graesser and F.A. Cozzarelli, 6/7/89, (PB90-164146/AS).
- NCEER-89-0019 "Nonlinear Dynamic Analysis of Three-Dimensional Base Isolated Structures (3D-BASIS)," by S. Nagarajaiah, A.M. Reinhorn and M.C. Constantinou, 8/3/89, (PB90-161936/AS).
- NCEER-89-0020 "Structural Control Considering Time-Rate of Control Forces and Control Rate Constraints," by F.Y. Cheng and C.P. Pantelides, 8/3/89, (PB90-120445/AS).
- NCEER-89-0021 "Subsurface Conditions of Memphis and Shelby County," by K.W. Ng, T-S. Chang and H-H.M. Hwang, 7/26/89, (PB90-120437/AS).
- NCEER-89-0022 "Seismic Wave Propagation Effects on Straight Jointed Buried Pipelines," by K. Elhmadi and M.J. O'Rourke, 8/24/89, (PB90-162322/AS).
- NCEER-89-0023 "Workshop on Serviceability Analysis of Water Delivery Systems," edited by M. Grigoriu, 3/6/89, (PB90-127424/AS).
- NCEER-89-0024 "Shaking Table Study of a 1/5 Scale Steel Frame Composed of Tapered Members," by K.C. Chang, J.S. Hwang and G.C. Lee, 9/18/89, (PB90-160169/AS).
- NCEER-89-0025 "DYNA1D: A Computer Program for Nonlinear Seismic Site Response Analysis - Technical Documentation," by Jean H. Prevost, 9/14/89, (PB90-161944/AS).
- NCEER-89-0026 "1:4 Scale Model Studies of Active Tendon Systems and Active Mass Dampers for Aseismic Protection," by A.M. Reinhorn, T.T. Soong, R.C. Lin, Y.P. Yang, Y. Fukao, H. Abe and M. Nakai, 9/15/89, (PB90-173246/AS).
- NCEER-89-0027 "Scattering of Waves by Inclusions in a Nonhomogeneous Elastic Half Space Solved by Boundary Element Methods," by P.K. Hadley, A. Askar and A.S. Cakmak, 6/15/89, (PB90-145699/AS).
- NCEER-89-0028 "Statistical Evaluation of Deflection Amplification Factors for Reinforced Concrete Structures," by H.H.M. Hwang, J-W. Jaw and A.L. Ch'ng, 8/31/89, (PB90-164633/AS).
- NCEER-89-0029 "Bedrock Accelerations in Memphis Area Due to Large New Madrid Earthquakes," by H.H.M. Hwang, C.H.S. Chen and G. Yu, 11/7/89, (PB90-162330/AS).
- NCEER-89-0030 "Seismic Behavior and Response Sensitivity of Secondary Structural Systems," by Y.Q. Chen and T.T. Soong, 10/23/89, (PB90-164658/AS).
- NCEER-89-0031 "Random Vibration and Reliability Analysis of Primary-Secondary Structural Systems," by Y. Ibrahim, M. Grigoriu and T.T. Soong, 11/10/89, (PB90-161951/AS).
- NCEER-89-0032 "Proceedings from the Second U.S. - Japan Workshop on Liquefaction, Large Ground Deformation and Their Effects on Lifelines, September 26-29, 1989," Edited by T.D. O'Rourke and M. Hamada, 12/1/89, (PB90-209388/AS).
- NCEER-89-0033 "Deterministic Model for Seismic Damage Evaluation of Reinforced Concrete Structures," by J.M. Bracci, A.M. Reinhorn, J.B. Mander and S.K. Kunnath, 9/27/89.
- NCEER-89-0034 "On the Relation Between Local and Global Damage Indices," by E. DiPasquale and A.S. Cakmak, 8/15/89, (PB90-173865).
- NCEER-89-0035 "Cyclic Undrained Behavior of Nonplastic and Low Plasticity Silts," by A.J. Walker and H.E. Stewart, 7/26/89, (PB90-183518/AS).
- NCEER-89-0036 "Liquefaction Potential of Surficial Deposits in the City of Buffalo, New York," by M. Budhu, R. Giese and L. Baumgrass, 1/17/89, (PB90-208455/AS).

- NCEER-89-0037 "A Deterministic Assessment of Effects of Ground Motion Incoherence," by A.S. Veletsos and Y. Tang, 7/15/89, (PB90-164294/AS).
- NCEER-89-0038 "Workshop on Ground Motion Parameters for Seismic Hazard Mapping," July 17-18, 1989, edited by R.V. Whitman, 12/1/89, (PB90-173923/AS).
- NCEER-89-0039 "Seismic Effects on Elevated Transit Lines of the New York City Transit Authority," by C.J. Costantino, C.A. Miller and E. Heymsfield, 12/26/89, (PB90-207887/AS).
- NCEER-89-0040 "Centrifugal Modeling of Dynamic Soil-Structure Interaction," by K. Weissman, Supervised by J.H. Prevost, 5/10/89, (PB90-207879/AS).
- NCEER-89-0041 "Linearized Identification of Buildings With Cores for Seismic Vulnerability Assessment," by I-K. Ho and A.E. Aktan, 11/1/89.
- NCEER-90-0001 "Geotechnical and Lifeline Aspects of the October 17, 1989 Loma Prieta Earthquake in San Francisco," by T.D. O'Rourke, H.E. Stewart, F.T. Blackburn and T.S. Dickerman, 1/90, (PB90-208596/AS).
- NCEER-90-0002 "Nonnormal Secondary Response Due to Yielding in a Primary Structure," by D.C.K. Chen and L.D. Lutes, 2/28/90.
- NCEER-90-0003 "Earthquake Education Materials for Grades K-12," by K.E.K. Ross, 4/16/90.
- NCEER-90-0004 "Catalog of Strong Motion Stations in Eastern North America," by R.W. Busby, 4/3/90.
- NCEER-90-0005 "NCEER Strong-Motion Data Base: A User Manual for the GeoBase Release (Version 1.0 for the Sun3)," by P. Friberg and K. Jacob, 3/31/90.
- NCEER-90-0006 "Seismic Hazard Along a Crude Oil Pipeline in the Event of an 1811-1812 Type New Madrid Earthquake," by H.H.M. Hwang and C-H.S. Chen, 4/16/90.
- NCEER-90-0007 "Site-Specific Response Spectra for Memphis Sheahan Pumping Station," by H.H.M. Hwang and C.S. Lee, 5/15/90.
- NCEER-90-0008 "Pilot Study on Seismic Vulnerability of Crude Oil Transmission Systems," by T. Ariman, R. Dobry, M. Grigoriu, F. Kozin, M. O'Rourke, T. O'Rourke and M. Shinozuka, 5/25/90.
- NCEER-90-0009 "A Program to Generate Site Dependent Time Histories: EQGEN," by G.W. Ellis, M. Srinivasan and A.S. Cakmak, 1/30/90.
- NCEER-90-0010 "Active Isolation for Seismic Protection of Operating Rooms," by M.E. Talbott, Supervised by M. Shinozuka, 6/8/9.
- NCEER-90-0011 "Program LINEARID for Identification of Linear Structural Dynamic Systems," by C-B. Yun and M. Shinozuka, 6/25/90.
- NCEER-90-0012 "Two-Dimensional Two-Phase Elasto-Plastic Seismic Response of Earth Dams," by A.N. Yiagos, Supervised by J.H. Prevost, 6/20/90.
- NCEER-90-0013 "Secondary Systems in Base-Isolated Structures: Experimental Investigation, Stochastic Response and Stochastic Sensitivity," by G.D. Manolis, G. Juhn, M.C. Constantinou and A.M. Reinhorn, 7/1/90.
- NCEER-90-0014 "Seismic Behavior of Lightly-Reinforced Concrete Column and Beam-Column Joint Details," by S.P. Pessiki, C.H. Conley, P. Gergely and R.N. White, 8/22/90.
- NCEER-90-0015 "Two Hybrid Control Systems for Building Structures Under Strong Earthquakes," by J.N. Yang and A. Daniellians, 6/29/90.

- NCEER-90-0016 "Instantaneous Optimal Control with Acceleration and Velocity Feedback," by J.N. Yang and Z. Li, 6/29/90.
- NCEER-90-0017 "Reconnaissance Report on the Northern Iran Earthquake of June 21, 1990," by M. Mehrain, 10/4/90.
- NCEER-90-0018 "Evaluation of Liquefaction Potential in Memphis and Shelby County," by T.S. Chang, P.S. Tang, C.S. Lee and H. Hwang, 8/10/90.
- NCEER-90-0019 "Experimental and Analytical Study of a Combined Sliding Disc Bearing and Helical Steel Spring Isolation System," by M.C. Constantinou, A.S. Mokha and A.M. Reinhorn, 10/4/90.
- NCEER-90-0020 "Experimental Study and Analytical Prediction of Earthquake Response of a Sliding Isolation System with a Spherical Surface," by A.S. Mokha, M.C. Constantinou and A.M. Reinhorn, 10/11/90.
- NCEER-90-0021 "Dynamic Interaction Factors for Floating Pile Groups," by G. Gazetas, K. Fan, A. Kaynia and E. Kausel, 9/10/90.
- NCEER-90-0022 "Evaluation of Seismic Damage Indices for Reinforced Concrete Structures," by S. Rodríguez-Gómez and A.S. Cakmak, 9/30/90.
- NCEER-90-0023 "Study of Site Response at a Selected Memphis Site," by H. Desai, S. Ahmad, G. Gazetas and M.R. Oh, 10/11/90.
- NCEER-90-0024 "A User's Guide to Strongmo: Version 1.0 of NCEER's Strong-Motion Data Access Tool for PCs and Terminals," by P.A. Friberg and C.A.T. Susch, 11/15/90.
- NCEER-90-0025 "A Three-Dimensional Analytical Study of Spatial Variability of Seismic Ground Motions," by L-L. Hong and A.H.-S. Ang, 10/30/90.



National Center for Earthquake Engineering Research
State University of New York at Buffalo